



Brownian Particles in Nonequilibrium Solvents

DISSERTATION

for the award of the degree

“Doctor rerum naturalium”

of the Georg-August-Universität Göttingen

within the doctoral program

Physics

of the Georg-August University School of Science (GAUSS)

submitted by

Boris Müller

from Waiblingen, Germany

Göttingen, 2019

Thesis committee

Prof. Dr. Matthias Krüger
Institut für Theoretische Physik,
Georg-August-Universität Göttingen

Prof. Dr. Marcus Müller
Institut für Theoretische Physik,
Georg-August-Universität Göttingen

Dr. Claus Heussinger
Institut für Theoretische Physik,
Georg-August-Universität Göttingen

Members of the examination board

Prof. Dr. Matthias Krüger
Institut für Theoretische Physik,
Georg-August-Universität Göttingen

Prof. Dr. Marcus Müller
Institut für Theoretische Physik,
Georg-August-Universität Göttingen

Further members of the examination board

Prof. Dr. Reiner Kree
Institut für Theoretische Physik,
Georg-August-Universität Göttingen

Prof. Dr. Tim Salditt
Institut für Röntgenphysik,
Georg-August-Universität Göttingen

Prof. Dr. Peter Sollich
Institut für Theoretische Physik,
Georg-August-Universität Göttingen

Prof. Dr. Annette Zippelius
Institut für Theoretische Physik,
Georg-August-Universität Göttingen

Date of the oral examination

December 10, 2019

Statutory Declaration

I herewith formally declare that

- I have written the submitted thesis independently.
- I did not use any outside support except for the quoted literature and other sources mentioned at the end of this paper.
- I clearly marked and separately listed all the literature and all other sources which I employed while producing this academic work, either literally or in content.
- the thesis was not used in the same or in a similar version to achieve an academic grading or is being published elsewhere.
- the digital version of my thesis is identical to the attached bound copies.

Göttingen, December 19, 2019

Boris Müller

List of publications

- [1] B. Müller and M. Krüger. Anisotropic particles near surfaces: Propulsion force and friction. *Phys. Rev. A*, 93:032511, 2016
- [2] B. Müller, R. Incardone, M. Antezza, T. Emig, and M. Krüger. Many-body heat radiation and heat transfer in the presence of a nonabsorbing background medium. *Phys. Rev. B*, 95:085413, 2017
- [3] K. Asheichyk, B. Müller, and M. Krüger. Heat radiation and transfer for point particles in arbitrary geometries. *Phys. Rev. B*, 96:155402, 2017
- [4] J. Berner, B. Müller, J. R. Gomez-Solano, M. Krüger, and C. Bechinger. Oscillating modes of driven colloids in overdamped systems. *Nat. Commun.*, 9(1):999, 2018
- [5] B. Müller, J. Berner, C. Bechinger, and M. Krüger. Properties of a nonlinear bath: Experiments, theory, and a stochastic Prandtl-Tomlinson model. *arXiv:1909.12812*, 2019

Abstract

Colloidal particles suspended in purely viscous (Newtonian) solvents have played a crucial role in understanding nonequilibrium processes and in the development of statistical physics out of equilibrium. The theoretical description of these systems usually rests on the assumption of a clear separation of time scales between the slow dynamical variables of probe particles and the fast dynamical variables of molecular solvent particles. In this so-called Markovian limit, the dynamical evolution equation of a probe particle's position is generally memory-free, that is, its current state contains all the information about future states. A suitable theoretical description is then provided in terms of Langevin equations in which the interaction force between probe particle and bath is separated into a systematic friction force and a fluctuating noise force. In the limit of infinite time scale separation, the random collisions of individual solvent molecules with the probe particle are statistically independent and the well-established model of Gaussian white noise can be used. The assumption of bath equilibrium in Newtonian fluids remains valid even when colloidal particles are strongly driven through the bath (e.g. active particles or by external forces) as is shown by remarkable agreement with all known experiments.

In recent years, viscoelastic fluids have entered the limelight of both theory and experiment. These fluids comprise a huge variety of systems such as biological fluids, semi-dilute polymer solutions, micellar systems, or dense colloidal suspensions. Most importantly, they are characterized by large structural relaxation times that can be comparable to or even larger than those of colloidal motion. The reason for the slow relaxation of these fluids lies in their complex microstructure that allows for the storage and dissipation of energy. Depending on externally imposed deformations they may exhibit either liquid- or solid-like behavior. If a particle is driven through such a viscoelastic bath, the assumption of a rapidly relaxing thermal bath is no longer applicable. Due to the elastic component of the bath, the microstructural deformation induced by the probe motion leads to a nontrivial back reaction of the bath on the probe particle. In this sense, the history of the probe particle is important and memory effects need to be invoked. The equation of motion becomes non-Markovian, i.e. future states of the probe depend on all previous states.

In this thesis, we thoroughly investigate and extend the theory of Brownian motion in complex fluids in and out of equilibrium. The theoretical analysis of these systems is performed on different levels of description. Starting from a microscopic point of view, we derive the effective equation of motion of a colloidal particle suspended in a complex equilibrium bath by well-known projection operator techniques. The

derivation is feasible for both Liouville dynamics and overdamped (Smoluchowski) dynamics. In the resulting linear generalized Langevin equation, we carefully investigate the influence of nonlinear particle-bath coupling on the friction memory kernel in a small time expansion. We find that for a harmonically confined tracer particle the memory kernel exhibits intriguing interdependencies, which can be shown to arise only in nonlinear baths. For example, the memory kernel shows a dependence on properties of the external potential, it can depend on the mass of the colloid, or, in the overdamped case, on its bare diffusivity. We demonstrate that these effects are indeed found in an experimental system of a harmonically confined colloidal silica particle suspended in a wormlike micellar solution. This system is known to behave strongly viscoelastically as it has a structural relaxation time on the order of seconds. After a detailed numerical analysis of experimental trajectories, we develop a simple model system of two nonlinearly coupled Brownian particles and study the influence of different interaction potentials. We find that a stochastic Prandtl-Tomlinson model accurately describes the experimental findings.

We then establish a connection of the equilibrium results with active microrheology within the framework of linear-response theory. In particular, we examine the limiting cases of an infinitely stiff trap and a very weak trap on the basis of a linear generalized Langevin equation and relate the results to previous work by other authors. We confirm that the microrheological friction coefficient of a trapped particle in general depends on the properties of the confining potential. In order to provide a suitable description beyond the linear-response regime, we derive a nonlinear Langevin equation in orders of probe displacement by making use of a recently presented novel approach of nonlinear response theory based on path integral techniques. We extend the generalized Langevin equation from second to third order and abstract the underlying structure of the exact microscopic equation in a phenomenological model. The nonlinear generalized Langevin equation is then linearized both in equilibrium and under nonequilibrium steady state conditions (constant velocity driving of the harmonically trapped particle). The derived linearized equation in the comoving frame proves useful in the description of the experimental micellar system, where in the nonequilibrium steady state we observe oscillating modes in the particle's mean conditional displacement. These oscillating modes are strictly ruled out in an overdamped equilibrium system. It turns out that a suitable model to describe these oscillations requires negative memory modes in the memory kernel of the linearized generalized Langevin equation. By using an extended Maxwell- or Jeffreys-like model with a negative contribution, we can successfully match the experimental data. We close the discussion by revisiting the stochastic Prandtl-Tomlinson model in nonequilibrium where we investigate the flow curve and the mean conditional displacement which show similar behavior as the experiment on a qualitative basis. We find that a three-particle extension of the model might be a good candidate to capture also the nonequilibrium effects of the complex experimental system.

Results of this thesis were published in Ref. [4] (presented in Chapter 6) and in the more recent work in Ref. [5] (presented in Chapter 3 and 4).

Contents

List of publications	i
Abstract	iii
1 Introduction	1
2 The system: confined Brownian particle in a viscoelastic solvent	7
3 Detecting nonlinear properties of an equilibrium bath	11
3.1 Microscopic starting point	11
3.2 Application of Zwanzig-Mori formalism	14
3.2.1 Derivation of equations of motion	14
3.2.2 Small time expansion of memory kernel	16
3.2.3 Overdamped dynamics	18
3.3 Experiment: A random walker in a wormlike micellar bath	22
3.4 Brownian dynamics simulations	29
3.4.1 Rescaling of the equations of motion	31
3.4.2 Harmonic coupling	32
3.4.3 Double-well interaction potential	35
3.4.4 Stochastic Prandtl-Tomlinson model	37
3.5 Stochastic Prandtl-Tomlinson model and experiments	40
4 Connection to microrheology and limiting cases	45
4.1 Linear-response theory of a colloid in confinement	46
4.2 The case of a very stiff trap $\kappa \rightarrow \infty$	48
4.3 The case of a very weak trap $\kappa \rightarrow 0$	50
4.4 Stationary limit	51
4.5 Nonlinear external potential	53
5 Nonlinear Langevin equation	57
5.1 Standard response formalism	57
5.2 Path integral formalism	59
5.3 Derivation of nonlinear Langevin equation	62
5.4 Phenomenological equation	67
5.4.1 Particle in equilibrium	68
5.4.2 Particle in a nonequilibrium steady state	72
6 Oscillating modes of overdamped driven colloids	79
6.1 State of the art	79

6.2	The regime of measurement	81
6.3	Experimental observations	82
6.4	Negative memory modes	88
6.5	Stochastic Prandtl-Tomlinson model in nonequilibrium	96
	Summary and outlook	101
	Zusammenfassung	103
	A Nonlinear external potential in overdamped dynamics	107
	B Entropic and frenetic part – An example	109
	Bibliography	111
	Acknowledgments	123
	Curriculum vitae	125

1 Introduction

Fluctuation-induced phenomena are an intrinsic and significant part of our (physical) world. Although often not visible to the naked eye, fluctuations are generally present and due to their ubiquity play an important role in many fields of physics [6–11]. They reflect the inherent statistical nature of physical systems as they describe the deviation of a particular realization of an observable (e.g. a single trajectory of a probe particle suspended in a liquid) from its ensemble average [12]. A statistical description is typically inevitable to approximate the dynamics of a given complex system as even with today’s computational power of modern supercomputers it is impossible to simulate a many-body problem consisting of the order of $\sim 10^{23}$ particles (corresponding to Avogadro’s constant [13]). Besides, the lack of knowledge or accessibility of initial conditions in an experimental system renders a formally exact theoretical description unfeasible and sometimes also not desirable [14].

Most intuitively, fluctuations appear in the form of thermal fluctuations in matter, indicating the thermal motion of its constituents (molecules and atoms) [7]. But even in the absence of matter and/or at the absolute zero of temperature, so-called quantum zero-point fluctuations form a fluctuating (quantum) vacuum with measurable consequences for physical observables [15]. In quantum systems, fluctuations naturally enter the theoretical description via Heisenberg’s uncertainty principle [16], and are responsible for intriguing effects such as Casimir forces [9, 17].

At the macroscopic level fluctuations of a system are often negligible. The intuitive reason is that their relative amplitude with respect to the mean value of a corresponding (macroscopic) observable is comparably small. Mathematically, this is a consequence of the central limit theorem [8]. This fundamental theorem of probability theory states that the probability distribution of the sum of N *independent* random variables (e.g. denoting the energies of particles in a non-interacting system or the positions of different time steps in a random walk [8]) converges in the limiting case of large N to a Gaussian distribution, although the distribution of individual random variables is assumed arbitrary. It is found that the relative fluctuations (normalized by the mean) of the sum of the N variables scales as $\sim 1/\sqrt{N}$ [8]. In the thermodynamic limit $N \rightarrow \infty$, the influence of fluctuations in such a system thus converges to zero. On the other hand, this result tells us that by scaling down our system size (or equivalently the length scale of entities we investigate) there is a regime where fluctuations are important.

A paradigmatic example of a fluctuation-induced phenomenon is the erratic and

jiggling motion of a mesoscopic particle (typically referred to as a colloidal or Brownian particle) suspended in a fluid (a liquid or a gas). The Brownian or colloidal length scale is roughly between 1 nm and 10 μm [18]. On this length scale, a continuum description of the interactions with the bath (constituted by the individual solvent particles) is applicable (due to a separation of length scales), and the thermal motion of the particle induced by random collisions with the solvent molecules is of the order of the particle size on experimental time ranges [18]. A particle of this size suspended in a liquid then performs what has become known as a random walk. The effect of Brownian motion was first observed by Scottish botanist Robert Brown [19]. He examined the thermal motion of various pollen grains of different plants under a simple microscope. From his observations Brown drew the conclusion that the effect is independent of the nature of dust particles but depends on their respective sizes. However, at the time of Brown's experimental observations in 1828 a theoretical explanation for the yet peculiar behavior of particles did not exist. It took until the beginning of the next century that Einstein [20], Sutherland [21], and Smoluchowski [22] provided the theoretical framework to explain the random motion of the mesoscopic particles. They attributed the irregular motion of mesoscopic particles suspended in a liquid to the thermal motion of molecular solvent particles. Most prominently, the authors derived the well-known Stokes-Einstein-Sutherland relation which connects the diffusion coefficient D of a spherical colloidal particle to the viscosity η of the solvent [20, 21],

$$D = \frac{k_B T}{6\pi\eta R}. \quad (1.1)$$

In this relation k_B denotes Boltzmann's constant, T is the temperature, and R is the radius of the colloid. Notably, the relation is a special version of a more fundamental theorem in statistical mechanics nowadays known as the fluctuation-dissipation theorem [23–25], which will be discussed for the case of linear viscoelastic media in more detail in Chapter 4. Shortly after these seminal works, Langevin presented a theory of Brownian motion based on a stochastic equation of motion for the mesoscopic particle [26]. He successfully applied Newton's second law to the case of a Brownian particle by separating the instantaneous total force into a deterministic part (friction force) and a stochastic part (random force/noise). Langevin attributed the latter contribution to the random kicks induced by the surrounding solvent molecules. The Langevin equation in its original form for the one-dimensional motion of a spherical Brownian particle in direction x reads [26]

$$m\ddot{x}(t) = -6\pi\eta R\dot{x}(t) + f(t). \quad (1.2)$$

Starting from this stochastic equation of motion Langevin computed the mean-squared displacement $\langle(x(t) - x(0))^2\rangle_{\text{eq}}$ of a free particle in a liquid thereby confirming the Stokes-Einstein-Sutherland relation. The theoretical framework developed at the time shared the similarity that it was in strong support of the atomic/molecular hypothesis of matter, a question which was, despite strong indications, still unsettled back then. It needed the experimental work of Perrin in 1910 to clarify the issue once and for all [27]. Perrin conducted measurements to determine Avogadro's

constant by several methods and also verified Einstein's and Langevin's prediction in terms of the Stokes-Einstein-Sutherland relation.

After the pioneering work on Brownian motion, more recent developments during the past decades have focused on advancing towards a description of systems far from equilibrium [28]. Nonequilibrium conditions provide a novel theoretical challenge as well-established theorems (such as the fluctuation-dissipation theorem [8]) can no longer be invoked in general, and additional assumptions must be imposed¹. Within this context, colloidal particles in purely viscous (Newtonian²) solvents have played a considerable role [30, 35–37]. They are an almost ideal realization of a random walker as their relaxation times ($\sim 10^{-9}$ s) are many orders of magnitude larger than those of the surrounding solvent molecules ($\sim 10^{-14}$ s) [18]. The separation of time scales of the slow degrees of freedom of the system (the colloidal particle) and the fast degrees of freedom (the solvent molecules) allows the statistical properties of the random force in Eq. (1.2) to be accurately described by Gaussian white noise. In the limit of infinite time scale separation, the statistical properties of the noise are fully specified by its first and second moment [11, 12, 18, 38],

$$\langle f(t) \rangle_{\text{eq}} = 0, \quad \langle f(t)f(t') \rangle_{\text{eq}} = 2k_B T \gamma \delta(t - t'). \quad (1.3)$$

In this equation, γ is the friction coefficient of the colloid (equal to $\gamma = 6\pi\eta R$ in the case of a spherical particle [18]). Note that the second moment of the noise yields yet another form of the fluctuation-dissipation theorem. It connects the force fluctuations in equilibrium with the dissipative part of the system, i.e. the particle's friction coefficient. Due to the rapid relaxation of bath degrees of freedom in a Newtonian liquid, the statistical properties of the random force do not change even when the particle is strongly driven through the fluid, as e.g., in the case of swimmers or imposed by external forces, and therefore, as experiments confirmed (see Ref. [39] for an overview), the equilibrium assumption of the bath remains valid. The surrounding heat bath thus acts as an inert equilibrium thermostat and only a small number of degrees of freedom (the particle position) is driven out of equilibrium in Newtonian systems. The assumption of weak coupling between probe particle and heat bath has led to an extension of fundamental concepts of classical thermodynamics, such as heat, work, energy, and entropy to be applicable to microscopic systems [40]. In the course of this development, various theoretical relations, commonly known as fluctuation relations, have been derived [41–47]. They restrict the general shape of distribution functions of thermodynamic variables on the mesoscopic scale and, ultimately, introduced the new field of stochastic thermodynamics [32, 39, 47]. On the experimental side, the precise control of colloidal particles by optical fields has provided the opportunity to immediately test theoretical predictions against exper-

¹We refer the reader to Refs. [29–33] for a discussion of fluctuation-dissipation theorems in nonequilibrium.

²Common examples of approximately purely viscous fluids under normal ambient conditions are, e.g., water, air, alcohol, or glycerin [34]. Purely viscous fluids can be characterized by Newton's law [11], i.e. for an incompressible and isotropic Newtonian fluid the shear stress σ is related to the shear rate $\dot{\gamma} = v_x/dy$ via the linear equation $\sigma = \eta\dot{\gamma}$, with η the (dynamic) shear viscosity of the fluid.

imental observations in model systems [30, 35–37].

The rich phenomenology and fundamental theoretical insight gleaned in the study of colloidal motion in Newtonian solvents raises the question of how the particle is affected by a more complex type of bath. In this respect, viscoelastic fluids have attracted considerable interest over the past years both on the experimental side and in theory [48–58]. Viscoelastic materials show distinct rheological properties as compared to Newtonian fluids due to their own complex microstructure. The class of viscoelastic material encompasses a huge variety of systems, such as biological fluids, polymer solutions, micellar systems, or dense colloidal suspensions. Since viscoelastic behavior can occur in many different forms, understanding of these fluids is significant both from a fundamental research point of view and in terms of industrial applications. Such baths allow for the storage and dissipation of energy, and their response to externally imposed deformations may show either liquid- or solid-like behavior. As a consequence, they exhibit large structural relaxation times³ that can easily become comparable to the time scales associated with Brownian motion. The large relaxation time of the bath leads to a situation where (macroscopically) many degrees of freedom are out of equilibrium when a colloidal particle is driven through a viscoelastic bath. The coupling of these degrees of freedom to a colloidal probe particle is expected to lead to a variety of new phenomena.

In this thesis, we aim to refine the well-established theory of Brownian motion in Newtonian solvents to be applicable to the case of nonequilibrium baths, realized by viscoelastic fluids. The study of driven colloids in viscoelastic fluids opens up a new field of research in statistical physics: The (confined) random walker in a nonequilibrium background. We start with a general introduction of the considered system in Chapter 2, where we discuss in particular the length and time scales of the system. Before we turn to nonequilibrium, we first investigate in Chapter 3 the properties of a complex equilibrium bath by well-known projection operator techniques in both Liouville and Smoluchowski dynamics. We find intriguing interdependencies in the friction memory kernel of the effective evolution equation of the probe particle by performing a small time expansion. The so-called “fluctuation renormalization” is a clear marker of nonlinear interactions between tracer particles and bath. The findings are indeed confirmed by the experimental system of a wormlike micellar solution, which we introduce and analyze in equilibrium in this chapter. A simple theoretical model system of two coupled Brownian particles (a stochastic Prandtl-Tomlinson model) allows us to match the experimental results on a quantitative level. Motivated by the observations in the effective evolution equation of the probe motion, we connect the results to well-known linear-response coefficients of microrheology in Chapter 4. We find that the interdependencies indeed translate to these coefficients. In particular, we study the limiting cases of an infinitely stiff confinement potential and a very weak one, respectively. We thereby confirm the observation of other authors that the two driving modes are distinct in the case of (active) microrheology

³See, e.g., Ref. [53] for the observation of elastic properties of a micellar bath, which after sudden removal of a perturbation induced by the motion of a colloidal tracer particle leads to a recoil effect of the particle.

and that the friction coefficient depends on the properties of the external confinement. In Chapter 5, we derive a nonlinear generalized Langevin equation up to third order in probe displacement by using a novel approach of nonlinear response theory based on path integrals. The derivation of a nonlinear Langevin equation is a prerequisite for a theoretical description far from equilibrium. The exact microscopic derivation of the equation of motion of the probe particle allows the extraction of a phenomenological nonlinear Langevin equation. This equation is then linearized in both equilibrium and under nonequilibrium steady state conditions by treating the nonlinearity as a perturbation of the linear system. In Chapter 6, the linearized equation is used to describe experimental results of a driven colloidal particle in a moving trap under stationary conditions. The experimental trajectories in a worm-like micellar solution exhibit a novel oscillatory mode in the comoving frame. Such particle oscillations in the mean conditional displacement are strictly ruled out for overdamped systems in equilibrium. The nonlinearity in the equation of motion renders the transformation into the comoving frame and the linearization nontrivial. We find that the linearized memory kernel and noise become functions of the dragging velocity of the trap. An extension of the classical Maxwell- or Jeffreys-like model for the memory kernel by negative memory modes yields a convenient phenomenological description of the experimental findings. At the end of the chapter we revisit the stochastic Prandtl-Tomlinson model under nonequilibrium conditions. We find that the extension to a three-particle model appears to be a good candidate to reproduce the experimental observations for the nonequilibrium steady state on a qualitative level. The thesis closes with a summary of the main results and a brief outlook regarding future work.

2 The system: confined Brownian particle in a viscoelastic solvent

We consider a system of a (harmonically) confined Brownian particle suspended in a complex viscoelastic solvent (see Figure 2.1 for a sketch). Viscoelastic materials occur in a large variety of systems such as biological fluids, polymer suspensions, micellar systems, or dense colloidal systems, and show distinct rheological properties compared to simple (Newtonian) fluids due to their complex microscopic structure [59]. The latter allows these kind of materials to store and dissipate energy and adds an elastic component to the properties of the bath. Such a behaviour is clearly distinct from the one of Newtonian fluids like water, alcohol, or glycerol which are typically well approximated by having a purely viscous impact on the motion of a probe particle [11]. As a consequence, the response of a viscoelastic material to an externally imposed deformation, e.g. induced by the motion of a probe particle, is strikingly different compared to the one of a Newtonian liquid.

In active microrheology [60–62], a mesoscopic particle, e.g. a colloid, is driven through a viscoelastic bath and thereby a shear deformation in the bath is locally induced. The motion of the particle may be characterized by a shear (strain) rate $\dot{\gamma}$. In a linear-response experiment (i.e. we consider sufficiently small shear rates) the resulting shear stress $\sigma(t)$ of the viscoelastic material is determined by the linear shear modulus $G(t)$ [63],

$$\sigma(t) = \int_{-\infty}^t G(t-t')\dot{\gamma}(t') dt' . \quad (2.1)$$

Notably, the shear stress of the solvent at time t depends not only on the instantaneous value of shear rate $\dot{\gamma}(t)$ but on the complete history of imposed shear rates. The memory of the viscoelastic bath will turn the effective equation of motion of the probe particle non-Markovian, i.e. future states of the particle depend on all previous states. On the other hand, when the system has no memory at all (the so-called Markovian approximation $G(t) \sim \delta(t)$), the current state of the probe contains all information about future states.

Equation (2.1) is a prime example of what we call a linear-response relation. The linear-response function G mediates the influence of a time-dependent perturbation (here the shear rate $\dot{\gamma}(t)$ induced by the driven particle) to the response of the system (the resulting shear stress of the bath). As mentioned before, such a linear relation is exact only in the case of sufficiently small shear rates and/or linear viscoelastic

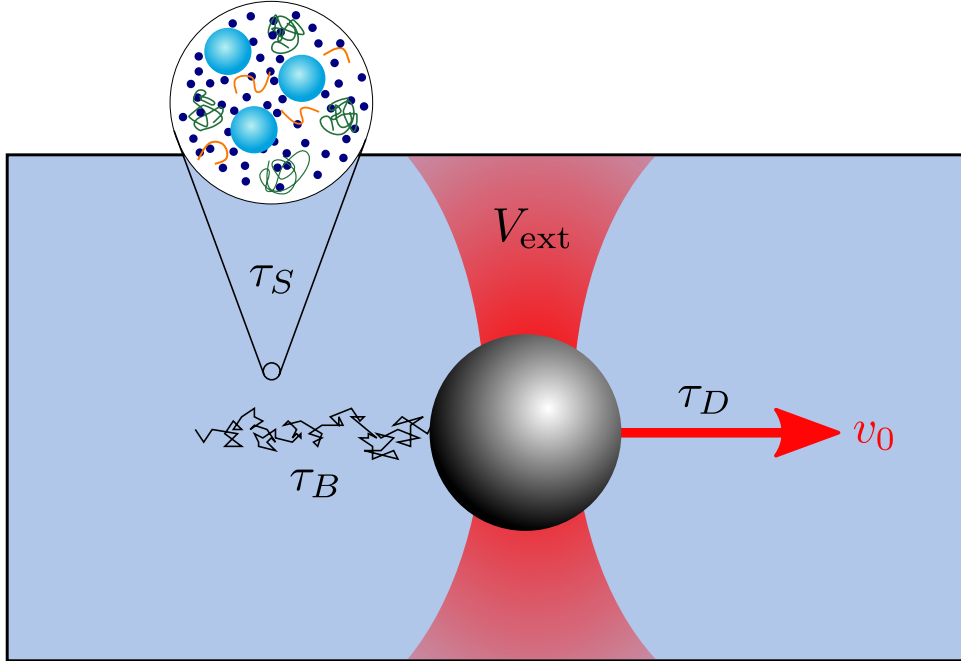


Figure 2.1: The considered system: A Brownian particle suspended in a complex viscoelastic bath, e.g. consisting of nanocolloids (blue), polymers (green), or wormlike micelles (orange). The latter constituents are much smaller than the particle but still large compared to the molecular solvent (dark blue dots), so that all length scales are well separated. The particle is confined by an external (harmonic) potential V_{ext} and performs Brownian motion in the limited configurational space. Nonequilibrium properties of the bath can e.g. be probed by dragging the particle at constant velocity v_0 through the bath. τ_D denotes the timescale of driving, τ_B is the timescale of Brownian fluctuations, and τ_S provides the (structural) relaxation time of the solvent.

material. In general, the full response behaviour of viscoelastic baths appears to be more complex either due to a nonlinear coupling between particle and bath and/or nonlinear interactions within the bath itself. In the case of a nonlinear bath an extension to nonlinear response theory is inevitable. In this way, the response relation in Eq. (2.1) needs to be recast in form of a so-called Volterra series where higher-order terms in shear rate will appear [64]. The response functions which depend on multiple frequencies in Fourier domain (in contrast to the single frequency dependence of the linear response function) are then referred to as nonlinear response functions (see Chapter 5 for a detailed discussion of nonlinear response theory).

An important aspect of the system for an appropriate theoretical description is given in terms of its length and time scales. In this context, it is important to point out that the viscoelastic fluid is made up of mesoscopic (Brownian) particles itself. In this work, we will focus on the case where bath particles are much smaller than the Brownian probe particle under investigation. This has the clear advantage that we can assume our findings to have no dependence on size ratios of tracer and bath particle. The mesoscopic bath particles on the other hand are assumed to be still

large compared to the solvent molecules. Due to the separation of length scales between tracer particle and bath particles a continuum description of the bath is expected to be applicable.

In order to keep the probe particle in focus (a relevant issue of diffusive Brownian particles in experimental systems [65, 66]), an external trapping potential is required. In recent years, tremendous progress in optical experimental techniques has led to a standard tool usually referred to as an optical tweezer [35, 53, 61, 67]. By means of optical tweezers (or in other words optical traps), it is possible to sort out and isolate individual Brownian particles in a sample. The trapping mechanism is achieved by a highly focused Gaussian laser beam shining onto the sample and exerting piconewton forces $\mathbf{F}_{\text{ext}} = -\nabla_{\mathbf{r}}V_{\text{ext}}(\mathbf{r})$. Note that by tuning the refractive indices of dielectric colloid and bath accordingly (the latter with lower refractive index), one can ensure that the light forces act only on the colloidal probe particle. For typical displacements from the position of the center of the trap, \mathbf{r}_{pot} , the imposed external potential on the particle is given by a harmonic potential [68],

$$V_{\text{ext}}(\mathbf{r}) = \frac{1}{2}\kappa|\mathbf{r} - \mathbf{r}_{\text{pot}}|^2, \quad (2.2)$$

where $\mathbf{r} = (x, y)$ is the position of the particle's barycenter. The colloid thus experiences a linear optical restoring force when being displaced from the center of the trap. The stiffness of the trap κ signifies the strength of the optical trap and can be easily manipulated in the experiment by changing the laser light intensity.

The sensitive control of optical tweezers allows the particle to be dragged through the viscoelastic background, e.g. by constant velocity on a straight line $\mathbf{v}_0 = (v_0, 0)$. In such an active microrheological experiment the driving itself sets an important time scale of the system which we denote as τ_D . This time scale is related to the inverse of the locally-induced shear rate, i.e. $\tau_D = 2R/v_0$, where $2R$ is the diameter of the dragged particle. It is therefore a measure for the characteristic rate of local deformation of the complex microstructure of the viscoelastic fluid. The second important time scale is given in terms of the Brownian diffusion time τ_B . This is the time it takes the particle to diffuse its own diameter, i.e. $\tau_B = 2R^2/D$, with D the diffusion constant. Most importantly – for the method of this thesis – is the last time scale τ_S of the solvent. As pointed out before, τ_S is typically very small in simple (Newtonian) fluids. Consequently, even if the probe particle is driven far away from equilibrium by high dragging velocities v_0 , the bath retains its equilibrium state due to the clear separation of time scales of probe and bath particles. This statement, however, is no longer true in case of viscoelastic baths. Due to the large structural relaxation time scale of the bath, (macroscopically) many degrees of freedom are out of equilibrium when the probe particle is driven through the bath. Indeed, by means of a recoil experiment in an entangled viscoelastic network of worm-like micelles, the bath relaxation time was revealed to be of the order of seconds [53]. In fluid dynamics, there is typically also the time scale of inertia τ_I , that describes the transition from ballistic to diffusive motion [18]. As we operate in the regime of very small Reynolds numbers ($\sim 10^{-9}$), viscous forces clearly dominate over inertial forces

and we assume τ_I to be small and negligible. This makes a theoretical description via overdamped dynamics feasible, where one assumes the momentum coordinates of the Brownian particles to be relaxed to thermal equilibrium. Furthermore, we note that in the theoretical description we will neglect hydrodynamic interactions to keep the theoretical approaches as simple as possible. In principle, these interactions are contained in Hamilton dynamics (the starting point of the next chapter) and we expect them to make no qualitative difference to the questions we raise.

In fluid dynamics, it has become common practice to introduce dimensionless numbers in order to classify different kinds of systems accordingly [69]. We have already encountered the Reynolds number, specifying the ratio of inertial to viscous forces. The introduced time scales give rise to additional dimensionless numbers that may prove useful in terms of classification of systems.

The first dimensionless number is the so-called Weissenberg number [69, 70], a measure of how strongly the solvent is perturbed by the driving of the probe particle. It is defined as the ratio of solvent relaxation time to the relaxation time set by the driving,

$$Wi \equiv \frac{\tau_S}{\tau_D} = \frac{v_0 \tau_S}{2R}. \quad (2.3)$$

For Newtonian fluids Wi is irrelevant due to the very small relaxation time τ_S of the solvent. For viscoelastic solvents, as considered in this thesis, however, the Weissenberg number can be of order unity, $Wi \sim 1$. In this regime, nonlinear non-Newtonian behaviour is expected to occur.

The second ratio we may introduce is given by the ratio of the solvent relaxation time and Brownian diffusion time. For this ratio there is no commonly used name known in literature, and we may define

$$M \equiv \frac{\tau_S}{\tau_B} = \frac{D\tau_S}{2R^2}. \quad (2.4)$$

For Newtonian fluids, $M \ll 1$, and the solvent relaxes almost instantaneously from the perspective of the Brownian particle. This renders the effective dynamics of the probe particle Markovian as assumed in Langevin's original publication (see Eq. (1.2)). If τ_S , however, is large and/or τ_B is small, then the description by a Markovian Langevin equation will no longer be correct. In this regime, a non-Markovian Langevin equation will naturally take into account memory effects of the solvent. Finally, the Péclet number, describing the strength of the driving relative to the particle's random motion [18],

$$Pe \equiv \frac{\tau_B}{\tau_D} = \frac{Rv_0}{D}, \quad (2.5)$$

is then already fixed. It turns out that this number which can take values in different regimes is less relevant in the performed study.

3 Detecting nonlinear properties of an equilibrium bath

Langevin equations provide a powerful method to describe the effective dynamics of a reduced set of degrees of freedom in a fluidic system. The general notion of these equations is to coarse grain the particle-bath interactions, thereby implicitly integrating out the bath degrees of freedom. The procedure is accomplished by *postulating* a random force or noise term in the equations of motion of the particle under study, turning them into stochastic differential equations. A rigorous link starting from microscopic equations of motion is important, however, to justify such an approach. The connection between microscopic models and Langevin equations can be established by well-known projection operator techniques first introduced by Zwanzig and Mori [71, 72]. In this chapter, we want to introduce these techniques for a particle-bath system in thermal equilibrium. The analysis is performed in the two cases of Hamilton dynamics as well as overdamped dynamics. We find that nonlinear properties of the system modify linear coefficients in the effective evolution equation of the probe particle in equilibrium. The results presented in this chapter and in the subsequent Chapter 4 are based to a large extent on the findings published in Ref. [5]¹.

3.1 Microscopic starting point

In classical mechanics, the dynamics of a macroscopic system consisting of N particles is determined by Hamilton's equations of motion [73]

$$\dot{\mathbf{q}}_i = \frac{\partial H}{\partial \mathbf{p}_i}, \quad \dot{\mathbf{p}}_i = -\frac{\partial H}{\partial \mathbf{q}_i}. \quad (3.1)$$

The classical microscopic Hamiltonian $H(\mathbf{q}, \mathbf{p}, t)$ of the system is a function of all $6N$ phase space variables given by positions $\mathbf{q} \equiv \mathbf{q}_1, \dots, \mathbf{q}_N$ and momenta

¹B. Müller, J. Berner, C. Bechinger, and M. Krüger. Properties of a nonlinear bath: Experiments, theory, and a stochastic Prandtl-Tomlinson model. *arXiv:1909.12812*, 2019. This article is licensed under a Non-exclusive License to Distribute (see <https://arxiv.org/licenses/nonexclusive-distrib/1.0/license.html>). Any reprint and/or adaptation of figures taken from this reference will be indicated in the corresponding figure caption in this and the subsequent chapter.

$\mathbf{p} \equiv \mathbf{p}_1, \dots, \mathbf{p}_N$ of the individual particles and, in general, may also be an explicit function of time. It reflects the total energy of the system which can be written as a sum of kinetic and potential energies. The dynamical evolution of the system can either be described by its so-called phase space trajectory $\mathbf{X}(t) \equiv (\mathbf{q}(t), \mathbf{p}(t))^T$ or, equivalently, in terms of a time-dependent probability distribution function $f(\mathbf{X}, t)$. By integrating the latter over an infinitesimal phase space element $d\mathbf{X}$, one obtains the probability to find the system at time t in a microscopic state corresponding to this volume element of phase space. Since the probability is a conserved quantity (the system must be somewhere in phase space), one has the normalization condition [11, 12]

$$\int d\mathbf{X} f(\mathbf{X}, t) = 1, \quad \forall t \quad (3.2)$$

which must be fulfilled for all times t . In physics, conserved quantities imply a conservation law in the form of a continuity equation. For the evolution of the phase space distribution function f one thus finds [11, 12]

$$\frac{\partial}{\partial t} f(t) = -\mathcal{L}f(t), \quad (3.3)$$

where for brevity we omitted the phase space dependence. This equation is known as the Liouville equation and describes the time evolution of the phase space distribution function f [11, 73]. It is determined by the Liouville operator \mathcal{L} which is a first-order differential operator given by [11, 12]

$$\mathcal{L} = \{ \cdot, H \} = \frac{\partial H}{\partial \mathbf{p}} \cdot \frac{\partial}{\partial \mathbf{q}} - \frac{\partial H}{\partial \mathbf{q}} \cdot \frac{\partial}{\partial \mathbf{p}}, \quad (3.4)$$

where we introduced the classical Poisson bracket $\{ \cdot, \cdot \}$. A similar evolution equation can be derived for an arbitrary dynamical phase space variable $A(\mathbf{q}, \mathbf{p})$ that does not explicitly depend on time t . By taking its total time derivative, and together with Hamilton's equation (3.1), one finds [11, 12]

$$\frac{\partial}{\partial t} A(t) = \mathcal{L}A(t). \quad (3.5)$$

Notably, there is a change of sign in comparison to Eq. (3.3). For the case of an equilibrium heat bath, as considered in this chapter, the Hamiltonian H does not explicitly depend on time. We recall again that the Liouville equation (for phase space distribution function f or dynamical phase space variable A) contains all the microscopic degrees of freedom of a system. Often, however, one is interested only in a certain subset of *relevant* variables and details of other microscopic degrees of freedom are not crucial for an appropriate theoretical description. This idea is accounted for by well-known projection operator techniques as was first discovered by Zwanzig and Mori [71, 72]. In this theoretical framework, any dynamical observable represents a vector in Hilbert space. The inner product associated with this Hilbert

space is given by [11, 12]

$$(A, B) = \int d\mathbf{X} f_{\text{eq}}(\mathbf{X}) A(\mathbf{X}) B^*(\mathbf{X}) = \langle A, B^* \rangle_{\text{eq}}, \quad (3.6)$$

weighted with the equilibrium distribution function f_{eq} . The Liouville operator, being anti-Hermitian with respect to this inner product [12], may now be separated into a part of relevant and irrelevant variables [12]

$$\mathcal{L} = \mathbf{P}\mathcal{L} + (\mathbf{1} - \mathbf{P})\mathcal{L}, \quad (3.7)$$

where the projector \mathbf{P} , projecting onto the subspace of relevant variables A , has been introduced. Its action on a variable B reads

$$\mathbf{P}B = (B, A) \cdot (A, A)^{-1} \cdot A. \quad (3.8)$$

By using Dyson's operator identity [12]

$$e^{t\mathcal{L}} = e^{t(\mathbf{1}-\mathbf{P})\mathcal{L}} + \int_0^t ds e^{(t-s)\mathcal{L}} \mathbf{P}\mathcal{L} e^{s(\mathbf{1}-\mathbf{P})\mathcal{L}}, \quad (3.9)$$

one can recast the Liouville equation for dynamical phase space variables Eq. (3.5) into the form of a linear non-Markovian generalized Langevin equation for an observable A of interest (which can be vector in space of observables) [12]

$$\frac{\partial}{\partial t} A(t) = i\mathbf{\Omega} \cdot A(t) - \int_0^t ds \mathbf{M}(s) \cdot A(t-s) + F(t). \quad (3.10)$$

The matrices (defined in space of observables) are given by

$$i\mathbf{\Omega} = (\mathcal{L}A, A) \cdot (A, A)^{-1}, \quad (3.11)$$

$$\mathbf{M}(t) = (F(t), F(0)) \cdot (A, A)^{-1}. \quad (3.12)$$

The exact mathematical rearrangement of the Liouville equation has led to linear equations of motion for the subset of relevant variables only. The process of integrating out irrelevant degrees of freedom to arrive at Eq. (3.10) is at cost of rendering the equations non-Markovian and also gives rise to a random force (noise) $F(t)$. This random force is given by the projected dynamics

$$F(t) = e^{t(\mathbf{1}-\mathbf{P})\mathcal{L}} (\mathbf{1} - \mathbf{P})\mathcal{L}A. \quad (3.13)$$

Notably, the noise term is orthogonal to the subspace of relevant variables A for all times t as can be seen by expanding the propagator of projected dynamics in powers of t . Besides, the equilibrium noise correlator in Eq. (3.12) is linked to the memory matrix \mathbf{M} . This relation may be identified with a non-Markovian variant of the fluctuation-dissipation theorem.

3.2 Application of Zwanzig-Mori formalism

We want to apply the abstract formalism of Zwanzig and Mori presented in the previous section to the case of a colloidal particle in confinement suspended in a complex bath as considered in this thesis. In order to keep the analysis as simple as possible, we consider a *one-dimensional* system, expecting the qualitative discussion to be equivalent in higher dimensions.

3.2.1 Derivation of equations of motion

We start from the following microscopic Hamiltonian,

$$H = \frac{p^2}{2m} + V_{\text{ext}}(x) + \sum_{j=1}^N \frac{p_j^2}{2m_j} + V_{\text{int}}(\{\xi_j\}). \quad (3.14)$$

Here, m is the mass of the colloid (spatial position x , momentum p), and $V_{\text{ext}}(x)$ is an external potential acting on it, e.g., imposed by optical forces as mentioned before. m_j are the masses of the N bath particles. p_j denote their corresponding momenta. The potential V_{int} is the interaction potential of the $N + 1$ particles involved, and is not necessarily pairwise additive. We assume V_{int} , however, to be translational invariant, i.e. it does not change under displacing all particles by the same vector. Consequently, it can be given in terms of the N relative coordinates $\{\xi_j\}$, where $\xi_j \equiv q_j - x$ is the distance between the tracer and the j -th bath particle.

So far, the choice of *relevant* variables has been arbitrary and we can choose it whatever we like it to be. For the explicit example of a colloid in a complex bath, however, it is most natural to choose the degrees of freedom of the probe particle as the subspace of relevant variables. Hence, we determine $A = (x, p)^T$, i.e. the vector formed by its position and momentum. The action of the projection operator on a variable B as defined in Eq. (3.8) is then given by the sum

$$\mathbf{P}B = \langle Bx \rangle_{\text{eq}} \langle x^2 \rangle_{\text{eq}}^{-1} x + \langle Bp \rangle_{\text{eq}} \langle p^2 \rangle_{\text{eq}}^{-1} p. \quad (3.15)$$

We want to derive the equations of motion for $A = (x, p)^T$ in the form of Eq. (3.10). The first quantity we need to compute is the so-called *frequency matrix* $i\mathbf{\Omega}$. It contains the inverse of the matrix $(\langle A, A \rangle_{\text{eq}})_{ij} = \langle A_i, A_j \rangle_{\text{eq}}$ which is found to be

$$\langle A, A \rangle_{\text{eq}}^{-1} = \begin{pmatrix} \langle x^2 \rangle_{\text{eq}}^{-1} & 0 \\ 0 & \langle p^2 \rangle_{\text{eq}}^{-1} \end{pmatrix}. \quad (3.16)$$

Here, we used that $\langle xp \rangle_{\text{eq}} = 0$ since spatial coordinates and momenta do not couple in the Hamiltonian (3.14), and the mean of position and momentum turns out to be zero in equilibrium. The next matrix we need to compute is $\langle \mathcal{L}A, A \rangle_{\text{eq}}$. The

Liouville operator for the given system reads explicitly

$$\mathcal{L} = \frac{\partial H}{\partial p} \left(\frac{\partial}{\partial x} - \sum_j \frac{\partial}{\partial \xi_j} \right) + \frac{\partial H}{\partial p_j} \frac{\partial}{\partial \xi_j} - \left(\frac{\partial H}{\partial x} - \sum_j \frac{\partial H}{\partial \xi_j} \right) \frac{\partial}{\partial p} - \frac{\partial H}{\partial \xi_j} \frac{\partial}{\partial p_j}, \quad (3.17)$$

where we used Einstein's summation convention, i.e. we sum over indices that appear twice in products. With this representation, we find

$$\langle \mathcal{L}A, A \rangle_{\text{eq}} = \begin{pmatrix} 0 & \langle p^2 \rangle_{\text{eq}}/m \\ -k_B T & 0 \end{pmatrix}. \quad (3.18)$$

Here, we used the fact the correlator of the external force $F_{\text{ext}}(x) = -V'_{\text{ext}}(x)$ and x equals $\langle F_{\text{ext}}(x)x \rangle_{\text{eq}} = -k_B T$ and that the average force acting on the tracer particle due to interactions with bath particles vanishes in equilibrium, i.e. $\langle F_{\text{int}} \rangle_{\text{eq}} = \sum_j \langle \partial_{\xi_j} V_{\text{int}} \rangle_{\text{eq}} = 0$. Finally, the frequency matrix takes on the form

$$i\mathbf{\Omega} = \begin{pmatrix} 0 & 1/m \\ -\kappa & 0 \end{pmatrix}, \quad (3.19)$$

where we defined the effective spring constant $\kappa = k_B T / \langle x^2 \rangle_{\text{eq}}$ which depends on V_{ext} (via the equilibrium distribution f_{eq}) and thermal energy $k_B T$. Notably, it is independent of the interaction potential V_{int} .

The memory matrix $\mathbf{M}(t)$ has a more involved form in comparison to the frequency matrix in Eq. (3.19), as it contains the projected dynamics, and no closed form for it is known in general. However, as a start we can provide its matrix structure for the given system. This becomes evident by computing the noise evaluated at time $t = 0$,

$$F(0) = (\mathbf{1} - \mathbf{P})\mathcal{L}A = \begin{pmatrix} 0 \\ F_{\text{int}} \end{pmatrix}. \quad (3.20)$$

We reiterate that $F_{\text{int}} = -\partial_x V_{\text{int}}$ is the force acting on the tracer particle due to interactions with bath particles. From this the matrix structure of $\mathbf{M}(t)$ becomes clear,

$$\mathbf{M}(t) = \begin{pmatrix} 0 & 0 \\ 0 & \Gamma(t)/m \end{pmatrix}, \quad (3.21)$$

where we introduced the so-called *friction memory kernel* $\Gamma(t)$

$$\Gamma(t) = m \langle e^{t(\mathbf{1}-\mathbf{P})\mathcal{L}} (\mathbf{1} - \mathbf{P})\mathcal{L}p, \mathcal{L}p \rangle_{\text{eq}} \langle p^2 \rangle_{\text{eq}}^{-1}. \quad (3.22)$$

The exact equations of motion for the colloidal particle in confinement in contact

with a complex bath in thermal equilibrium are thus given by

$$\dot{x}(t) = p(t)/m, \quad (3.23)$$

$$m\ddot{x}(t) = -\kappa x(t) - \int_0^t ds \Gamma(s)\dot{x}(t-s) + F(t). \quad (3.24)$$

In equilibrium, the first moment of the noise vanishes, i.e. $\langle F(t) \rangle_{\text{eq}} = 0$, and the second moment is given by the fluctuation-dissipation theorem

$$\langle F(t)F(0) \rangle_{\text{eq}} = k_B T \Gamma(t), \quad t \geq 0. \quad (3.25)$$

Although the applied technique is well known, it is worth reminding that despite the fact that the Hamiltonian in Eq. (3.14) contains nonlinear contributions V_{ext} and V_{int} , the resulting equations of motion (3.23) and (3.24) are inherently linear in x and p . The nonlinear character of V_{ext} and V_{int} finds its way into the linear coefficients appearing in Eq. (3.24). The shaping of linear coefficients by the underlying nonlinear interactions of system's constituents is widely known, and appears, for example, also in the linear optical response given by permittivity ε or permeability μ . For a typical solid, these quantities known from electrodynamics are functions of temperature T [74], one reason for it being the nonlinear interactions of atoms.

By using the fact that the noise term is orthogonal to the subspace of relevant variables for all times t , we can derive an exact linear transport equation for the equilibrium position correlator $C_{xx}(t) \equiv \langle x(t)x(0) \rangle_{\text{eq}}$ of the colloid. Multiplying Eq. (3.24) by x and by taking the equilibrium ensemble average on both sides of the equation, one obtains

$$m\ddot{C}_{xx}(t) = -\kappa C_{xx}(t) - \int_0^t ds \Gamma(s)\dot{C}_{xx}(t-s). \quad (3.26)$$

Even though one cannot give the memory kernel Γ in closed-form, this equation may be used as a prototypical example for various phenomenological models of memory kernels.

3.2.2 Small time expansion of memory kernel

Here, we continue on another route and expand the memory kernel in a small time expansion. Such an expansion will provide valuable insight into the principal structure of the memory kernel and we will discover intriguing interdependencies, which can be shown to arise only in nonlinear baths. In general, the series expansion of the memory kernel in time t to any order may be written as

$$\Gamma(t) = \sum_{n=0}^{\infty} \frac{\Gamma^{(2n)}}{(2n)!} t^{2n}. \quad (3.27)$$

Note that only even powers of t contribute due to the intrinsic time reversal symmetry, $\Gamma(t) = \Gamma(-t)$, as can be seen from Eq. (3.12). By expanding the operator exponential in Eq. (3.22), and using the anti-Hermitian property of the Liouville operator, $\mathcal{L} = -\mathcal{L}^\dagger$, the Taylor coefficients in Eq. (3.27) are found to be given by the quadratic form

$$\Gamma^{(2n)} = (-1)^n m \langle p^2 \rangle_{\text{eq}}^{-1} \langle [(\mathbf{1} - \mathbf{P})\mathcal{L}]^{n+1} p^2 \rangle_{\text{eq}}. \quad (3.28)$$

For simplicity, we restrict ourselves to the case of a harmonic external potential, $V_{\text{ext}}(x) = \frac{1}{2}\kappa x^2$. In this way, we may also isolate physical effects caused by the nonlinearity of the bath. We have already computed parts of the memory kernel evaluated at $t = 0$ in Eq. (3.20). By virtue of Eq. (3.28), we find

$$\Gamma(t = 0) = \Gamma^{(0)} = \beta \langle F_{\text{int}}^2 \rangle_{\text{eq}}. \quad (3.29)$$

The leading term for short times depends on the variance of the interaction force (we have $\langle F_{\text{int}} \rangle_{\text{eq}} = 0$) acting upon the colloidal particle in the presence of bath particles. While this dependence is generally expected, already the second Taylor coefficient is more interesting. For the second coefficient we find

$$\Gamma^{(2)} = -\frac{1}{m} \sum_{j,k} \langle \partial_j F_{\text{int}} ; \partial_k F_{\text{int}} \rangle_{\text{eq}} - \sum_j \frac{1}{m_j} \langle (\partial_j F_{\text{int}})^2 \rangle_{\text{eq}}, \quad (3.30)$$

where we introduced the covariance $\langle A ; B \rangle = \langle AB \rangle - \langle A \rangle \langle B \rangle$. The first term on the right-hand side of (3.30) depends on the mass m of the colloidal particle. The presence of such a term is surprising because it contradicts the naive expectation that the friction kernel should only depend on properties of the bath, and be independent of the tracer mass. Notably, it carries the covariance of force gradients as a prefactor and is thus absent in the harmonic coupling case, as e.g. employed in the models by Caldeira-Leggett [75]. This term is hence a signature of nonlinear coupling of the colloidal particle to the bath. Computation of the next higher-order term in the small-time expansion of the memory kernel reveals another interesting dependence. The Taylor coefficient to quartic order in t reads

$$\Gamma^{(4)} = \frac{\kappa}{m^2} \sum_{j,k} \langle \partial_j F_{\text{int}} ; \partial_k F_{\text{int}} \rangle_{\text{eq}} + \mathcal{O}(\kappa^0). \quad (3.31)$$

The friction kernel does not only depend on properties of bath and tracer, but also on the stiffness κ of the external harmonic potential. This is surprising as well since in the Hamiltonian (3.14) the external potential is in no way coupled to the bath degrees of freedom. The dependence showing up in the small time expansion of the memory kernel has indeed been observed in recent computer simulations of molecular solutes in water [76]. As already noted for the previous coefficient, the term also depends on the mass of the tracer particle. Both dependencies (on m and κ) are exclusively present in the case of nonlinear coupling to the bath, and hence not visible in purely linear systems. The computation of higher-order coefficients becomes more and more complex because of the appearance of many different terms.

However, higher-order terms in t share the similarity that they take on the form

$$\Gamma^{(2n)} = (-1)^n \frac{\kappa^{n-1}}{m^n} \sum_{j,k} \langle \partial_j F_{\text{int}} ; \partial_k F_{\text{int}} \rangle_{\text{eq}} + \mathcal{O}(\kappa^{n-2}) \quad n \geq 2. \quad (3.32)$$

This result is a consequence of the cyclicity of the recurrent application of the Liouville operator in Eq. (3.28). The intriguing interdependencies hence appear in any order $n \geq 2$ of Taylor coefficients in the small time expansion.

The effect of nontrivial dependencies in linear coefficients due to nonlinear interactions is sometimes referred to as “fluctuation renormalization” [12, 77, 78]. Indeed, the covariance of gradients of the interaction force is a quantity specifying the strength of fluctuations (here the fluctuations in the gradient of interaction forces with respect to the position of the tracer particle). The effect may therefore be considered as an anomalous enhancement of these fluctuations which occurs only in the presence of nonlinear interactions.

Notice that the effects studied in this section rely solely on the nonlinear coupling between tracer particle and bath. It does not require a nonlinear coupling among bath particles themselves. The latter will enter the probe’s effective evolution equation only if the motion of the probe strongly disturbs the thermal equilibrium of the bath, i.e. when the nonlinear response of the bath is probed by the tracer particle. Although in the equilibrium or near-equilibrium case the particle feels the nonlinear coupling to the bath, its motion is still influenced only by the linear back reaction of the bath.

The findings of this section are important to develop a basic understanding of how a nonlinear tracer-bath coupling affects the probe motion in equilibrium. In a nonequilibrium scenario, new physical effects are supposed to occur which have their origin in the bath dynamics itself. Indeed, this case has been recently studied in Ref. [54] via a new approach combining a path-integral description and nonlinear response theory. The authors found that nonlinear bath dynamics enter the probe’s dynamical evolution equation in second-order response theory giving rise to a novel time scale originating from changes in the dynamical activity of the bath. We will discuss this new approach and extend it to third order in Chapter 5.

3.2.3 Overdamped dynamics

In this section, we change the underlying dynamics from Hamilton dynamics to overdamped dynamics. In overdamped dynamics, we consider the same microscopic system as before but coarse grain the interaction of molecular solvent particles. A theoretical description for the degrees of freedom of interacting Brownian particles (as we consider in the case of a colloidal particle in a viscoelastic bath) may then be

given in terms of (nonlinear) Langevin equations [18]

$$\gamma_i \frac{\partial \mathbf{r}_i}{\partial t} = \mathbf{F}_i + \mathbf{f}_i. \quad (3.33)$$

Here, we have already assumed the overdamped limit, i.e. viscous forces dominate over inertial forces, and we omitted the latter. For a better differentiation between systematic and random forces, we denote \mathbf{F}_i as the total force acting on particle i due to external and interaction forces with other Brownian particles, and \mathbf{f}_i as the corresponding random force invoked by the molecular solvent. In this description, the noise is assumed to be white Gaussian with second moments fulfilling [18]

$$\langle f_i^\alpha(t) f_j^\beta(t') \rangle = 2k_B T \gamma_i \delta_{ij} \delta_{\alpha\beta} \delta(t - t'), \quad (3.34)$$

i.e., the noises of different particles and different directions at different times are assumed to be uncorrelated.

As nonlinear stochastic equations are generally very difficult to be approached analytically, an alternative description in terms of the probability distribution function $P(\mathbf{X} \equiv \{\mathbf{r}_i\}, t)$ is typically more practical. There are many different routes to derive the evolution equation for $P(\mathbf{X}, t)$ known as the Smoluchowski equation in the overdamped limit [18, 38]. It is given in terms of the Smoluchowski operator Ω and reads in the absence of hydrodynamic interactions (and assuming isotropic diffusion matrices D_i) [18, 38]

$$\begin{aligned} \partial_t P(\mathbf{X}, t) &= \Omega P(\mathbf{X}, t), \\ \Omega &= \sum_i D_i \nabla_{\mathbf{r}_i} \cdot [\nabla_{\mathbf{r}_i} - \beta \mathbf{F}_i]. \end{aligned} \quad (3.35)$$

The Smoluchowski equation is valid on the Brownian (or diffusive) timescale where the momentum coordinates of the Brownian particles are relaxed to thermal equilibrium. It provides an effective description where the phase space coordinates of the solvent molecules are long relaxed. In contrast to the Liouville equation, the Smoluchowski equation is a second-order partial differential equation and is sometimes referred to as a drift-diffusion equation [38]. The reason for it is that the second-order derivative term is associated with diffusion (cf. the diffusion equation [38]), while the first-order derivative term describes a drift term, e.g. of a particle in a flowing medium.

Of particular importance is the Hermitian conjugate, Ω^\dagger , of the Smoluchowski operator because it appears in the definition of equilibrium correlation functions [18]

$$C_{AB}(t) = \int d\mathbf{X} P_{\text{eq}} B^* e^{\Omega^\dagger t} A = \langle B^* e^{\Omega^\dagger t} A \rangle_{\text{eq}}. \quad (3.36)$$

The phase space functions A and B are arbitrary and in general complex. It is

straightforward to show that this operator takes on the form [18]

$$\Omega^\dagger = \sum_i D_i (\nabla_{\mathbf{r}_i} + \beta \mathbf{F}_i) \cdot \nabla_{\mathbf{r}_i}. \quad (3.37)$$

Notably, the adjoint operator is Hermitian with respect to the weighted inner product (weighted with the equilibrium distribution function P_{eq}) [18], i.e.

$$\langle A^* \Omega^\dagger B \rangle_{\text{eq}} = \langle B \Omega^\dagger A^* \rangle_{\text{eq}} = - \left\langle \sum_i D_i \frac{\partial A^*}{\partial \mathbf{r}_i} \cdot \frac{\partial B}{\partial \mathbf{r}_i} \right\rangle_{\text{eq}}. \quad (3.38)$$

In principle, a similar analysis as in the previous section is feasible by simply replacing the Liouville operator \mathcal{L} with the Hermitian conjugate of the Smoluchowski operator Ω^\dagger . By taking the overdamped limit $m \rightarrow 0$ in Eq. (3.24), we seek for an equation of the form

$$0 = -\kappa x(t) - \int_0^t ds \Gamma(s) \dot{x}(t-s) + f(t). \quad (3.39)$$

However, by making the choice $A = x$ in Eq. (3.10), the tracer's position and not its velocity is linked to the memory kernel Γ . A simple partial integration can currently not resolve this issue due to the projected dynamics that appear in the boundary terms. Nevertheless, a direct mapping by means of Eq. (3.36) appears to be a promising way to identify the memory kernel in the small time regime. A small time expansion of the position autocorrelation function yields

$$C_{xx}(t) = \langle x(t)x(0) \rangle_{\text{eq}} = \frac{k_B T}{\kappa} + \sum_{n=1}^{\infty} \frac{t^n}{n!} \langle x(\Omega^\dagger)^n x \rangle_{\text{eq}}. \quad (3.40)$$

On the other hand, the correlation function of the defining equation (3.39) can be easily computed in Laplace space as

$$\hat{C}_{xx}(s) = \frac{\frac{k_B T}{\kappa} \hat{\Gamma}(s)}{s \hat{\Gamma}(s) + \kappa}, \quad (3.41)$$

with Laplace transforms $\hat{h}(s) = \int_0^\infty dt e^{-st} h(t)$. Now, by taking the Laplace transform of Eq. (3.40) and together with Eq. (3.41) we find the relation

$$\frac{\frac{k_B T}{\kappa} \hat{\Gamma}(s)}{s \hat{\Gamma}(s) + \kappa} = \frac{k_B T}{\kappa} \frac{1}{s} + \sum_{n=1}^{\infty} \frac{1}{s^{n+1}} \langle x(\Omega^\dagger)^n x \rangle_{\text{eq}}. \quad (3.42)$$

In a small time expansion the memory kernel is expected to take on the following form

$$\Gamma(t) = \gamma_\delta \delta(t) + \sum_{n=0}^{\infty} \frac{\Gamma^{(n)}}{n!} t^n. \quad (3.43)$$

The expansion scheme for the overdamped case differs with respect to Eq. (3.27) in two ways. First, it is a nonanalytic function of time, exhibiting an instantaneous response $\sim \delta(t)$. The addition of this term is clear as in the overdamped limit inertial timescales $\tau_I = m/\gamma$ are shifted to zero and consequently no ballistic regime in the mean-squared displacement of the tracer particle can emerge. Secondly, as a consequence of this nonanalyticity, even and odd powers of t appear in the expansion.

In the following, we restrict ourselves to the case of two coupled Brownian particles in one dimension. Again, we expect the analysis to be qualitatively unchanged for higher dimensions or additional particles. The coupled system of equations of motion reads

$$\begin{aligned}\gamma\dot{x}(t) &= -V'_{\text{int}}(x - q) - \partial_x V_{\text{ext}}(x(t)) + F(t), \\ \gamma_b\dot{q}(t) &= V'_{\text{int}}(x - q) + F_b(t).\end{aligned}\tag{3.44}$$

Just like for the case of Hamilton dynamics, we take the external potential acting upon the tracer particle to be harmonic, $V_{\text{ext}} = \frac{1}{2}\kappa x^2$. The particle interacts via an arbitrary interaction potential $V_{\text{int}}(x - q)$ with the second Brownian particle (the bath particle). The noise sources of tracer and bath particle are still assumed to be white Gaussian and independent (see Eq. (3.34)). A Laplace transformation of the expansion in Eq. (3.43) together with Eq. (3.42) allows us to directly map the memory kernel $\Gamma(t)$ to the Smoluchowski dynamics. A straightforward computation yields the following coefficients

$$\gamma_\delta = \gamma\tag{3.45}$$

$$\Gamma^{(0)} = \beta\langle F_{\text{int}}^2 \rangle_{\text{eq}}\tag{3.46}$$

$$\begin{aligned}\Gamma^{(1)} &= -\frac{1}{\gamma}\langle F_{\text{int}}^{(1)} ; F_{\text{int}}^{(1)} \rangle_{\text{eq}} \\ &\quad + \frac{1}{\gamma_b} \left(\beta\langle F_{\text{int}}^2 F_{\text{int}}^{(1)} \rangle_{\text{eq}} + \langle F_{\text{int}} F_{\text{int}}^{(2)} \rangle_{\text{eq}} \right)\end{aligned}\tag{3.47}$$

$$\Gamma^{(2)} = \frac{\kappa}{\gamma^2}\langle F_{\text{int}}^{(1)} ; F_{\text{int}}^{(1)} \rangle_{\text{eq}} + \mathcal{O}(\kappa^0)\tag{3.48}$$

⋮

$$\Gamma^{(n)} = (-1)^n \frac{\kappa^{n-1}}{\gamma^n} \langle F_{\text{int}}^{(1)} ; F_{\text{int}}^{(1)} \rangle_{\text{eq}} + \mathcal{O}(\kappa^{n-2}) \quad n \geq 2.\tag{3.49}$$

A direct comparison to the Taylor coefficients found for Hamilton dynamics shows that the dependence on colloidal mass m is here, in the overdamped case, mirrored by the dependence of γ in Eq. (3.47). The dependence on the bare tracer friction γ is noteworthy, as again, it contradicts the naive expectation that the memory kernel should only depend on bath properties. Similarly to the case of Hamilton dynamics, the term involves the variance of the interaction force gradient. In this way, it is a signature of nonlinear interactions between tracer particle and bath, being absent in the harmonic coupling case. Higher-order terms in the small time expansion of Γ exhibit again a dependence on the trap stiffness κ of the external potential. This dependence carries over for orders $n \geq 2$, where the prefactor is

always linked to the covariance of the derivative of the interaction force. We may conclude that the “fluctuation renormalization” as discussed in the previous section appears to be an effect independent of the dynamics, visible only for nonlinearly interacting particle-bath systems.

3.3 Experiment: A random walker in a wormlike micellar bath

In this section, we want to examine the properties of a particular experimental system in thermal equilibrium, a harmonically trapped colloidal particle in a worm-like micellar bath. The provision of experimental data is part of a joint collaboration with the group of Clemens Bechinger at the University of Konstanz. The Bechinger group has gathered vast experience in the experimental treatment of viscoelastic fluids over the past years [4, 52, 53, 56, 57]. The experimental setup and measurement of data – as presented in this thesis – were performed by Johannes Berner, who himself is a PhD student in said group. Here, we will analyze the raw experimental data in different meaningful ways.

The experimental study is conducted in an equimolar solution of surfactant, cetylpyridinium chloride monohydrate (CPyCl, Sigma-Aldrich, crystalline, 99.0 – 102.0%) and salt, sodium salicylate (NaSal, Sigma-Aldrich, Reagentplus TM, $\geq 99.5\%$) in deionised water at a concentration of 7 mM. In such suspensions, it is well known that micellar structures will emerge after sufficiently long mixture time at temperatures close to room temperature [49]. Micelles can be considered as compound structures or aggregations of colloids composed of ionic surfactants typically with a hydrophilic headgroup and hydrophobic tail. These kind of amphiphilic molecules can self-assemble into various microstructures such as wormlike micelles, spherical micelles, or liquid crystal structures. The precise structure depends on detailed characteristics of the system such as molecular geometry of individual molecules, the ratio of volume to length of hydrophilic heads and hydrophobic tail, and so on [49]. In general, the behaviour of such systems is well understood and easily tunable from an experimental point of view [79–83]. The given experimental system is known to yield a wormlike micellar structure, where individual micelles form and deform dynamically. In this way, a highly entangled microstructure is established where thermal motion leads to dynamical phenomena like reptation, or formation and deformation of individual micelles.

Most significantly, the distinct microstructure of wormlike micelles allows for the storage and dissipation of energy thus leading to distinct rheological properties as compared to simple viscous fluids. This becomes evident in micro- and/or macrorheological experiments, where one typically shears the fluid in a pre-determined manner or time protocol [53]. By measuring the response to an external perturbation as a function of time, one can determine the structural stress relaxation time τ_S of

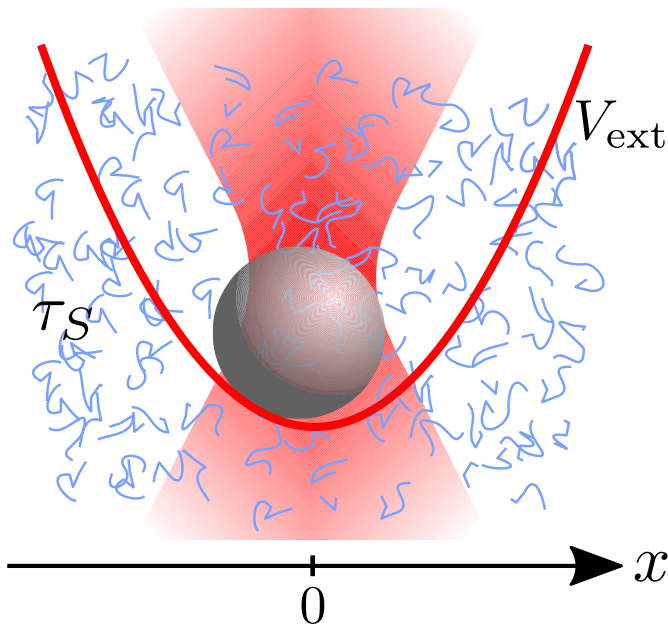


Figure 3.1: The experimental system: A silica microsphere is confined by a harmonic trap $V_{\text{ext}}(x) = \frac{1}{2}\kappa x^2$ and suspended in a highly viscoelastic wormlike micellar solution with a structural relaxation time τ_S of the order of seconds. Reprinted and adapted from Ref. [5].

the viscoelastic fluid. Such an experiment was performed by Juan Ruben Gomez-Solano [53], a member of the Bechinger group, where a similar viscoelastic fluid was examined as the one we investigate in this thesis. In this study, the motion of a harmonically trapped particle was monitored as it was dragged through the bath and finally released from its confinement. After removal of the trap the authors found that the particle recoiled into the direction opposite to its original dragging velocity. The observed transient dynamics is attributed to the recovery or relaxation of the deformed fluidic microstructure. The relaxation of the displacement of the particle can be conveniently described by a double-exponential decay, where the faster relaxation time is attributed to the viscous impact of the molecular solvent, and the slower relaxation gives rise to the stress relaxation time τ_S . The latter was determined to be on the order of more than one second in a wormlike micellar solution.

The experimental system under consideration in this thesis (see Fig. 3.1 for a sketch) exhibits a structural relaxation time of $\tau_S = 2.5 \pm 0.2$ s as determined by microrheological and macrorheological measurements at $T = 298$ K, thereby giving rise to highly non-Newtonian properties [4, 53]. The length of wormlike micelles is typically found between 100 and 1000 nm [80], and the characteristic mesh size is on the order of 30 nm [84].

Optical trapping of a single colloidal silica particle of diameter $2R = 2.73 \mu\text{m}$ is achieved by a highly focused Gaussian laser beam (wavelength $\lambda = 1070$ nm). Hydrodynamic interactions with the walls are avoided by moving the focal plane into

the middle plane of the sample cell. The particle in the center of the sample cell of height $90\ \mu\text{m}$ has at least a distance of $40\ \mu\text{m}$ to any wall. The observable of interest is the fluctuating displacement of the particle from the center of the trap. In two dimensions the displacement vector $\mathbf{r}(t)$ is tracked by means of video microscopy at a rate of more than 100 fps. The spatial accuracy or resolution of the system is given by $4\ \text{nm}$ [85]. During the measurement the temperature of the sample cell is kept constant at $T = 298 \pm 0.2\ \text{K}$, realized by coupling it to a thermostat.

Due to the isotropy of the given system in equilibrium we restrict ourselves to one dimension and denote the displacement of the particle from the center of the trap in this dimension as $x(t)$. A sample trajectory of the particle is shown in Fig. 3.2. As one would expect in equilibrium, the particle performs random fluctuations within the trap and can be perceived as an almost ideal realization of a random walker. A more informative analysis of the particle's trajectory is shown in Fig. 3.3 where we present the probability distribution $P(x)$ in form of a histogram. The distribution of x is in excellent agreement with Boltzmann statistics (red lines). From the Boltzmann distribution $P_{\text{eq}}(x) \sim \exp(-V_{\text{ext}}(x)/k_B T)$ we may extract the trap stiffness κ of the optical trap by using a parabolic fit function $V_{\text{ext}}(x) = \frac{1}{2}\kappa x^2$. For the given trajectory we find $\kappa = 7.42\ \mu\text{N}/\text{m}$ which is confirmed by a direct computation via the equipartition theorem $\kappa = \frac{k_B T}{\langle x^2 \rangle}$.

While the equilibrium probability distribution $P_{\text{eq}}(x)$ gives us information about the trap stiffness κ of the external potential, it does not provide any insight regarding the nonlinearity of the bath. In order to address properties of the latter, we need to consider the dynamics of the particle in the bath. In the following, we consider the case of a free particle (in the absence of the trap, i.e. $\kappa = 0$) in the wormlike micellar solution. A well-known measure of nonlinearity is given by the self-dynamic structure factor [18, 86],

$$S_s(k, t) \equiv \langle \exp(ik(x(0) - x(t))) \rangle \equiv \exp(-D(k, t)k^2 t). \quad (3.50)$$

The self-dynamic structure factor (sometimes also referred to as self-intermediate scattering function [87]) is a quantity known from light scattering experiments. It is the time-dependent correlation function of the Fourier transform of the microscopic single-particle density $\rho(\tilde{x}) = \delta(\tilde{x} - x)$. The time correlation function provides insight into the dynamics of sinusoidal density fluctuations of wavelength $\lambda = 2\pi/k$ of a single particle interacting with other Brownian particles. In a classical light scattering experiment, the N particles are considered as scattering centers and the scattered light commonly shows interference effects. The self-dynamic structure factor gives information on the incoherent part of the scattered light (while for the coherent part the time-dependent positions of the other particles also need to be taken into account [11]). It is obvious, however, that already the self-dynamic structure factor provides information on the properties of the bath since the bath particles influence the dynamics of the tracer particle via interactions.

On the right-hand side of Eq. (3.50), we defined the diffusion coefficient $D(k, t)$,

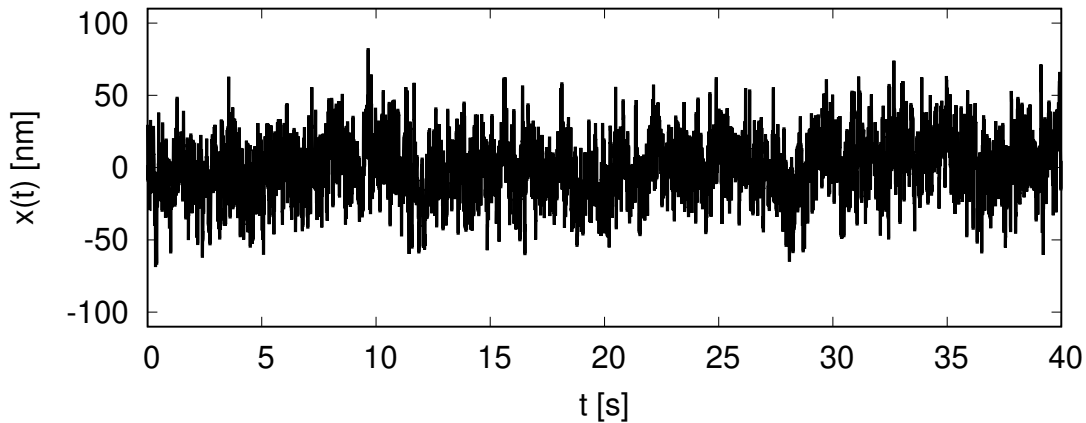


Figure 3.2: Experimental trajectory of a harmonically confined colloidal silica particle suspended in a wormlike micellar bath in thermal equilibrium. Provision and use of experimental raw data granted by Johannes Berner (Bechinger group, University of Konstanz).

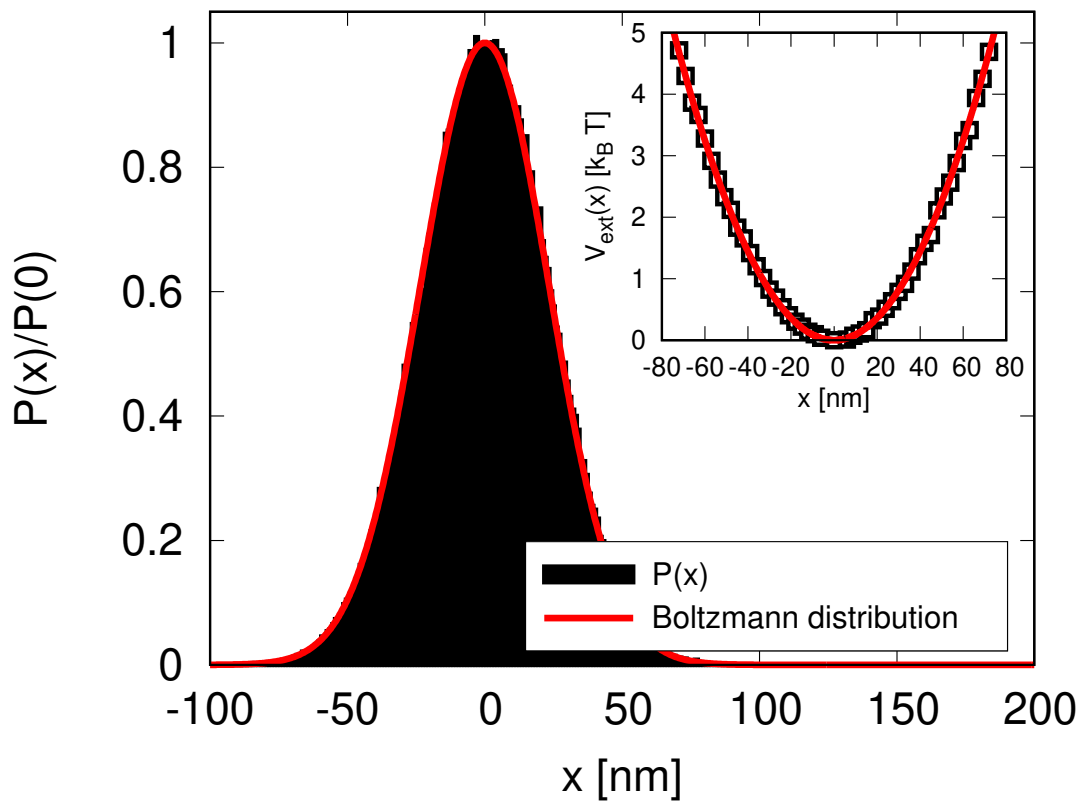


Figure 3.3: Main graph: Probability distribution $P(x)$ of particle positions relative to the center of the harmonic trap in a wormlike micellar bath in thermal equilibrium. The distribution is well described by the Boltzmann distribution shown as a red line. Inset: Extraction of trap stiffness κ from a parabolic fit (solid line) of the measured trap potential (symbols). Reprinted and adapted from Ref. [5].

which, due to interactions with the surrounding Brownian particles, now is a function of wavenumber k and time t . Note that diffusion processes in comparable complex systems have recently attracted a lot of interest [88–90]. If the probability distribution of particle displacements is Gaussian (as found in purely linear systems), the ensemble average can be moved into the exponential to yield

$$\langle \exp(-ik\Delta x(t)) \rangle = \exp\left(-\frac{1}{2}k^2\langle \Delta x(t)^2 \rangle\right), \quad (3.51)$$

where we abbreviated $\Delta x(t) = x(t) - x(0)$. In linearly interacting systems, the diffusion coefficient hence shows no k -dependence in D , so that a k -dependence is a good indicator for non-Gaussian and nonlinear processes. In a small wavenumber expansion, the self-dynamic structure factor is linked to the mean squared displacement and one finds [18]

$$S_s(k, t) = 1 - \frac{k^2}{2}\langle \Delta x(t)^2 \rangle + \mathcal{O}(k^4). \quad (3.52)$$

On the other hand, a small- k expansion of the right-hand side of Eq. (3.50) yields

$$S_s(k, t) = 1 - D(k=0, t)k^2t + \mathcal{O}(k^4). \quad (3.53)$$

Comparison of the two expansions reproduces the well-known Einstein relation in one dimension [20],

$$\langle \Delta x(t)^2 \rangle = 2D(k=0, t)t, \quad (3.54)$$

valid on timescales that are much larger than any relaxation time of the system. This requirement is certainly fulfilled for the long-time diffusion coefficient accessible in an experimental trajectory that is recorded for more than 30 minutes. From the definition of the diffusion coefficient for interacting systems in Eq. (3.50), we obtain the long-time free diffusion coefficient as

$$\lim_{t \rightarrow \infty} D(k, t) = -\lim_{t \rightarrow \infty} \frac{1}{k^2t} \log(\langle \exp(-ik\Delta x(t)) \rangle). \quad (3.55)$$

In Fig. 3.4, we show the k -dependence of $D(k, t \rightarrow \infty)$ normalized on $D(0, t \rightarrow \infty) = 204.8 \text{ nm}^2/\text{s}$ for an interval of experimentally accessible wavenumbers. The analysis reveals that D indeed depends on k for the given system, starting to decrease at a wavenumber of around $k \approx 10^7 \text{ m}^{-1}$. This value of wavenumber is connected to a length scale $2\pi/k$ of roughly 600 nm and appears to be a good estimate for typical length scales of wormlike micelles [80, 84].

The long-time diffusion coefficient strongly depends on the length scales probed by the particle. As the particle probes length scales comparable to the length scale of (nonlinear) interaction with the bath (recall that the length scale of wormlike micelles is found between 100 and 1000 [80], and the typical mesh size is on the order of 30 nm [84]), it apparently experiences a greater resistance in its motion

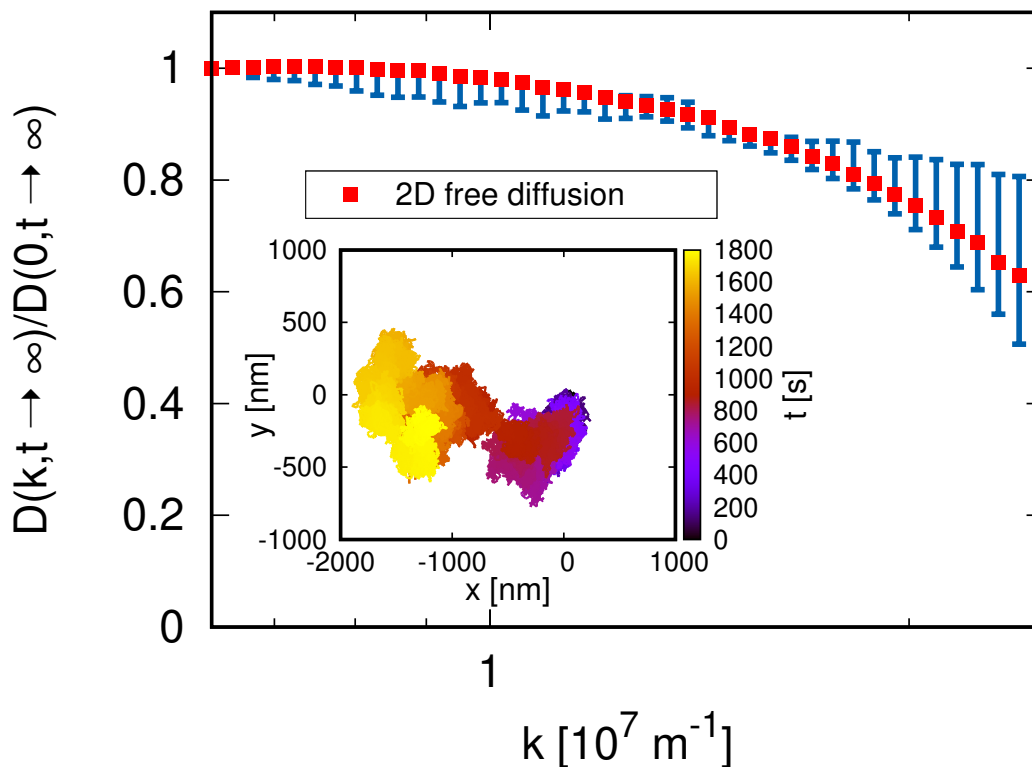


Figure 3.4: Normalized wavenumber-dependent free ($\kappa = 0$) diffusion coefficient $D(k, t \rightarrow \infty)$ of a colloidal silica particle in a wormlike micellar bath in thermal equilibrium. The statistical error is estimated by partitioning the measured trajectory (cf. inset) into two independent subsets. Provision and use of experimental raw data granted by Johannes Berner (Bechinger group, University of Konstanz). Reprinted from Ref. [5].

which is reflected in a decrease of the diffusion coefficient. On the other hand, in the regime of small wavenumbers, $k \rightarrow 0$, the particle probes the continuous properties of the bulk system and the diffusion coefficient saturates to a plateau value $D(0, t \rightarrow \infty)$.

We note that the experimental free diffusion coefficient D can only be resolved for a finite interval of k -values. The resolution of high k becomes numerically more and more unstable due to a sharper decay of the average in Eq. (3.55) and, ultimately, is limited by the finite spatial accuracy of about 4 nm in the experiment [85]. On the other hand, the small- k regime is limited by the finite size of the sample cell and the minimal distance to walls that is required to avoid hydrodynamical interactions with the sample cell itself.

The k -dependent free-diffusion coefficient is a first indication of the pronounced nonlinear properties of the experimental system in the absence of confinement. We proceed with the case of harmonic confinement and clarify the question whether

the intriguing interdependencies found in Sec. 3.2 indeed show up in the experimental system. In the previous section, we have shown that integrating out degrees of freedom of bath particles results in memory effects for the remaining degrees of freedom of the tracer particle. In the regime of small Reynolds number, we can neglect inertial forces and assume an equation of motion in the form of an overdamped generalized Langevin equation

$$\int_0^t ds \Gamma(s) \dot{x}(t-s) = -\kappa x(t) + f(t). \quad (3.56)$$

We are interested in the memory kernel Γ that describes the time-dependent friction force acting upon the tracer particle. A direct analysis in time domain is difficult since the memory kernel appears as a convolution with the tracer particle's velocity. By making use of the convolution theorem, however, the friction force reduces to a product of Laplace transforms in Laplace space and we can express the memory kernel $\hat{\Gamma}(s)$ as

$$\hat{\Gamma}(s) = \frac{\kappa \hat{C}_{xx}(s)}{\frac{k_B T}{\kappa} - \hat{C}_{xx}(s)s}. \quad (3.57)$$

In this derivation, we used that the equal time correlation function equals $C_{xx}(0) = \langle x^2 \rangle_{\text{eq}} = \frac{k_B T}{\kappa}$, i.e., the bath is prepared in thermal equilibrium at $t = 0$. Section 3.2 revealed interesting dependencies of the friction kernel Γ on the bare friction γ of the tracer particle or the trap stiffness κ of the external potential. While the former dependence might be tested by changing the particle size (recall Stokes's law for spherical particles $\gamma = 6\pi\eta R$), we will restrict ourselves to the variation of κ . This is easily accomplished in the experiments by varying the laser light intensity, and also allows comparison to results of Ref. [76].

In Fig. 3.5, we show the memory kernel in Laplace space extracted from experimental data and calculated via Eq. (3.57) for three different values of stiffnesses. We clearly see a dependence of the memory kernel on κ as was theoretically predicted in Sec. 3.2. For large values of s (corresponding to small times t), the three curves collapse to a single line. This behaviour is generally expected as in the limit $s \rightarrow \infty$ the tracer particle will only experience the solvent friction. For larger times t (smaller s values), nonlinear interactions with micelles dominate the friction force experienced by the colloidal probe particle, and the value of $\hat{\Gamma}(s)$ increases. In this regime, the dependence on κ becomes evident, and we observe the anticipated fluctuation renormalization. Finally, in the limit $s \rightarrow 0$ the Laplace-transformed memory kernel, $\hat{\Gamma}(s=0) = \int_0^\infty dt \Gamma(t)$, is expected to saturate to a constant plateau value because of the finite memory of the system. This regime, however, is difficult to access experimentally due to the finite measurement time of trajectories and the limited spatial resolution. Note that the equilibrium correlation functions, $\langle x(t)x(0) \rangle_{\text{eq}}$, required to compute the curves in the main graph are shown in the inset of Fig. 3.5.

The analysis of the tracer particle in harmonic confinement has shown another strong signature of nonlinear coupling between tracer particle and micellar bath in the

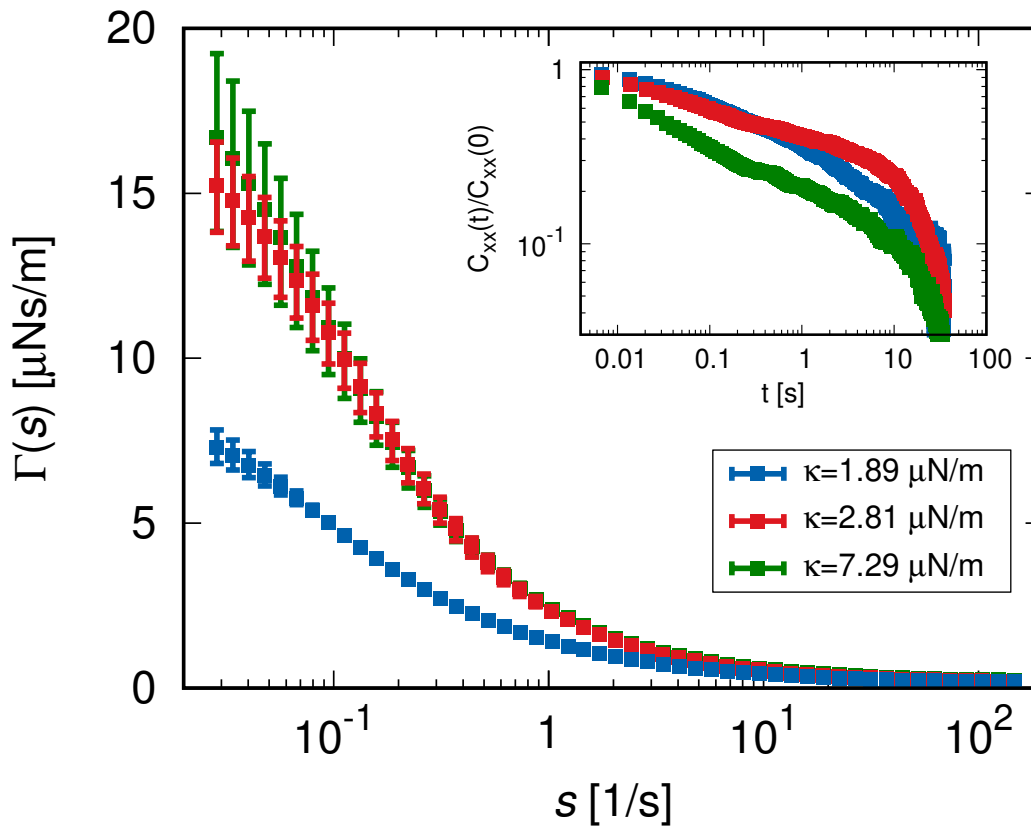


Figure 3.5: Experimental memory kernel $\hat{\Gamma}(s)$ of a harmonically confined colloidal silica particle in a wormlike micellar solution. The kernel is shown in Laplace space for three values of trap stiffness κ . The statistical error is estimated by partitioning the measured trajectories into two independent subsets. The inset shows the corresponding equilibrium time correlation functions $C_{xx}(t) \equiv \langle x(t)x(0) \rangle_{\text{eq}}$ from experimental data. Provision and use of experimental raw data granted by Johannes Berner (Bechinger group, University of Konstanz). Reprinted and adapted from Ref. [5].

experimental system. Since analytical methods for nonlinear systems are typically limited to expansion or approximate schemes, we aim to develop a simple model system to numerically reproduce the impact of a nonlinear tracer-bath coupling on the effective dynamics of the probe particle.

3.4 Brownian dynamics simulations

The starting point of Brownian dynamics simulations is the overdamped system of (nonlinearly) coupled equations of motion as given in Eq. (3.33). In contrast to molecular dynamics simulations [91, 92], the technique is based on stochastic equations of motions rather than on deterministic ones. In this sense, it uses an already coarsened-grained version of Newton's equation of motion where the kinetics

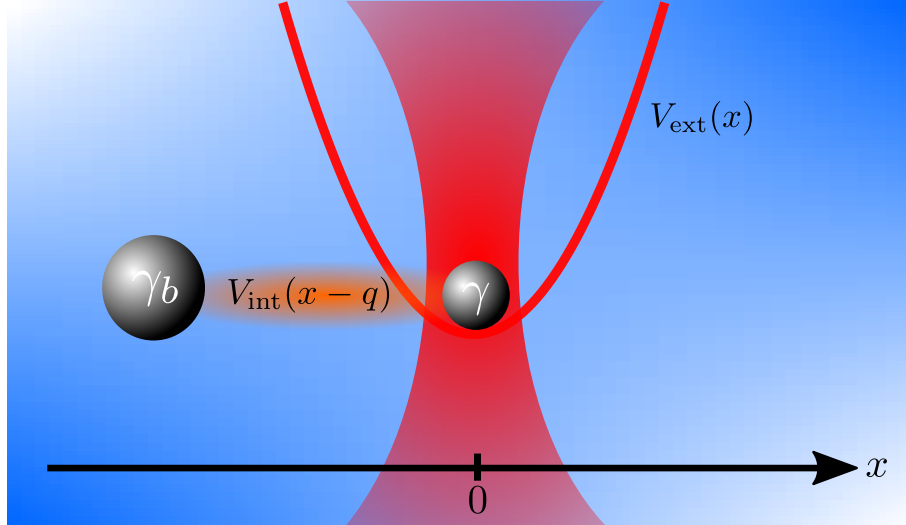


Figure 3.6: Model system of tracer and bath. The tracer particle (coordinate x) is confined by a harmonic potential $V_{\text{ext}}(x) = \frac{1}{2}\kappa x^2$, and coupled to the bath via an interaction potential $V_{\text{int}}(x - q)$, where q is the coordinate of the bath particle. Reprinted from Ref. [5].

of molecular solvent particles is accounted for by a noise term/fluctuating force. The coarse graining is rendered possible due to the clear separation of length and time scales between molecular solvent particles and mesoscopic Brownian particles. In comparison to conventional molecular dynamics simulations the technique allows to simulate much larger time scales because of the reduction of explicit degrees of freedom that enter the equations of motion. Brownian dynamics simulations have proven useful in a variety of different systems [93–97]. The technique is of particular importance in the study of spatio-temporal evolution or rheological properties of complex fluids such as polymers, proteins, DNA molecules, or colloidal solutions [98].

Here, we apply the method to a simple model of two nonlinearly coupled Brownian particles in the overdamped limit. This is a minimal model of a tracer-bath system where the elastic properties of the bath are taken into account by a coupled Brownian particle which mimics the bath itself. The tracer particle is considered to be in external confinement, V_{ext} , and the equations of motion are given by the coupled system already presented in Eq. (3.44),

$$\begin{aligned}\gamma\dot{x}(t) &= -V'_{\text{int}}(x - q) - \partial_x V_{\text{ext}}(x(t)) + F(t), \\ \gamma_b\dot{q}(t) &= V'_{\text{int}}(x - q) + F_b(t).\end{aligned}$$

The noise sources of tracer and bath particles are assumed to be white Gaussian, and independent $(i, j) \in \{F, F_b\}$,

$$\langle F_i(t) \rangle_{\text{eq}} = 0, \quad \langle F_i(t) F_j(t') \rangle_{\text{eq}} = \delta_{ij} 2k_B T \gamma_i \delta(t - t'). \quad (3.58)$$

Note that the friction coefficient of the bath γ_b is assumed to be much larger than the bare friction γ of the tracer particle. Again, we want to consider the case of harmonic confinement, i.e. $V_{\text{ext}} = \frac{1}{2}\kappa x^2$. A sketch of this simple model system is provided in Fig. 3.6.

3.4.1 Rescaling of the equations of motion

In the following, we aim to study this system by using specific forms of V_{int} . In order to generalize the results, it is convenient to recast the equations of motion into a dimensionless form. Such rescaling is often sensible to identify crucial time and length scales and to avoid rounding errors in numerical simulations. A reasonable choice is given by

$$\bar{x} = \frac{x}{d_0}, \quad \bar{t} = \frac{t}{\tau_B}, \quad \dot{\bar{x}} = \frac{\dot{x}}{\bar{v}}. \quad (3.59)$$

d_0 is a typical length scale set by the interaction potential V_{int} (see, e.g., Eq. (3.64) below for d_0). The Brownian time scale $\tau_B = \frac{d_0^2}{D} = \frac{d_0^2\gamma}{k_B T}$ is associated with the time it takes the tracer particle to (freely) diffuse a typical length scale of the interaction potential. And $\bar{v} = D/d_0$ is of the order of the mean velocity linked to the diffusive motion of the tracer particle. In these dimensionless units, the equations of motion turn into

$$\begin{aligned} \dot{\bar{x}} &= -\bar{\kappa}\bar{x} + \bar{F}_{\text{int}} + \bar{F}, \\ \bar{\gamma}_b\dot{\bar{q}} &= -\bar{F}_{\text{int}} + \bar{F}_b. \end{aligned} \quad (3.60)$$

We introduced the following rescaled parameters and forces

$$\bar{\kappa} = \frac{\kappa}{k_B T}, \quad \bar{\gamma}_i = \frac{\gamma_i}{\gamma}, \quad \bar{F}_{\text{int}}(\bar{\xi}) = \frac{F_{\text{int}}(\xi)}{\frac{k_B T}{d_0}}, \quad \bar{F}_i(\bar{t}) = \frac{F_i(t)}{\frac{k_B T}{d_0}}, \quad (3.61)$$

where the interaction force acting upon the tracer particle reads $F_{\text{int}} = -V'_{\text{int}}(\xi)$ with relative coordinate $\xi \equiv x - q$. The noise sources in these units take on the form

$$\langle \bar{F}_i(\bar{t}) \rangle_{\text{eq}} = 0, \quad \langle \bar{F}_i(\bar{t}) \bar{F}_j(\bar{t}') \rangle_{\text{eq}} = \delta_{ij} 2\bar{\gamma}_i \delta(\bar{t} - \bar{t}'). \quad (3.62)$$

The trap stiffness κ in the simulations is given in units of $k_B T/d_0^2$, so that the length associated with the tracer's motion in the trap, $\sqrt{\langle x^2 \rangle_{\text{eq}}} = \sqrt{k_B T/\kappa}$ (or equivalently $\sqrt{\langle \bar{x}^2 \rangle_{\text{eq}}} = 1/\sqrt{\bar{\kappa}}$ in rescaled units), is compared to the length scale d_0 that appears in the interaction potential. In the following, we set $\bar{\gamma}_b = 10$ to consider a massive bath particle, and vary the value of $\bar{\kappa}$ in the given rescaled units.

In order to compute the free diffusion coefficient and the memory kernel from simulated trajectories and to compare them to the experimental results in the previous section, we deploy a stochastic Runge-Kutta method of weak convergence order three [99]. Note that a high-convergence-order algorithm in combination with sufficient

statistics is essential for our analysis, as will be demonstrated in the subsequent section.

3.4.2 Harmonic coupling

The simplest choice of possible interaction between the tracer particle and the bath particle is a harmonic coupling, $V_{\text{int}}(\xi) = \frac{1}{2}\kappa_l\xi^2$, i.e. the interaction force on the tracer particle in Eq. (3.44) and (3.60), respectively, reads

$$F_{\text{int}}(\xi) = -\kappa_l\xi \quad \iff \quad \bar{F}_{\text{int}}(\bar{\xi}) = -\bar{\xi}. \quad (3.63)$$

Note that spatial variables are naturally rescaled by

$$d_0 = \sqrt{\frac{k_B T}{\kappa_l}}, \quad (3.64)$$

the length scale associated with the long-time limit of the root mean squared displacement of the relative coordinate ξ . The case of linear coupling can be treated analytically [12, 75, 100]. By explicitly integrating out the bath degree of freedom, one obtains the following linear non-Markovian Langevin equation for the tracer particle

$$\int_{-\infty}^t ds \Gamma(t-s)\dot{x}(s) = -\kappa_l x(t) + \tilde{F}(t). \quad (3.65)$$

The memory kernel and noise depend on the properties of the bath particle and take on the form

$$\Gamma(t) = 2\gamma\delta(t) + \kappa_l e^{-\frac{\kappa_l}{\gamma_b}t}, \quad (3.66)$$

$$\tilde{F}(t) = F(t) + \frac{\kappa_l}{\gamma_b} \int_{-\infty}^t ds e^{-\frac{\kappa_l}{\gamma_b}(t-s)} F_b(s). \quad (3.67)$$

The effective noise \tilde{F} is a linear combination of Gaussian random variables and as a consequence is a Gaussian random variable itself. It is easy to verify that its first and second moment is given by

$$\langle \tilde{F}(t) \rangle_{\text{eq}} = 0, \quad \langle \tilde{F}(t)\tilde{F}(t') \rangle_{\text{eq}} = k_B T \Gamma(|t-t'|). \quad (3.68)$$

Note that this result can be generalized to a heat bath of N harmonic oscillators that are bilinearly coupled to the tracer particle and where the coupling constant might differ for different particles [12, 75]. In this way, many interaction time scales enter the effective description of the tracer particle. As was expected from the analysis in Sec. 3.2 and literature [12, 75, 100], the memory kernel $\Gamma(t)$ in Eq. (3.66) depends only in a trivial way on γ and on bath properties, i.e., γ_b and the interaction strength κ_l .

The equation of motion (3.65) can be solved most easily in Fourier or Laplace space. By application of the convolution theorem, we find

$$\tilde{x}(\omega) = \frac{\tilde{f}(\omega)}{i\omega\tilde{\Gamma}_+(\omega) + \kappa}, \quad (3.69)$$

with Fourier transform $\tilde{h}(\omega) = \int_{-\infty}^{\infty} dt e^{-i\omega t} h(t)$, and where we defined $\Gamma_+(t) \equiv \Gamma(t)\theta(t)$ with $\theta(t)$ the Heaviside step function². By means of the Wiener-Khintchine theorem [38], we find for the spectral density of the position correlation function

$$\langle |x(\omega)|^2 \rangle = \frac{2k_B T \operatorname{Re}[\tilde{\Gamma}_+(\omega)]}{|i\omega\tilde{\Gamma}_+(\omega) + \kappa|^2}. \quad (3.70)$$

Computation of the inverse Fourier transform, $h(t) = \frac{1}{2\pi} \int_{-\infty}^{\infty} \tilde{h}(\omega)$, of the spectral density in Eq. (3.70) yields the equilibrium time correlation function $C_{xx}(t)$, and we find

$$C_{xx}(t) = \frac{k_B T}{\kappa} e^{-\frac{t}{\tau}} \left(\cosh(\omega_0 t) + \left(\frac{1}{\tau} - \frac{\kappa}{\gamma} \right) \frac{\sinh(\omega_0 t)}{\omega_0} \right) \quad t \geq 0. \quad (3.71)$$

In this equation, we defined the time scale τ and frequency ω_0 which depend on the properties of tracer and bath particle according to

$$\tau = \frac{2\gamma\gamma_b}{\gamma\kappa_l + \gamma_b(\kappa + \kappa_l)}, \quad \omega_0 = \sqrt{\frac{1}{\tau^2} - \frac{\kappa\kappa_l}{\gamma\gamma_b}} > 0. \quad (3.72)$$

We may rewrite the hyperbolic functions in Eq. (3.71) in terms of exponentials to find

$$C_{xx}(t) = \frac{k_B T}{\kappa} \left(\lambda_1 e^{-\frac{t}{\tau_1}} + \lambda_2 e^{-\frac{t}{\tau_2}} \right), \quad t \geq 0. \quad (3.73)$$

The correlation function is given in terms of a double exponential decay with relaxation times

$$\tau_{1/2} = \left(\frac{1}{\tau} \pm \omega_0 \right)^{-1} \quad (3.74)$$

and amplitudes

$$\lambda_1(\omega_0) = \frac{\kappa\tau - \gamma(1 - \omega_0\tau)}{2\gamma\omega_0\tau}, \quad \lambda_2(\omega_0) = \lambda_1(-\omega_0), \quad \lambda_1 + \lambda_2 = 1. \quad (3.75)$$

Note that the equal time correlation function in Eq. (3.73) reproduces the equipartition theorem, $C_{xx}(0) = \langle x^2 \rangle_{\text{eq}} = \frac{k_B T}{\kappa}$, and the position of the tracer particle becomes uncorrelated for large times, $\lim_{t \rightarrow \infty} C_{xx}(t) = 0$. In the limit of large κ , the correla-

²We use here the half-maximum convention of the Heaviside theta function [101], i.e. $\theta(0) \equiv 1/2$.

tion function reduces to

$$C_{xx}(t) \stackrel{\kappa \gg 1}{\cong} \frac{k_B T}{\kappa} \left(e^{-t/\tau_1} + \frac{\kappa_l}{\kappa} e^{-t/\tau_2} \right). \quad (3.76)$$

We observe a decoupling of time scales, $\tau_1 = \gamma/\kappa$ of the tracer motion in the trap, and, $\tau_2 = \gamma_b/\kappa_l$ of the bath particle motion in the interaction potential. Moreover, the amplitude factors are well separated in terms of magnitude, with the second prefactor $\kappa_l/\kappa \ll 1$ in the limit of large κ .

With the analytical results in Eq. (3.66) and (3.71) at hand we can test the quality of numerical simulations, applied to Eq. (3.60). The generalized Langevin equation (3.65) can be rewritten in terms of the rescaled units introduced earlier in Eqs. (3.59) and (3.61). We find

$$\int_{-\infty}^{\bar{t}} ds \bar{\Gamma}(\bar{t} - \bar{s}) \dot{\bar{x}}(\bar{s}) = -\bar{\kappa} \bar{x}(\bar{t}) + \bar{F}(\bar{t}), \quad (3.77)$$

where we defined the rescaled memory kernel $\bar{\Gamma}(\bar{t}) = \frac{\Gamma(t)}{\frac{k_B T}{d_0^2}}$. Note that Γ is rescaled in the same units as the trap stiffness κ . We aim to plot the Laplace-transformed memory kernel $\hat{\Gamma}(s) = \int_0^\infty dt e^{-st} \Gamma(t)$. In dimensionless units, this quantity needs to be rescaled according to $\bar{\Gamma}(\bar{s}) = \frac{\hat{\Gamma}(s)}{\gamma}$, where the frequency parameter s scales in an inverse manner compared to the time variable, i.e. $\bar{s} = s\tau_B$.

The simulations are used to create particle trajectories $x(t)$ from which the correlation function $C_{xx}(t) = \langle x(t)x(0) \rangle_{\text{eq}}$ is computed. By numerically evaluating its Laplace transforms and by using the relation found in Eq. (3.57), we obtain the simulated memory kernel $\hat{\Gamma}(s)$ in Laplace space. $\hat{\Gamma}(s)$ needs to be compared to the analytical result which is found from the representation in time domain in Eq. (3.66),

$$\hat{\Gamma}(s) = \gamma + \frac{\kappa_l}{s + \frac{\kappa_l}{\gamma_b}}. \quad (3.78)$$

In the limit of large s (small times) the particle diffuses freely, while for small s (large times) the two particles have the same mean velocities due to the bounded potential. This circumstance is reflected in the two limits,

$$\hat{\Gamma}(s=0) = \gamma + \gamma_b, \quad \lim_{s \rightarrow \infty} \hat{\Gamma}(s) = \gamma. \quad (3.79)$$

In Fig. 3.7, we show the results for the harmonic coupling for different values of κ . The simulated data points for $\hat{\Gamma}(s)$ (main graph) and $C_{xx}(t)$ (inset) follow well the analytical forms (solid lines). As expected, $\hat{\Gamma}(s)$ exhibits no dependence on the trap stiffness κ and the simulated curves take identical forms for values of κ spanning five orders of magnitude. The correlation function $C_{xx}(t)$, however, shown in the inset of Fig. 3.7 exhibits a strong dependence on κ which was expected from Eq. (3.73). Note that the extraction of $\hat{\Gamma}(s)$ requires high numerical accuracy of the correlation

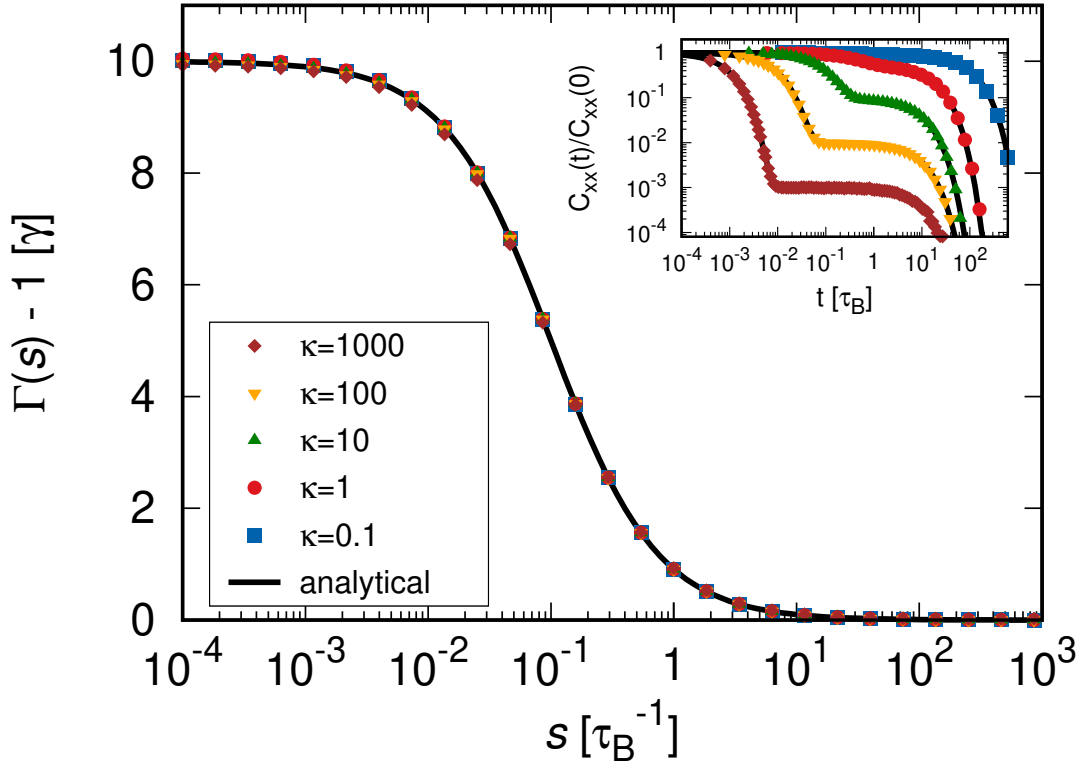


Figure 3.7: Main graph: Memory kernel $\hat{\Gamma}(s) - 1$ for harmonic coupling in units of tracer friction γ , in Laplace space, as obtained in numerical simulations, for different values of κ . The black line represents the analytical solution given in Eq. (3.78). The trap stiffness κ is given in units of $k_B T / d_0^2$ and the friction coefficient of the bath particle has been fixed to $\gamma_b = 10\gamma$. Inset: Simulated correlation function $\langle x(t)x(0) \rangle_{\text{eq}}$ plotted against the analytical solution Eq. (3.71). Reprinted and adapted from Ref. [5].

function, as may be illustrated by considering the case of $\kappa = 10^3$: In the limit of large κ both the time scales and amplitudes of the double exponential decay in the correlation function are well separated (cf. Eq. (3.76)), and a transient plateau is emerging. Even though the value of this plateau is very small ($\sim 10^{-3}$ for $\kappa = 10^3$) and can easily be overlooked, it is essential to obtain the correct value of $\hat{C}_{xx}(s)$ as $s \rightarrow 0$.

3.4.3 Double-well interaction potential

After this first numerical test of the principal analysis in the previous section, which allowed direct comparison to analytical results, we want to go one step further and consider a nonlinear interaction potential. A natural extension of the harmonic

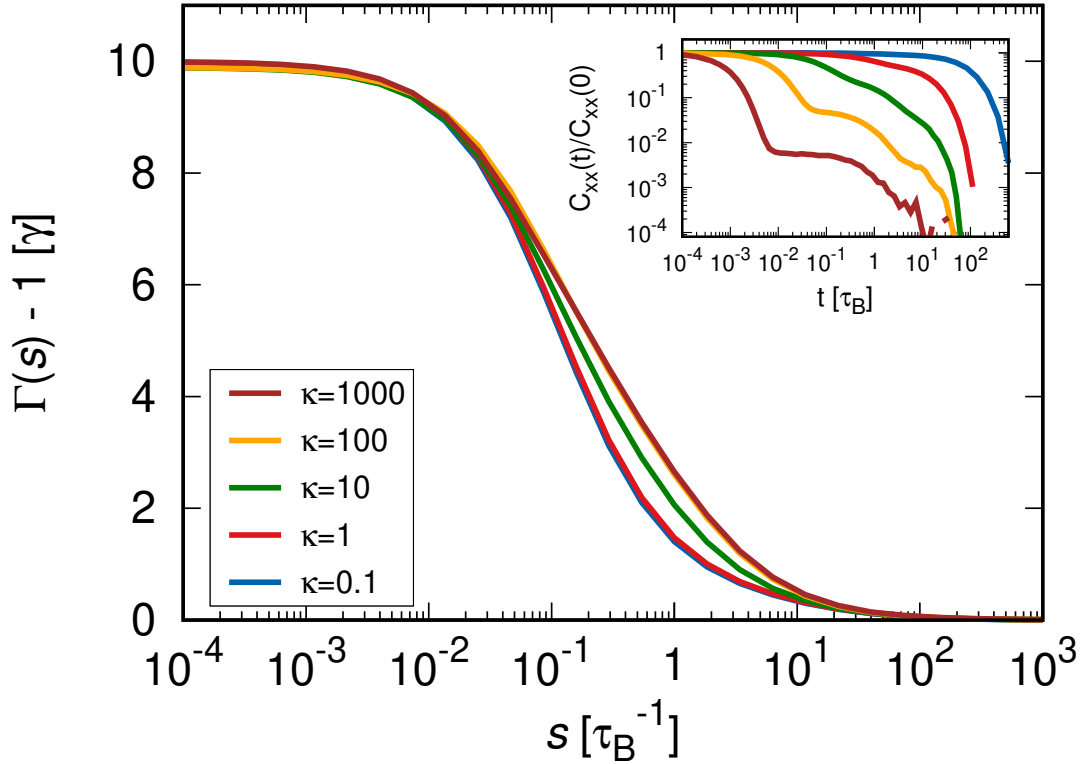


Figure 3.8: Main graph: Memory kernel $\hat{\Gamma}(s) - 1$ for a double-well coupling in units of tracer friction γ , in Laplace space, as obtained in numerical simulations, for different values of κ . The trap stiffness κ is given in units of $k_B T/d_0^2$, the barrier height is set to $V_0 = k_B T$, and the friction coefficient of the bath particle has been fixed to $\gamma_b = 10\gamma$. Inset: Simulated correlation function $\langle x(t)x(0) \rangle_{\text{eq}}$. Reprinted and adapted from Ref. [5].

potential is a symmetric double-well potential of the form

$$V_{\text{int}}(\xi) = \frac{V_0}{d_0^4} (\xi - d_0)^2 (\xi + d_0)^2. \quad (3.80)$$

In this potential, V_0 is the height of the potential barrier between the wells, and d_0 is half the distance between their minima. Its counterpart in two dimensions, the so-called Mexican hat potential, is of significance in field-theory to illustrate of what has become known as spontaneous-symmetry breaking [102]. Note that for a single particle moving in a double-well potential interesting barrier-crossing kinetics were found for a one-dimensional Langevin equation with bi-exponential memory only recently [103]. From the interaction potential we find the corresponding force by taking its derivative

$$F_{\text{int}}(\xi) = \frac{4V_0(d_0^2 - \xi^2)\xi}{d_0^4} \iff \bar{F}_{\text{int}}(\bar{\xi}) = 4\bar{V}_0(1 - \bar{x}^2)\bar{x}. \quad (3.81)$$

In rescaled units the barrier height $\bar{V}_0 = \frac{V_0}{k_B T}$ is given in units of thermal energy $k_B T$. By performing the same numerical analysis as in the previous section, we find the results illustrated in Fig. 3.8. In contrast to the case of harmonic coupling, the memory kernel $\hat{\Gamma}(s)$ is now dependent on the external trap stiffness for finite values of s . However, for small and large values of s , $\hat{\Gamma}(s)$ takes still the same limiting values as for the harmonic coupling, shown in Fig. 3.7. This behaviour is somewhat expected since for large s , the colloid, as before, does not notice the presence of the bath. In the reverse limit of small s , the two particles behave again as a composite particle, with the sum of bare friction coefficients. As will be discussed in Chapter 4, this value equals the microrheological friction coefficient measured in a linear response experiment where due to the bounded potential both particles move at the same velocity in the stationary state. In the intermediate regime of finite s values the relative coordinate ξ may cross the barrier and the time scale linked to its mean first-passage time comes into play. On this time scale, the nonlinearity of the potential affects the tracer's motion in the trap and we indeed observe the fluctuation renormalization as predicted in Eq. (3.48).

3.4.4 Stochastic Prandtl-Tomlinson model

We now look for a model where the fluctuation renormalization in the memory kernel is also visible for $s = 0$. Such a model is particularly important to correctly describe the experimental curves of the wormlike micellar bath presented in Fig. 3.5. As implied by the observations in the previous section, we need a model where colloid and bath particle are not bound. This brings us to the so-called Prandtl-Tomlinson (PT) model. The PT model is popular in the field of frictional processes on the atomic scale and was introduced by Prandtl to describe plastic deformations in crystals as well as dry friction [104]. Prandtl considered the situation of a point mass in a periodic potential that is damped by a frictional force and harmonically coupled to a host solid. The theoretical framework derived by Prandtl has been extensively deployed and modified to be applicable to a wide range of physical applications [105]. Most prominently, it well describes the damped motion of a nanotip of an atomic force microscope driven over a (corrugated) surface [106–108].

We thus use a sinusoidal interaction potential of the PT model-like form,

$$V_{\text{int}}(\xi) = V_0 \cos\left(\frac{2\pi}{d_0}\xi\right), \quad (3.82)$$

with a wavelength d_0 and amplitude V_0 . The interaction force used in Eq. (3.44) and (3.60), respectively, then reads

$$F_{\text{int}}(\xi) = V_0 \frac{2\pi}{d_0} \sin\left(\frac{2\pi}{d_0}\xi\right) \iff \bar{F}_{\text{int}}(\bar{\xi}) = 2\pi \bar{V}_0 \sin(2\pi\bar{\xi}), \quad (3.83)$$

where again the rescaled amplitude $\bar{V}_0 = \frac{V_0}{k_B T}$ is given in units of thermal energy

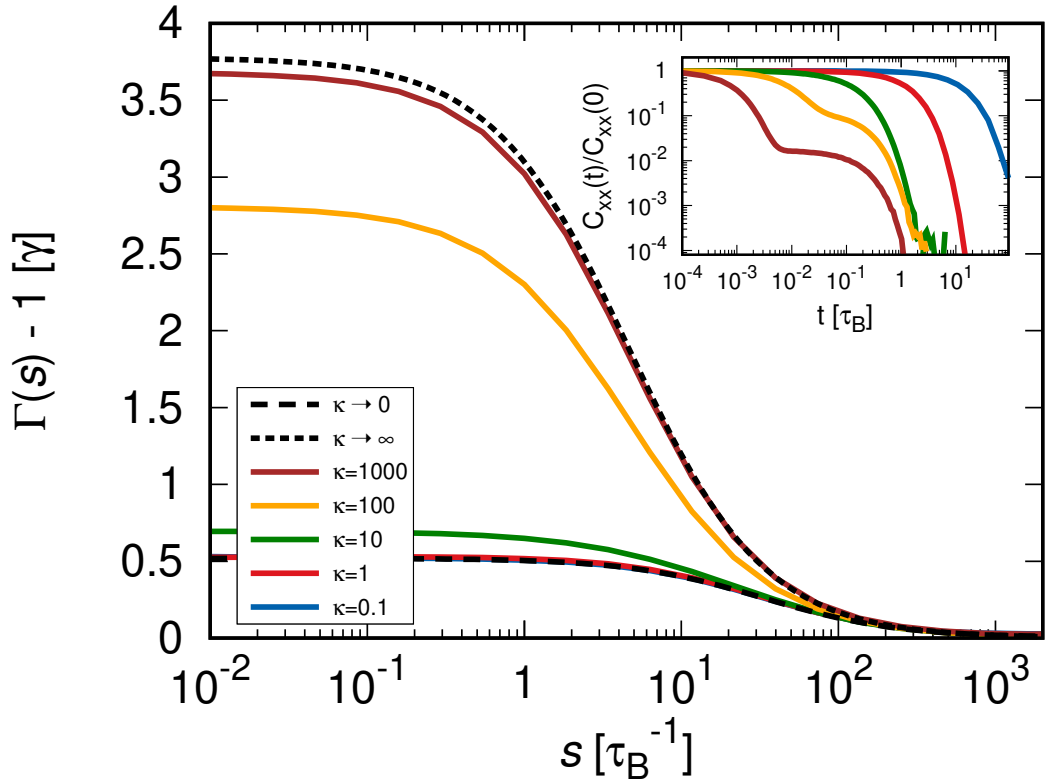


Figure 3.9: Main graph: Memory kernel $\hat{\Gamma}(s) - 1$ for stochastic Prandtl-Tomlinson model in units of tracer friction γ , in Laplace space, as obtained in numerical simulations, for different values of κ . The trap stiffness κ is given in units of $k_B T/d_0^2$, the barrier height is set to $V_0 = k_B T$, and the friction coefficient of the bath particle has been fixed to $\gamma_b = 10\gamma$. Inset: Simulated correlation function $\langle x(t)x(0) \rangle_{\text{eq}}$. The limiting curves for $\kappa \rightarrow 0$ and $\kappa \rightarrow \infty$ shown in the main graph will be discussed in Secs. 4.2 and 4.3. Reprinted and adapted from Ref. [5].

and is set to unity in the simulations. The model employed in this section is an extension of the original PT model: Here, the *interaction potential* of Brownian particles is mimicked by a sinusoidal potential. As a consequence, the potential is not fixed in space, but describes the interaction with a bath particle, which by itself is stochastic with finite friction and diffusion coefficients (given through γ_b). By taking into account that in the experimental system the micellar bath is indeed a non-static background with a finite relaxation time, this appears to be a promising simple model system to reproduce the properties of the experiment.

Before we turn to a quantitative comparison with the experimental results, we first want to discuss the findings of the stochastic PT model on a qualitative level. Figure 3.9 shows the results obtained from the simulations of the stochastic PT values for different values of κ given in units of $k_B T/d_0^2$. In contrast to the previous two sections, we see a strong dependence of $\hat{\Gamma}(s)$ on κ , and, as the potential is unbound, also in the limit $s \rightarrow 0$. This observation becomes intuitively clear by imagining

a linear response experiment where the confined tracer particle is dragged by a small constant velocity v_0 : If we constrain the bath coordinate for a moment, the light tracer particle steadily overcomes the recurrent barrier height of the sinusoidal potential. On the other hand, if we constrain the tracer coordinate, the heavier bath particle spends much more time in one of the potential sinks. In effect, for the unbounded potential the relative coordinate ξ increases over time, and the two particles take on different velocities on average. The friction force experienced by the particle now depends on the ratio of length scales associated with particle motion in the trap and wave length d_0 of the interaction potential. In this way, κ anomalously couples to the fluctuations of the interaction force gradient (as observed in Sec. 3.2.2) and affects the friction force even in the stationary state (where tracer and bath particle are assigned different mean velocities).

Note that the significance of length scales is also reflected in the rescaled units. The effect of fluctuation renormalization on the friction force of the tracer particle may be easily controlled/tuned by one of the three different but equivalent routes (we assume the ratio of friction coefficients γ_b/γ and barrier height V_0 to be fixed):

- We increase/decrease the trap stiffness κ of the harmonic trap, while keeping the bath temperature T and the interaction potential length scale d_0 fixed.
- We decrease/increase the temperature T of the bath, while keeping the trap stiffness κ and the length scale d_0 fixed.
- We increase/decrease the length scale d_0 of the interaction potential, while keeping κ and T fixed.

In the given range of rescaled parameters, the value $\hat{\Gamma}(s=0)$ differs by more than a factor of three between very large and very small values of κ . Note that this ratio can of course be tuned by changing the value of $\bar{\gamma}_b$ or \bar{V}_0 .

So far, the discussion of the stochastic PT model was about the tracer particle in (harmonic) confinement. In Sec. 3.3, we started the experimental analysis by studying the free diffusion case. We found that the long-time diffusion coefficient becomes a function of wavevector k for a particle suspended in a nonlinear bath. The same numerical analysis is feasible with the stochastic PT model where we compute $D(k, t \rightarrow \infty)$ from simulated trajectories performed at $\kappa = 0$. Figure 3.10 shows the simulation result of the long-time diffusion coefficient. The graph resembles – on a qualitative level – very closely the experimental curve in Fig. 3.4. The free-diffusion coefficient decreases with increasing k , and approaches limiting values for both large and small k . In the experimental system we traced this observation back to a corresponding length scale of dominant nonlinear interaction set by the micellar bath. Here, it is related to the chosen value of d_0 and in rescaled units the decay becomes visible at $k \sim d_0^{-1}$.

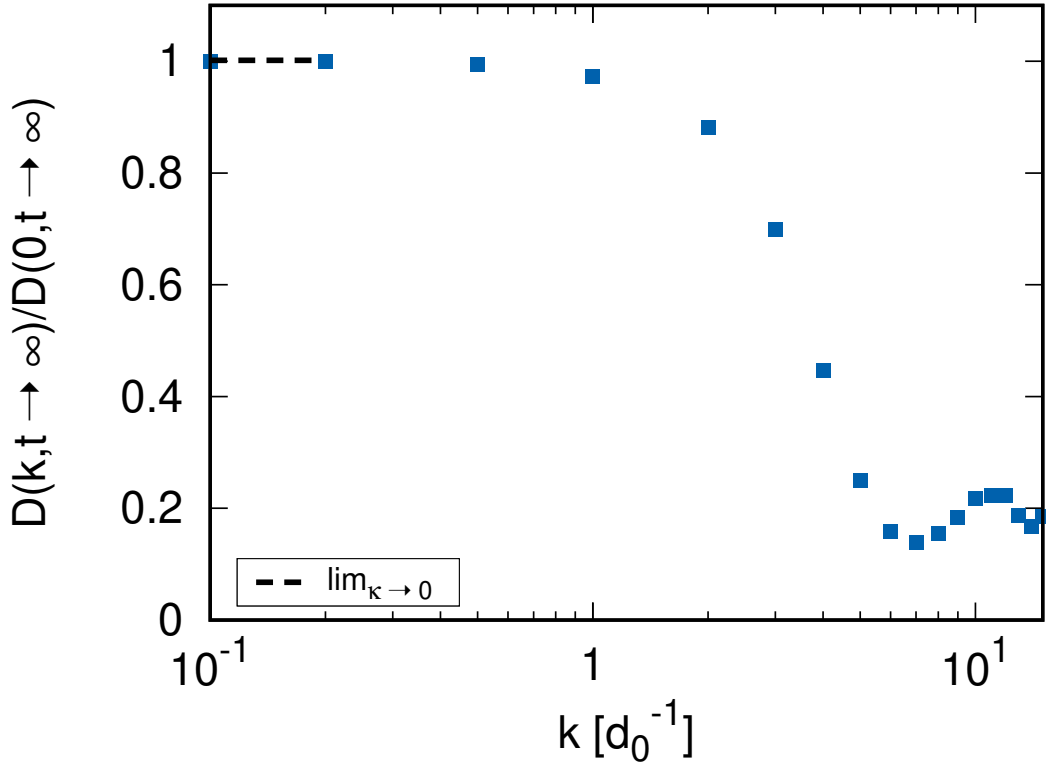


Figure 3.10: Normalized wavenumber-dependent long-time diffusion coefficient $D(k, t \rightarrow \infty)$ extracted from a free particle simulation of the stochastic PT model. The barrier height is set to $V_0 = k_B T$, and the friction coefficient of the bath particle has been fixed to $\gamma_b = 10\gamma$. Reprinted and adapted from Ref. [5].

3.5 Stochastic Prandtl-Tomlinson model and experiments

Encouraged by the qualitative agreement of the results of the stochastic Prandtl-Tomlinson model and the experimental micellar system in the previous section, we want to continue with a detailed and quantitative comparison between the simulation model and the experiment. We start with a comparison of the free diffusion coefficient and determine the model parameters in such fashion that we obtain best agreement with the experimental curve. The result of this mapping of the model on the experiment is presented in Fig. 3.11 and shows good agreement. The quantitative comparison of the SPT model with the experimental data can also be performed in the case of harmonic confinement. The comparison between model and experiment in terms of correlation function $\langle x(t)x(0) \rangle_{\text{eq}}$ and memory kernel $\hat{\Gamma}(s)$ is presented in Fig. 3.12 for three experimental trap stiffnesses κ . We restrict the simulation curves (black lines) to the range of experimentally accessible s values. The model parameters used in the creation of the simulated curves in Figs. 3.11 and 3.12 are provided in Table 3.1.

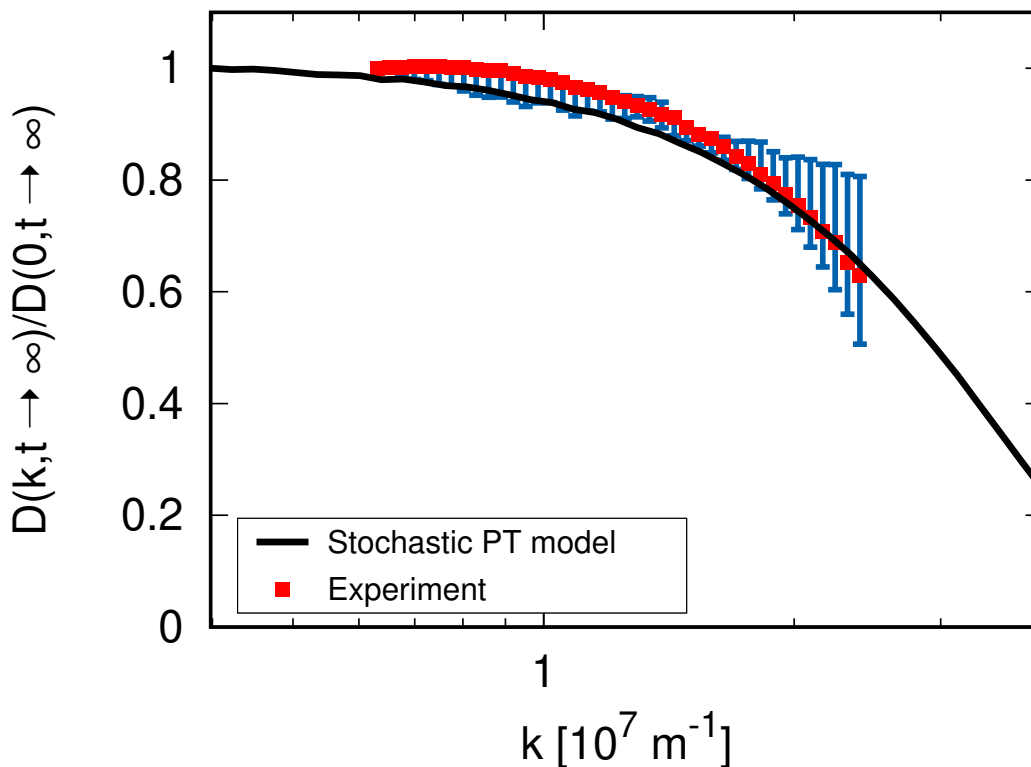


Figure 3.11: Normalized wavenumber-dependent long-time diffusion coefficient $D(k, t \rightarrow \infty)$ for a micellar bath as obtained from experiments, and in comparison to the simulated curve from the stochastic PT model. As in Fig. (3.4) above, bars indicate the statistical error estimated by partitioning the measured trajectory into two pieces. Provision and use of experimental raw data granted by Johannes Berner (Bechinger group, University of Konstanz). Reprinted from Ref. [5].

Ideally, one set of parameters of the SPT model should suffice to describe all experimental data shown in these figures. We have, however, allowed a slight variation of parameters to obtain optimal agreement by keeping in mind that the SPT is a very coarse representation of the micellar bath, which cannot reproduce its full dynamical complexity. On the other hand, possibilities for systematic errors in the experiment are taken into account by this freedom of parameters. We point out that optical traps as used in the experiment are usually optimized for trap stiffnesses that are smaller than the largest ones used here. Going beyond this regime may introduce (weak) effects like local heating, promotion of ageing effects, or a slight anharmonicity of trap shape. The latter is indeed reflected in the relative standard error for κ obtained from a parabolic fit of the experimentally measurement potential (see Fig. 3.3). It ranges from roughly 2% for the smallest value of κ to 5% for the largest one. We also note that the two-particle SPT model cannot correctly account for the prefactor $D(0, t \rightarrow \infty)$ used to normalize the data in Fig. 3.11. While this issue could potentially be fixed by adding more particles to the model (and thus more length scales), we cannot resolve it in the absence of more experimental data allow-

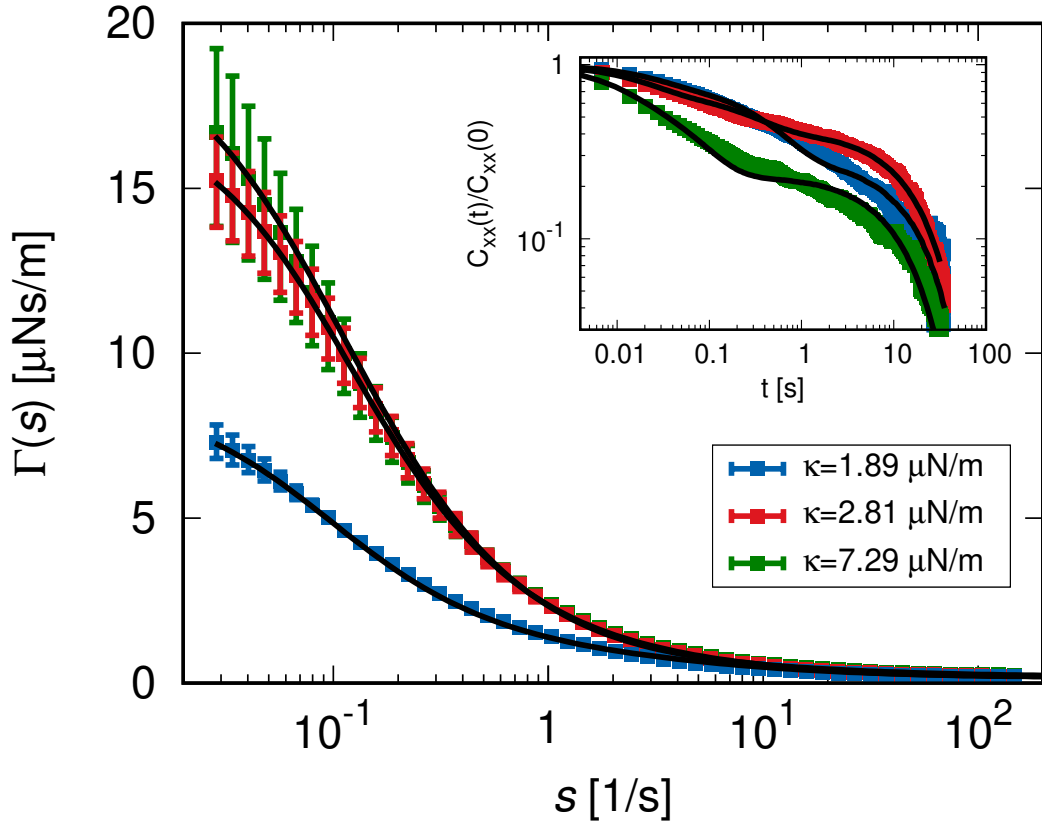


Figure 3.12: Main graph: Memory kernel $\hat{\Gamma}(s)$ of a micellar system, in Laplace space, as obtained from experimental data, for three values of κ . Error bars show the statistical error obtained from partitioning the measured trajectories into two pieces. Inset: Correlation function $\langle x(t)x(0) \rangle_{\text{eq}}$ from experimental data. In both main graph and inset, the solid black lines are obtained from the stochastic PT model, with parameters given in Table 3.1. Provision and use of experimental raw data granted by Johannes Berner (Bechinger group, University of Konstanz). Reprinted from Ref. [5].

ing a resolution of the diffusion coefficient for smaller wavenumbers k . We point out though that adding another distinct length scale does not affect the curves in Fig. 3.12 as it would only influence $\hat{\Gamma}(s)$ for values of s that are currently not resolvable experimentally. In view of these comments, the quantitative agreement between experimental data and the stochastic PT model is satisfactory and convincing.

The simulation parameters provided in Table 3.1 can be interpreted in terms of experimental scales of the micellar bath. The amplitude V_0 can be thought of as a potential barrier formed by micelles surrounding the tracer particle. It's value of the order of the thermal energy $k_B T$ appears to be reasonable. The length scale d_0 sets the dominant length scale of (nonlinear) interactions between tracer particle and bath. We find it to be on the order of a few hundred nanometers in great agreement with the typical sizes of micellar particles [84]. Finally, the relaxation time of the bath can be estimated from the value of γ_b and the curvature of V_{int} at

κ [$\mu\text{N}/\text{m}$]	V_0 [$k_B T$]	d_0 [nm]	γ [$\mu\text{Ns}/\text{m}$]	γ_b [$\mu\text{Ns}/\text{m}$]
0	2.1	98	0.16	148
1.89	1.9	210	0.18	66.7
2.81	2.11	210	0.168	68.2
7.29	1.4	120	0.189	148.3

Table 3.1: Parameters of the stochastic PT model used for the curves shown in Figs. 3.11 and 3.12.

its minimum. It is determined to be of the order of a few seconds for the values used in the simulations. This matches quite well the order of magnitude of the measured structural relaxation time measured in a recoil experiment [53]. In conclusion, the STP model is able to reproduce the experimental data, with physically plausible parameters.

4 Connection to microrheology and limiting cases

In conventional rheological measurements a macroscopic volume of a sample fluid is sheared between two solid surfaces of a given geometry. In principle, such a rheometer can be operated in two driving modes: constant shear stress and constant shear strain. On macroscopic length scales, however, these two modes yield the same result unless the correlation length of fluctuations becomes very large (e.g. near a critical point)¹. For small shear rates or in the regime of low Reynolds numbers the two solid surfaces moving at relative velocity v_0 induce a laminar or viscometric flow field in the fluid. A macrorheological measurement allows to deduce information on macroscopic length scales of the fluid under study such as viscous or elastic moduli of the bulk material. This is in contrast to microrheology where rheological properties of a fluid are probed by a small particle on the mesoscopic scale (typically a colloidal particle with diameter on the micron scale). In passive microrheology, rheological properties are tested by the fluctuating thermal motion of the colloid, while in active microrheology the probe particle is actively driven through the probe (e.g. in a constant velocity or constant force mode). On the length scale of the mesoscopic probe particle fluctuations are significant and no longer negligible. Since fluctuations differ depending on the mode of operation, measurable differences in response are found in different driving modes as was detailed pointed out in Ref. [60] for a model system of a colloidal probe particle in a suspension of hard spheres.

In this section, we want to establish ties between results from previous sections and the viscosity or friction coefficient obtained from microrheology [50, 55, 62, 109–113]. In contrast to the model system in Ref. [60] of colloidal hard spheres, we will perform this analysis on the level of a generalized Langevin equation without specifying the microscopic details of the bath (the impact of the bath is contained in the memory kernel $\Gamma(t)$ and noise of the effective dynamical description of the probe particle). In particular, we will study the limiting curves of $\hat{\Gamma}(s)$ for very large and very small values of κ which allows us to gain a better understanding of the limiting curves of $\hat{\Gamma}(s)$ in Fig. 3.9. The results of this chapter have partially already been presented in Ref. [5].

¹Fluctuations in shear rate at constant stress are expected to decay as $1/\sqrt{N}$ according to the central limit theorem and thus vanish in the thermodynamic limit.

4.1 Linear-response theory of a colloid in confinement

In a typical setting of (active) microrheology, a colloidal particle suspended in a complex fluid is confined by an external potential V_{ext} and the potential trap moves at a constant velocity v_0 . Due to the motion of the trap the Hamiltonian of the system becomes explicitly time dependent and in one dimension takes on the general form,

$$H(t) = H_0 + V_{\text{ext}}(x - v_0 t). \quad (4.1)$$

Here, we have separated the Hamiltonian into a part H_0 , that does not explicitly depend of time, and a time-dependent part induced by the moving potential $V_{\text{ext}}(x - v_0 t)$, which in the laboratory frame is a function of the difference $x - v_0 t$. In the following, we consider a small perturbation of the equilibrium state and expand the moving external potential to first order in dragging velocity v_0 . Furthermore, we switch on the perturbation at time $t = 0$. The Hamiltonian can then be written as

$$H(t) = H_{\text{eq}} + H_{\text{pert}}(t) = H_{\text{eq}} - V'_{\text{ext}}(x)v_0 t \theta(t) + \mathcal{O}(v_0^2), \quad (4.2)$$

where the time-independent part of V_{ext} was reabsorbed in the equilibrium Hamiltonian H_{eq} , and we introduced the perturbation Hamiltonian $H_{\text{pert}}(t)$. In the latter the ‘‘perturbation’’ $v_0 t \theta(t)$ couples to the phase space observable $V'_{\text{ext}}(x)$. We are interested in the change of mean force $\langle F_{\text{ext}} \rangle(t)$ exerted by the colloidal particle on the external potential (or vice versa) due to the perturbation of a moving potential. In the framework of linear-response theory, the fluctuation-dissipation theorem relates the response of a system to its equilibrium fluctuations [11]. Direct application of this fundamental theorem of statistical mechanics to the given Hamiltonian yields the relation

$$\langle F_{\text{ext}} \rangle(t) = \langle F_{\text{ext}}(x - v_0 t) \rangle_{\text{eq}} - \beta \int_0^t dt' \frac{d}{dt} \langle F_{\text{ext}}(t - t') F_{\text{ext}}(0) \rangle_{\text{eq}} v_0 t' + \mathcal{O}(v_0^2). \quad (4.3)$$

Note that in the equilibrium correlation function on the right-hand side the force of the static trap appears². We can get rid of the derivative by means of partial integration

$$\langle F_{\text{ext}} \rangle(t) = \langle F_{\text{ext}}(x - v_0 t) \rangle_{\text{eq}} + \beta \langle F_{\text{ext}}(x)^2 \rangle_{\text{eq}} v_0 t - \beta v_0 \int_0^t dt' \langle F_{\text{ext}}(t') F_{\text{ext}}(0) \rangle_{\text{eq}}. \quad (4.4)$$

²As a function of phase space variable x the force F_{ext} only implicitly depends on time. However, since the state x changes with time, so does F_{ext} .

In order to find the correct linear order in v_0 , we need to expand the equilibrium average $\langle F_{\text{ext}}(x - v_0 t) \rangle_{\text{eq}}$. By using

$$\langle F_{\text{ext}}(x - v_0 t) \rangle_{\text{eq}} = \underbrace{\langle F_{\text{ext}}(x) \rangle_{\text{eq}}}_{=0} - \langle F'_{\text{ext}}(x) \rangle_{\text{eq}} v_0 t + \mathcal{O}(v_0^2) \quad (4.5)$$

and realizing that $\langle F_{\text{ext}}(x)^2 \rangle_{\text{eq}} = \beta^{-1} \langle F'(x)_{\text{ext}} \rangle$, we finally find

$$\langle F_{\text{ext}} \rangle(t) = -\beta v_0 \int_0^t dt' \langle F_{\text{ext}}(t') F_{\text{ext}}(0) \rangle_{\text{eq}}. \quad (4.6)$$

The principle of action-reaction allows us to define the time-dependent friction coefficient by

$$\gamma(t) \equiv \frac{|\langle F_{\text{ext}} \rangle(t)|}{v_0} = \beta \int_0^t dt' \langle F_{\text{ext}}(t') F_{\text{ext}}(0) \rangle_{\text{eq}}. \quad (4.7)$$

We now want to consider the case of a harmonic potential,

$$V_{\text{ext}}(x - v_0 t) = \frac{1}{2} \kappa (x - v_0 t)^2. \quad (4.8)$$

Evaluation of Eq. (4.7) links the friction coefficient to the position correlation function of the colloid,

$$\gamma(t) = \frac{|\langle x \rangle(t) - v_0 t|}{v_0} = \beta \kappa^2 \int_0^t dt' \langle x(t') x(0) \rangle_{\text{eq}}. \quad (4.9)$$

In the long-time limit $t \rightarrow \infty$ the mean friction force becomes stationary and the integral on the right-hand side turns into the $s = 0$ value of $\hat{C}_{xx}(s)$. We aim to describe the effective particle dynamics by a linear generalized Langevin equation. By performing a small s expansion of $\hat{C}_{xx}(s)$ in Eq. (3.41)³,

$$\hat{C}_{xx}(s) \stackrel{s \ll 1}{\cong} \frac{\hat{\Gamma}(0)}{\beta \kappa^2} + \mathcal{O}(s), \quad (4.10)$$

we find a connection between the long-time friction coefficient of microrheology in linear response theory and the memory kernel defined in the generalized Langevin equation (3.39), given by

$$\gamma_{\text{lr}} \equiv \lim_{t \rightarrow \infty} \gamma(t) = \hat{\Gamma}(0) = \int_0^\infty dt' \Gamma(t'). \quad (4.11)$$

In the stationary state, the friction coefficient is simply given as the time integral of the memory kernel. The fluctuation renormalization of the memory kernel, i.e. dependence on parameters such as the colloidal mass or the trap stiffness κ , as discussed and analyzed in Sec. 3.2.2 and 3.2.3 thus translates to microrheological observations. Indeed, an effect of the stiffness κ on the measured microrheological

³Inclusion of the inertial force $m\ddot{x}$ does not change the result of the expansion

viscosity has been noticed before [60, 61, 67, 114].

4.2 The case of a very stiff trap $\kappa \rightarrow \infty$

The impact of the external trap on the particle's friction coefficient γ is naturally expected to become the stronger the stiffer the stiffness κ . In this section, we study the limiting case of a very stiff trap $\kappa \rightarrow \infty$. In principle, this limit is contained in Eq. (4.9) as the derived relation is valid for any non-zero value of stiffness κ . We want to link it to the memory kernel of the generalized Langevin equation in a way similar to Eq. (4.11). When being dragged through a complex fluid, the confined tracer particle can make excursions from the center of the trap to avoid collisions with bath particles which are limited by the restoring force of the trap (see left panel of Fig. 4.1). As the trap becomes stiffer, the restoring force on the particle increases and the amplitude of displacements attenuates. Ultimately, in the limit $\kappa \rightarrow \infty$, the particle is stuck in the potential minimum, unable to move as the restoring force is infinitely large. Consequently, the particle's velocity and acceleration in the generalized Langevin equation (3.24) can be set to zero when the trap is at rest. The particle still feels random kicks by the surrounding solvent particles which are almost immediately counterbalanced by the restoring external force. It is these random kicks in the large- κ limit that determine the particle position in the trap and we find

$$\lim_{\kappa \rightarrow \infty} \kappa^2 \langle x(t)x(0) \rangle_{\text{eq}} = \lim_{\kappa \rightarrow \infty} \langle f(t)f(0) \rangle_{\text{eq}}. \quad (4.12)$$

The non-Markovian fluctuation-dissipation theorem, $\langle f(t)f(0) \rangle_{\text{eq}} = \beta^{-1}\Gamma(|t|)$, relates the force fluctuations on the other hand to the memory kernel irrespective of the value of trap stiffness κ . By using this relation in Eq. (4.12), and via Eq. (4.9), we obtain in the limit $\kappa \rightarrow \infty$,

$$\lim_{\kappa \rightarrow \infty} \gamma(t) = \lim_{\kappa \rightarrow \infty} \int_0^t dt' \Gamma(t'). \quad (4.13)$$

Obviously, this equation is the extension of Eq. (4.11) for any t , valid for large κ . In Laplace space, we can solve for the memory kernel and find

$$\lim_{\kappa \rightarrow \infty} \hat{\Gamma}(s) = \lim_{\kappa \rightarrow \infty} s\hat{\gamma}(s). \quad (4.14)$$

The microrheological setup corresponding to the limit $\kappa \rightarrow \infty$ is the case where the colloidal particle is moving at constant velocity v_0 (fixed-velocity mode). The scenario is discussed in Ref. [60] for a hard-sphere suspension as sketched in the right panel of Fig. 4.1. The particle being confined in a very stiff trap and dragged at constant velocity through a complex bath cannot avoid collisions with bath particles by lateral displacements in the trap. This leads to an increase of the tracer particle's friction coefficient which in the description via a generalized Langevin equation is

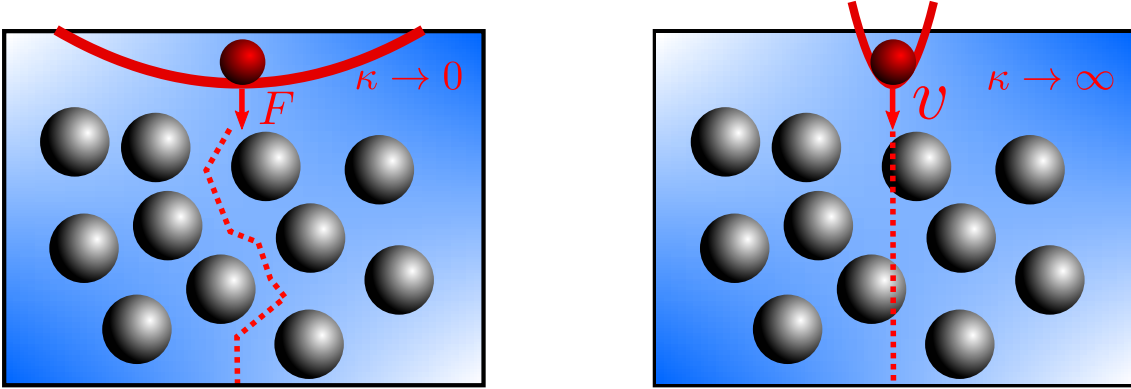


Figure 4.1: Illustration of limiting cases ($\kappa \rightarrow 0$ and $\kappa \rightarrow \infty$) of a particle being dragged through a complex fluid as amply discussed in Ref. [60]. In the left panel a tracer particle (red) confined by a weak harmonic potential can move laterally in the trap to make an excursion around the bath particles (fixed-force mode). In the right panel the tracer particle is strongly confined by the external potential and pushes all bath particles out of its way (fixed-velocity mode). We find simple relations for the memory kernel Γ of a generalized Langevin equation in terms of well-known linear response coefficients for these two modes.

reflected by a dependence of the memory kernel on the trap stiffness κ .

We may apply the previous discussion to our simple simulation model of two nonlinearly coupled Brownian particles introduced in Sec. 3.4. The external force instantaneously counterbalances two contributions in the limit $\kappa \rightarrow \infty$: The interaction force of the bath particle and the random force of solvent molecules. The force-force correlator acting on the tracer particle held at fixed position is given by

$$\lim_{\kappa \rightarrow \infty} \langle F_{\text{ext}}(t) F_{\text{ext}}(0) \rangle_{\text{eq}} = 2k_B T \gamma \delta(t) + \langle F_{\text{int}}(q(t)) F_{\text{int}}(q(0)) \rangle_{\text{eq}}, \quad (4.15)$$

By virtue of Eq. (4.6), we find the particle's friction coefficient

$$\lim_{\kappa \rightarrow \infty} \gamma(t) = \gamma + \beta \int_0^t dt' \langle F_{\text{int}}(q(t')) F_{\text{int}}(q(0)) \rangle_{\text{eq}}. \quad (4.16)$$

The position of the bath particle is governed by the equation of motion

$$\gamma_b \dot{q}(t) = -V'_{\text{int}}(q) + F_b(t). \quad (4.17)$$

For the stochastic PT model this limit is shown by the upper dashed line in Fig. 3.9.

4.3 The case of a very weak trap $\kappa \rightarrow 0$

In the reverse limit of vanishing trap stiffness, we perturb the particle by a small constant force F_0 . The system's Hamiltonian reads

$$H(t) = H_{\text{eq}} + H_{\text{pert}}(t) = H_{\text{eq}} - xF_0\theta(t) + \mathcal{O}(F_0^2), \quad (4.18)$$

where again the perturbation is switched on at $t = 0$ and the external perturbation couples to the tracer particle's position x . Application of the fluctuation-dissipation theorem yields the Einstein relation [11],

$$\mu(t) \equiv \frac{\langle v \rangle(t)}{F_0} = \frac{\beta}{2} \frac{d}{dt} \langle (x(t) - x(0))^2 \rangle_{\text{eq}}. \quad (4.19)$$

The time derivative of the mean-squared displacement can be expressed in terms of the time derivative of $C_{xx}(t)$, and in Laplace space we find

$$\hat{\mu}(s) = \frac{1}{s\hat{\Gamma}(s) + \kappa} = \frac{1}{s\hat{\Gamma}(s)} + \mathcal{O}(\kappa). \quad (4.20)$$

In the second step we expanded for small stiffnesses κ . Note that the two limits $s \rightarrow 0$ and $\kappa \rightarrow 0$ do not commute. This is a consequence of the fact that the probability distribution of the free particle is no longer normalizable in the limit of infinite time. We thus find [48, 115]

$$\lim_{\kappa \rightarrow 0} \hat{\Gamma}(s) = \lim_{\kappa \rightarrow 0} \frac{1}{s\hat{\mu}(s)}. \quad (4.21)$$

The memory kernel in the limit of vanishing trap stiffness κ is connected to the mobility μ of the particle in the absence of the trap. In the language of (active) microrheology this corresponds to a constant-force perturbation (fixed-force mode). In this limit, the particle may avoid collisions with bath particles as sketched in the left panel of Fig. 4.1. Note that equation (4.21) is a generalized form of the Stokes-Einstein-Sutherland relation in Eq. (1.1) [48]. The connection of $\hat{\mu}(s)$ to the diffusion coefficient may be established by rewriting the memory kernel in terms of the mean-squared displacement $\langle \Delta x^2(t) \rangle_{\text{eq}}$. On the Brownian time scale, i.e. we neglect inertial effects, one finds the relation [115]

$$\lim_{\kappa \rightarrow 0} \hat{\Gamma}(s) = \lim_{\kappa \rightarrow 0} \frac{2k_B T}{s^2 \langle \Delta \hat{x}^2(s) \rangle_{\text{eq}}} \quad (4.22)$$

in Laplace space. Introduction of the time-dependent diffusion coefficient as [11]

$$D(t) = \frac{1}{2} \frac{d}{dt} \langle \Delta x^2 \rangle_{\text{eq}} = \int_0^t dt' \langle v(t')v(0) \rangle_{\text{eq}}, \quad (4.23)$$

and conversion to Laplace domain together with Eq. (4.21) finally yields [48, 115]

$$\lim_{\kappa \rightarrow 0} \hat{\mu}(s) = \lim_{\kappa \rightarrow 0} \beta \hat{D}(s), \quad (4.24)$$

which is the most common form of the Stokes-Einstein-Sutherland relation generalized to the case of linear viscoelastic media.

The limiting curve $\lim_{\kappa \rightarrow 0} \hat{\Gamma}(s)$ for the model system of two nonlinearly coupled Brownian particles in Sec. 3.4 is found by measuring the diffusion process in the absence of external potential. We show it for the stochastic PT model in Fig. 3.9 as the lower dashed line.

In Sec. 3.3, we introduced a wavevector-dependent diffusion coefficient $D(k, t)$ to take into account the interactions of the tracer particle with surrounding Brownian particles. By comparison of Eqs. (3.54) and (4.23) we identify $D(t) = D(k = 0, t)$, and find in particular

$$D(0, t \rightarrow \infty) = \frac{1}{\beta \lim_{\kappa \rightarrow 0} \hat{\Gamma}(0)}. \quad (4.25)$$

In Fig. 3.4 we included the corresponding value of this relation as a dashed line computed from the limiting curve in Fig. 3.9. Note that no such relation has been obtained in the opposite limit for $k \rightarrow \infty$.

4.4 Stationary limit

The measurement of linear response coefficients, $\lim_{\kappa \rightarrow \infty} \gamma(t)$ and $\lim_{\kappa \rightarrow 0} \mu(t)$, provides information on the κ -dependence of the memory kernel $\Gamma(t)$ if the effective dynamics of the system is modeled by a linear generalized Langevin equation. In the long-time limit, the response coefficients become time independent, and approach constant values

$$\gamma_{\text{lr}} \equiv \lim_{t \rightarrow \infty} \gamma(t), \quad \mu_{\text{lr}} \equiv \lim_{t \rightarrow \infty} \mu(t). \quad (4.26)$$

In this limit, we obtain with Eq. (4.14) and (4.21)

$$\lim_{\kappa \rightarrow 0} \int_0^\infty dt' \Gamma(t') = \lim_{\kappa \rightarrow 0} \frac{1}{\mu_{\text{lr}}}, \quad (4.27)$$

$$\lim_{\kappa \rightarrow \infty} \int_0^\infty dt' \Gamma(t') = \lim_{\kappa \rightarrow \infty} \gamma_{\text{lr}}. \quad (4.28)$$

Since in the linear-response regime the memory kernel $\hat{\Gamma}(s)$ appears to increase in a monotonic way with increasing κ , we may conclude that a κ -dependence in $\hat{\Gamma}(0) = \int_0^\infty dt' \Gamma(t')$ only occurs if the linear response coefficients measured in the two modes

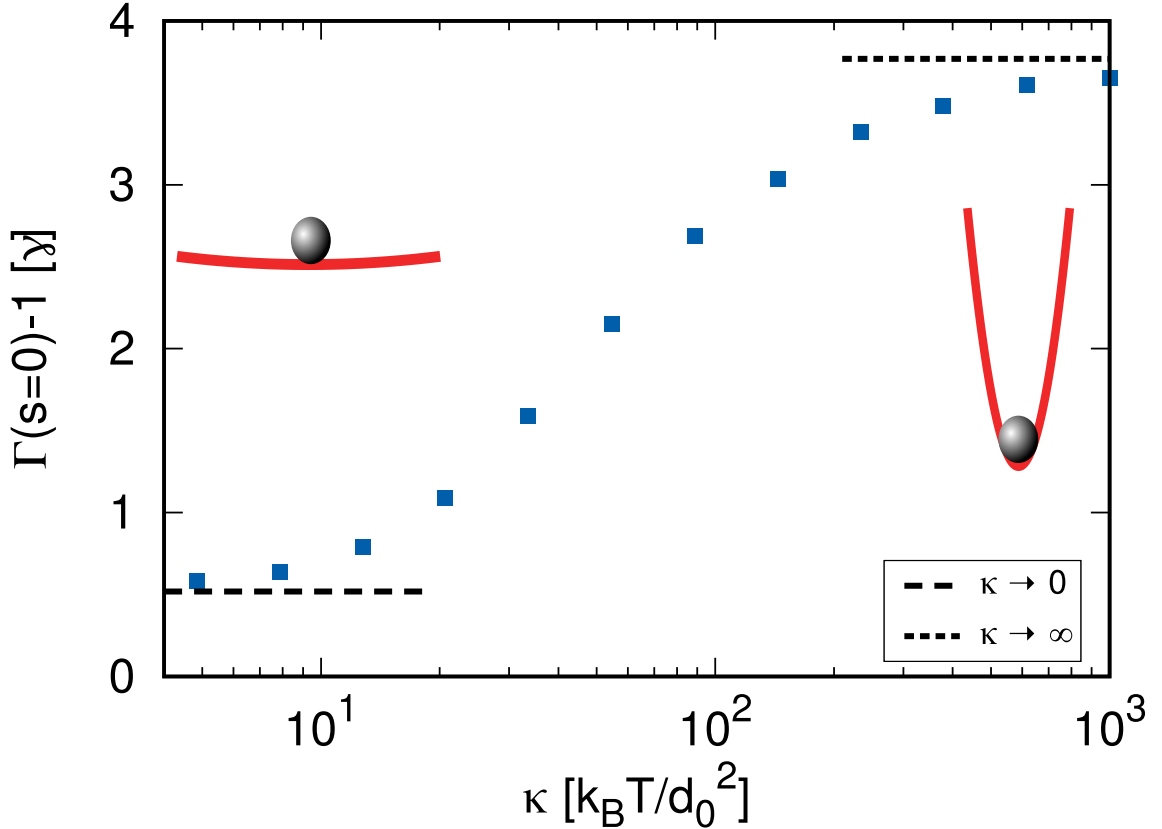


Figure 4.2: Long-time friction coefficient $\gamma_{\text{lr}} \equiv \lim_{t \rightarrow \infty} \gamma(t) = \hat{\Gamma}(0) = \int_0^\infty dt' \Gamma(t')$ of the particle in a slowly moving trap from the stochastic PT model. Dashed lines give the limiting cases $\kappa \rightarrow 0$ and $\kappa \rightarrow \infty$, respectively, corresponding to fixed-force and fixed-velocity mode as discussed in the text. Reprinted and adapted from Ref. [5].

of fixed-force and fixed-velocity differ, i.e. if $\lim_{\kappa \rightarrow 0} \frac{1}{\mu_{\text{lr}}} \neq \lim_{\kappa \rightarrow \infty} \gamma_{\text{lr}}$. Reversely, if the integrated memory kernel in the two limits shows a distinct result, then the two linear-response measurements of fixed-force and fixed-velocity in the stationary limit must be different. In particular for linearly coupled systems, no κ -dependence can occur in $\hat{\Gamma}(0)$ and for these kind of systems we have $\lim_{\kappa \rightarrow 0} \mu_{\text{lr}} = \lim_{\kappa \rightarrow \infty} \frac{1}{\gamma_{\text{lr}}}$ in the long-time limit, i.e. we cannot distinguish the fixed-forced mode from the fixed-velocity mode.

Figure 4.2 shows $\hat{\Gamma}(s = 0)$ as a function of stiffness κ , obtained in the stochastic Prandtl-Tomlinson model, including the two limiting cases for small and large κ . The curve asymptotically approaches the two limits of fixed-force and fixed-velocity, respectively, and in between shows a transient regime which is sometimes referred to as mixed-mode behaviour [60].

4.5 Nonlinear external potential

So far we have considered a harmonic external potential and obtained a fluctuation renormalization due to the nonlinear interaction between tracer particle and bath particles. In this section, we demonstrate that a related effect is caused by the presence of a nonlinear external potential. Again, we consider the one-dimensional case and expect the discussion to be qualitatively equivalent in higher dimensions. The system's Hamiltonian under study is given by [12]

$$H = \frac{p^2}{2m} + \frac{1}{2}ax^2 + \frac{1}{4}bx^4 + \sum_j \left\{ \frac{p_j^2}{2m_j} + \frac{1}{2}m_j\omega_j^2 \left(q_j - \frac{\gamma_j}{\omega_j^2}x \right)^2 \right\}. \quad (4.29)$$

Note that this Hamiltonian is of the Caldeira-Leggett type [75], assuming bilinear coupling between tracer particle and bath, but with a nonlinear external potential. The amplitude b gives the strength of the anharmonicity of the potential, γ_j is the coupling strength of the tracer particle to the j -th bath particle, the latter with eigenfrequency ω_j . Particle positions and momenta are denoted as before. Such a Hamiltonian has been considered by Zwanzig in Ref. [12] for the case $a = m = m_j = 1$. He derived the equations of motion in a perturbative manner to first order in b . We are not going to repeat the full derivation but provide the results for the case of arbitrary a , m , and m_j . In the same way as in Sec. 3.2.1 one can derive the equations of motion given in Eqs. (3.23) and (3.24). The effective spring constant $\kappa = k_B T / \langle x^2 \rangle_{\text{eq}}$ to first order in b is found to be

$$\kappa = a + \frac{3k_B T}{a}b + \mathcal{O}(b^2). \quad (4.30)$$

Similarly, for the noise we have

$$F(t) = \sum_j \gamma_j \left(p_j \frac{\sin(\omega_j t)}{\omega_j} + m_j \left(q_j - \frac{\gamma_j}{\omega_j^2}x \right) \cos(\omega_j t) \right) + b e^{t\mathcal{L}_0} \left(3 \frac{k_B T}{a} x - x^3 \right) + \mathcal{O}(b^2), \quad (4.31)$$

Note that \mathcal{L}_0 is the unperturbed Liouville operator, i.e. it depends on the Hamiltonian in Eq. (4.29) with $b = 0$. The memory kernel $\Gamma(t)$ can then be expressed via the fluctuation-dissipation theorem in Eq. (3.25) as

$$\Gamma(t) = \sum_j \frac{\gamma_j^2}{\omega_j^2} m_j \cos(\omega_j t) + \frac{b^2}{k_B T} \left\langle \left(3 \frac{k_B T}{a} x - x^3 \right) e^{t\mathcal{L}_0} \left(3 \frac{k_B T}{a} x - x^3 \right) \right\rangle_{\text{eq}} + \mathcal{O}(b^3). \quad (4.32)$$

We can simplify this representation of the memory kernel by realizing that for the leading order in b the correlation functions in the second term must be evaluated with respect to the unperturbed equilibrium probability distribution which is Gaussian. By using the property that the propagator $e^{t\mathcal{L}_0}$ can be distributed over products of functions and application of Wicks's theorem [38], we can use

$$\langle x(t)^3 x(0) \rangle_{\text{eq}} = 3 \langle x^2 \rangle_{\text{eq}} \langle x(t)x(0) \rangle_{\text{eq}} = \langle x(t)x(0)^3 \rangle_{\text{eq}}, \quad (4.33)$$

$$\langle (x(t)x(0))^3 \rangle_{\text{eq}} = 9\langle x^2 \rangle_{\text{eq}}^2 \langle x(t)x(0) \rangle_{\text{eq}} + 6\langle x(t)x(0) \rangle_{\text{eq}}^3. \quad (4.34)$$

Equation (4.32) thus reduces to

$$\Gamma(t) = \sum_j \frac{\gamma_j^2}{\omega_j^2} m_j \cos(\omega_j t) + \frac{6b^2}{k_B T} \langle x(t)x(0) \rangle_{\text{eq}}^3 + \mathcal{O}(b^3). \quad (4.35)$$

We need to compute the correlation function of the unperturbed system. It is most easily derived by solving the equation of motion (3.24) in Laplace space and we obtain

$$\hat{x}(s) = \frac{m(sx(0) + \dot{x}(0)) + \hat{\Gamma}(s)x(0) + \hat{F}(s)}{ms^2 + s\hat{\Gamma}(s) + a}. \quad (4.36)$$

The normalized correlation function in Laplace space yields

$$\frac{\langle \hat{x}(s)x(0) \rangle_{\text{eq}}}{\langle x^2 \rangle_{\text{eq}}} = \frac{ms + \hat{\Gamma}(s)}{ms^2 + s\hat{\Gamma}(s) + a}. \quad (4.37)$$

The memory kernel used in this equation is the one of the unperturbed problem ($b = 0$), i.e. with harmonic external potential. It is given by the limit $b \rightarrow 0$ in Eq. (4.35). So far we considered a discrete spectrum $\{\omega_j\}$ with coupling constants $\{\gamma_j\}$. In the thermodynamic limit the spectrum is continuous and we may replace discrete sums $\sum_j \rightarrow \int d\omega g(\omega)$, where $g(\omega)$ is a density of states, the coupling constants turn into a function of frequency $\gamma(\omega)$, and $m_j = \mu$ [12]. In the continuous case the memory kernel of the unperturbed problem becomes a Fourier integral,

$$\lim_{b \rightarrow 0} \Gamma(t) = \mu \int_0^\infty d\omega g(\omega) \frac{\gamma(\omega)^2}{\omega^2} \cos(\omega t). \quad (4.38)$$

Note that the memory kernel can take on various different forms depending on the choice of spectrum and coupling. If we assume, for example, that $g(\omega) \sim \omega^2$ is a quadratic function in frequency and $\gamma(\omega) = \gamma$, i.e. the coupling strength is independent of frequency, then $\lim_{b \rightarrow 0} \Gamma(t) \sim \delta(t)$ is proportional to the delta function. This describes the Markovian part of the memory kernel, while the correction term in Eq. (4.35) due to the nonlinearity in the Hamiltonian is non-Markovian. In the following, we consider this specific case and set $\lim_{b \rightarrow 0} \Gamma(t) = 2\gamma\delta(t)$. Computation of the inverse Laplace transform of Eq. (4.37) yields the familiar solution for the equilibrium correlator

$$C_{xx}(t) = \frac{k_B T}{a} \left(\lambda_1 e^{-\frac{t}{\tau_1}} + \lambda_2 e^{-\frac{t}{\tau_2}} \right), \quad t \geq 0. \quad (4.39)$$

The parameters of this solution now read

$$\tau_{1/2} = \left(\frac{1}{\tau} \pm \omega_0 \right)^{-1}, \quad \lambda_1(\omega_0) = \frac{a\tau - \gamma(1 - \omega_0\tau)}{2\gamma\omega_0\tau} - \frac{a}{2\gamma\omega_0}, \quad \lambda_2(\omega_0) = \lambda_1(-\omega_0), \quad (4.40)$$

where the amplitudes $\lambda_1 + \lambda_2 = 1$ sum again to unity and we used the abbreviations

$$\tau = \frac{2m}{\gamma}, \quad \omega_0 = \sqrt{\frac{1}{\tau^2} - \frac{a}{m}} = \frac{\sqrt{\gamma^2 - 4ma}}{2m}. \quad (4.41)$$

Depending on the value of the discriminant in ω_0 , the correlation function will either show exponentially decaying oscillatory behaviour ($\gamma^2 < 4ma$) or a purely exponential decay ($\gamma^2 > 4ma$). Note that in the overdamped limit the correlation function reduces to a single exponential decaying function

$$C_{xx}(t) \stackrel{\frac{m}{\gamma} \ll 1}{=} \frac{k_B T}{a} \exp\left(-\frac{t}{\gamma/a}\right), \quad (4.42)$$

where the relaxation time is set by the particle motion in the trap. We may now compute the time integral over the memory kernel in Eq. (4.35) up to quadratic order in b and find

$$\hat{\Gamma}(0) = \int_0^\infty dt \Gamma(t) = \left(1 + 2 \left(k_B T \frac{b}{a^2}\right)^2 \frac{5 \frac{ma}{\gamma^2} + 2}{\frac{ma}{\gamma^2} + 2}\right) \gamma + \mathcal{O}(b^3). \quad (4.43)$$

The correction term due to the anharmonicity in the potential exhibits a dependence on the mass m of the particle and on its bare friction coefficient γ . We regrouped the terms in Eq. (4.43) so that the two dimensionless parameter $k_B T \frac{b}{a^2} \ll 1$ and $\frac{ma}{\gamma^2}$ appear. Note that in the overdamped limit we have

$$\hat{\Gamma}(0) = \int_0^\infty dt \Gamma(t) \stackrel{\frac{m}{\gamma} \ll 1}{=} \left(1 + 2 \left(k_B T \frac{b}{a^2}\right)^2\right) \gamma + \mathcal{O}(b^3). \quad (4.44)$$

A related result may be derived in overdamped dynamics by application of projection operator techniques as outlined in Appendix A. It is important to point out, however, that in the case of a nonlinear external potential the time-integrated memory kernel is no longer connected to the microrheological friction coefficient. The relation we derived in Eq. (4.11) is exclusively valid for the case of a harmonic external potential. In general, the microrheological friction coefficient in linear-response theory is linked to the force-force correlator of the external potential as shown in Eq. (4.7).

For a single Brownian particle in overdamped dynamics it is easy to verify that the friction coefficient is always given by the bare friction coefficient of the particle irrespective of the shape of the external potential. The Hermitian conjugate of the one-particle Smoluchowski operator is given by

$$\Omega^\dagger = D(\partial_x + \beta F_{\text{ext}})\partial_x \quad (4.45)$$

with diffusion coefficient $D = (\beta\gamma)^{-1}$. The force-force correlator can be expressed

in terms of this operator as

$$\langle F_{\text{ext}}(0)F_{\text{ext}}(t) \rangle_{\text{eq}} = (D\beta)^{-2} \langle x\Omega^\dagger e^{\Omega^\dagger t} \Omega^\dagger x \rangle_{\text{eq}} = (D\beta)^{-2} \frac{d^2}{dt^2} \langle x e^{\Omega^\dagger t} x \rangle_{\text{eq}}. \quad (4.46)$$

We need to integrate the correlator over time and obtain

$$\int_0^\infty dt' \langle F_{\text{ext}}(0)F_{\text{ext}}(t') \rangle_{\text{eq}} = -(D\beta)^{-2} \langle x\Omega^\dagger x \rangle_{\text{eq}} = (D\beta^2)^{-1}. \quad (4.47)$$

Finally, by virtue of Eq. (4.7) we find

$$\gamma_{\text{lr}}^{\text{iso}} = \beta \int_0^\infty dt' \langle F_{\text{ext}}(0)F_{\text{ext}}(t') \rangle_{\text{eq}} = \gamma \quad (4.48)$$

in case of a single Brownian particle. For coupled Brownian particles the situation is more complex due to additional contributions to the friction coefficient via the interaction of bath particles. If we neglect indirect (hydrodynamic) interactions between the Brownian particles and only take into account direct interactions via an interaction potential $V_{\text{int}}(\{\xi_j\})$, we can rewrite the stationary limit of Eq. (4.7) according to

$$\gamma_{\text{lr}} = \gamma + \beta \int_0^\infty dt \langle F_{\text{int}}(0)F_{\text{int}}(t) \rangle_{\text{eq}}. \quad (4.49)$$

The additional contribution to the friction coefficient originates from the interaction force correlations acting upon the tracer particle. We note that for bath particles which are coupled to the tracer particle by a bounded potential (as e.g. considered in the Hamiltonian in Eq. (4.29)), we expect the additional term to yield the sum of their bare friction coefficients irrespective of the shape of the external potential. In this case, the bath particles move at the same velocity as the tracer particle in the stationary state if the latter is perturbed a small velocity.

5 Nonlinear Langevin equation

In the previous chapter, we observed that even in thermal equilibrium a nonlinear coupling of a colloidal particle to a complex bath leads to interesting effects in the effective probe dynamics of the probe. The fluctuation renormalization of linear coefficients due to a strong coupling between particle and bath also affected microrheological quantities such as the friction coefficient measured in a linear-response experiment where the probe particle is perturbed by a small velocity v_0 . In situations where the probe motion strongly perturbs the surrounding (complex) fluid, the linear description is expected not to be valid anymore. Under these circumstances the bath is driven far from equilibrium and the intrinsic nonlinear bath kinetics, i.e. the (nonlinear) dynamical behaviour of bath particles, will enter the effective dynamics of the probe particle.

In order to capture nonlinear effects in complex baths various theoretical techniques have been developed. They include, inter alia, density functional theory [116, 117], mode coupling theory [50, 58], or lattice models [118]. Another possible route to take into account nonlinear effects of the bath is provided by nonlinear response theory. A novel approach based on the level of real-space trajectories, i.e. incorporating path integral techniques, has been recently introduced [119] and applied to derive a Langevin description for probes in a nonlinear medium [54]. In Ref. [54] the authors use an expansion scheme around bath equilibrium and thereby derive a nonlinear Langevin equation to second order in probe displacement. The second-order term is significant only if either the probe is non-symmetric or if it is suspended in an anisotropic and/or inhomogeneous bath. In case of an isotropic and homogeneous system it must vanish due to symmetry considerations [54]. In this chapter, we present this novel approach of nonlinear-response theory and extend it to third-order in probe motion. To begin with, we first introduce the classical approach that is typically used in response theory.

5.1 Standard response formalism

In the standard scheme of nonlinear-response theory one starts from the evolution equation of the distribution function $P(t)$ which can be written as a linear operator

equation

$$\frac{\partial}{\partial t} P(t) = \Omega(t)P(t) \quad (5.1)$$

where $\Omega(t)$ e.g. denotes the Fokker-Planck operator. The perturbative part renders the operator explicitly time-dependent and the general solution to this equation is given by [120]

$$P(t) = e_+^{\int_{t_0}^t ds \Omega(s)} P(t_0). \quad (5.2)$$

In this relation “+” denotes a time-ordered exponential with earlier times standing on the right. Expansion of the time-ordered exponential yields the so-called Dyson series [121]

$$e_+^{\int_{t_0}^t ds \Omega(s)} = \sum_{n=0}^{\infty} U_n(t, t_0) = \frac{1}{n!} \int_{t_0}^t dt_1 \cdots \int_{t_0}^t dt_n \mathcal{T}\{\Omega(t_1) \cdots \Omega(t_n)\}, \quad (5.3)$$

where we introduced the time-ordering operator \mathcal{T} . The solution in Eq. (5.2) can be slightly rewritten so that the initial distribution $P(t_0)$ appears as a summand

$$P(t) = P(t_0) + \int_{t_0}^t dt' e_+^{\int_{t'}^t ds \Omega(s)} \Omega(t') P(t_0). \quad (5.4)$$

We now assume that the system is in equilibrium at some far time in the past, i.e. $P(t_0 \rightarrow -\infty) = P_{\text{eq}}$, so that

$$P(t) = P_{\text{eq}} + \int_{-\infty}^t dt' e_+^{\int_{t'}^t ds \Omega(s)} \Omega(t') P_{\text{eq}}. \quad (5.5)$$

The change of an arbitrary phase space observable B due to a time-dependent perturbation $\delta\Omega(t) = \Omega(t) - \Omega_e$ (with equilibrium operator Ω_e) may be expressed as

$$\langle B \rangle(t) - \langle B \rangle_{\text{eq}} = \int d\mathbf{X} \int_{-\infty}^t dt' (\delta\Omega(t') P_{\text{eq}}) e_-^{\int_{t'}^t ds \Omega^\dagger(s)} B. \quad (5.6)$$

Note that by repeated application of partial integration the Hermitian conjugate Ω^\dagger of the Fokker-Planck operator appeared and the time-ordering is reversed. We may introduce the response function $\chi(t, t') = \frac{\delta \langle B \rangle(t)}{\delta F(t')}$ by

$$\langle B \rangle(t) - \langle B \rangle_{\text{eq}} = \int_{-\infty}^t dt' \chi(t, t') F(t'). \quad (5.7)$$

In the following, we consider a perturbation by a potential force, $H_{\text{pert}}(t) = -AF(t)$, and one can show that for Fokker-Planck dynamics

$$\delta\Omega(t) P_{\text{eq}} = \beta C P_{\text{eq}} F(t). \quad (5.8)$$

Note that the defined phase space variable equals $C = -\Omega_e^\dagger A$. We may then express the response formula (5.6) in terms of an equilibrium correlation function

$$\langle B \rangle(t) - \langle B \rangle_{\text{eq}} = \beta \int_{-\infty}^t dt' \left\langle C \exp_- \left(\int_{t'}^t ds \Omega^\dagger(s) \right) B \right\rangle_{\text{eq}} F(t') \quad (5.9)$$

or the response function as

$$\chi(t, t') = \beta \left\langle C \exp_- \left(\int_{t'}^t ds \Omega^\dagger(s) \right) B \right\rangle_{\text{eq}}. \quad (5.10)$$

We can further simplify this representation by application of the so-called Dyson or Baker-Campbell-Hausdorff formula [8, 120]

$$U_-(t', t) = U_e(t - t') + \int_{t'}^t ds U_-(t', s) \delta\Omega^\dagger(s) U_e(t - s) \quad (5.11)$$

which can be proven directly by differentiation. Note that we used the abbreviations $U_-(t', t) = e^{\int_{t'}^t ds \Omega^\dagger(s)}$ and $U_e(t - t') = e^{\Omega_e^\dagger(t-t')}$ in the previous formula. The implicit equation may be iteratively substituted into Eq. (5.10) and for the perturbation via a conservative force field we find

$$k_B T \chi(t, t') = \langle CB(t-t') \rangle_{\text{eq}} + \int_{t'}^t ds \langle CU_e(s-t') \delta\Omega^\dagger(s) U_e(t-s) B \rangle_{\text{eq}} + \mathcal{O}(F^2). \quad (5.12)$$

Note that we truncated the series after the first nonlinear contribution which translates to a linear dependence on the force F in the response function. By neglecting this nonlinear contribution we recover the fluctuation-dissipation theorem. This theorem plays a preeminent role in statistical mechanics as it is universal with regard to the dynamics used in its derivation, i.e. it holds for any (equilibrium) system. This observation, however, is no longer true for the case of nonlinear response, where different types of dynamics (e.g. Liouville or Fokker-Planck dynamics) yield different results.

5.2 Path integral formalism

The novel approach of response formalism introduced in Ref. [119] is based on real-space trajectories rather than on specific bath dynamics. The path-integral formalism provides a unifying framework where the stochastic dynamics of the bath is implicitly contained in the trajectories of the tracer particle. It does not involve the Liouville equation or an expansion around the Fokker-Planck equation. In this section, we want to extend the response formalism to third order as derived in Ref. [119], a necessity to derive a nonlinear Langevin equation in probe displacement for an isotropic and homogeneous system. The expectation value of a path

observable $O = O(\omega)$ can be written as a path integral

$$\langle O(\omega) \rangle = \int \mathcal{D}\omega \mathcal{P}(\omega) O(\omega). \quad (5.13)$$

The integration over ω is meant to be over paths and $\mathcal{P}(\omega)$ is the weight function of each of the paths. We consider $\mathcal{P}(\omega)$ to be a perturbed dynamical ensemble that is linked to the equilibrium ensemble $\mathcal{P}_{\text{eq}}(\omega)$ via an action $\mathcal{A}_\varepsilon(\omega)$

$$\mathcal{P}(\omega) = e^{-\mathcal{A}_\varepsilon(\omega)} \mathcal{P}_{\text{eq}}(\omega) = e^{-\mathcal{A}_\varepsilon(\omega)} e^{-A_0(\omega)} P_{\text{eq}}(x_0). \quad (5.14)$$

At time $t = 0$ the system states are described by the Boltzmann distribution $P_{\text{eq}}(x_0)$ and the system is perturbed for $t > 0$. The time-dependent perturbation is present in the action \mathcal{A}_ε and is described by a small parameter $\varepsilon \ll 1$. It can be expanded into a Taylor series up to third order

$$\mathcal{A}_\varepsilon = \varepsilon \mathcal{A}'_0 + \frac{1}{2} \mathcal{A}''_0 \varepsilon^2 + \frac{1}{6} \mathcal{A}'''_0 \varepsilon^3 + \mathcal{O}(\varepsilon^4) \quad (5.15)$$

and vanishes in the limit $\varepsilon \rightarrow 0$. The analysis considerably simplifies if we consider a state observable $O(\omega) = O(x_t)$ which only depends on the state of the system at time t rather than on the whole path. It is useful to introduce the time-reversal operator θ which changes the temporal direction of a path $\omega = (x_s, 0 \leq s \leq t)$

$$(\theta\omega)_s = \pi x_{t-s}. \quad (5.16)$$

π is the kinematical time-reversal, e.g. it changes the sign of velocities. Applied to a state observable $O(x_t)$ we simply have $O(\theta\omega) = O(\pi x_0)$. The equilibrium distribution $\mathcal{P}_{\text{eq}}(\theta\omega) = \mathcal{P}_{\text{eq}}(\omega)$ must be invariant under time-reversal, and, by means of the Boltzmann distribution, the equilibrium average of a state observable fulfills $\langle O(\pi x_0) \rangle_{\text{eq}} = \langle O(x_0) \rangle_{\text{eq}} = \langle O(x_t) \rangle_{\text{eq}}$. Expansion of Eq. (5.13) for the case of a state variable with respect to ε yields

$$\begin{aligned} \langle O \rangle &= \langle O \rangle_{\text{eq}} - \varepsilon \langle \mathcal{A}'_0(\omega) O \rangle_{\text{eq}} - \frac{\varepsilon^2}{2} [\langle \mathcal{A}''_0(\omega) O \rangle_{\text{eq}} - \langle (\mathcal{A}'_0(\omega))^2 O \rangle_{\text{eq}}] \\ &\quad - \frac{\varepsilon^3}{6} [\langle \mathcal{A}'''_0(\omega) O \rangle_{\text{eq}} - 3 \langle \mathcal{A}'_0(\omega) \mathcal{A}''_0(\omega) O \rangle_{\text{eq}} + \langle (\mathcal{A}'_0(\omega))^3 O \rangle_{\text{eq}}] + \mathcal{O}(\varepsilon^4). \end{aligned} \quad (5.17)$$

Note that the right-hand side is expressed in terms of equilibrium expectations $\langle F(\omega) \rangle_{\text{eq}} = \int \mathcal{D}\omega \mathcal{P}_{\text{eq}}(\omega) F(\omega)$. Now we consider the time-reversed observable

$$\begin{aligned} \langle O\theta \rangle &= \langle O \rangle_{\text{eq}} - \varepsilon \langle \mathcal{A}'_0(\theta\omega) O \rangle_{\text{eq}} - \frac{\varepsilon^2}{2} [\langle \mathcal{A}''_0(\theta\omega) O \rangle_{\text{eq}} - \langle (\mathcal{A}'_0(\theta\omega))^2 O \rangle_{\text{eq}}] \\ &\quad - \frac{\varepsilon^3}{6} [\langle \mathcal{A}'''_0(\theta\omega) O \rangle_{\text{eq}} - 3 \langle \mathcal{A}'_0(\theta\omega) \mathcal{A}''_0(\theta\omega) O \rangle_{\text{eq}} + \langle (\mathcal{A}'_0(\theta\omega))^3 O \rangle_{\text{eq}}] + \mathcal{O}(\varepsilon^4). \end{aligned} \quad (5.18)$$

It is useful to decompose the action \mathcal{A}_ε into a time-symmetric part $D(\omega)$ and a time-antisymmetric part $S(\omega)$, i.e. $\mathcal{A}_\varepsilon = D - S/2$ with $D\theta = D$ and $S\theta = -S$. Note that these two parts are usually referred to as entropic and frenetic part in literature

[29, 122, 123]. If we consider the ratio of probabilities of forward and backward path, we find

$$\frac{P(\omega)}{P(\theta\omega)} = e^{S(\omega)}. \quad (5.19)$$

For stochastic microscopic reversible dynamics (e.g. (Markovian) Langevin dynamics [124]) Crooks' fluctuation theorem relates this ratio to the entropy production or dissipation of the nonequilibrium system [43] and is thus reasonably called the entropic part of the action. In a thermodynamical interpretation it is linked to the irreversibility of a dissipative nonequilibrium system as its entropy is increasing. Various theoretical relations, commonly known as fluctuation relations, have been derived to extend the notions of classical thermodynamics and to take into account the inherent stochasticity of systems on the mesoscopic scale [41, 42, 44–47]. The frenetic contribution D reflects the time-symmetric contribution that appears in the nonlinear response and is linked to a change of dynamical activity of the bath [29, 123] (recall that on a microscopical level of description Newton's equation of motion are inherently time-reversal symmetric). We provide a simple example of how to derive S and D for the case of overdamped Markovian diffusion in Appendix B. Subtracting Eq. (5.18) from Eq. (5.17) gives

$$\begin{aligned} \langle O(x_t) \rangle - \langle O(x_t) \rangle_{\text{eq}} &= \varepsilon \langle S'_0(\omega) O \rangle_{\text{eq}} - \frac{\varepsilon^2}{2} \langle [2D'_0(\omega)S'_0(\omega) - S''_0(\omega)] O \rangle_{\text{eq}} \\ &+ \frac{\varepsilon^3}{6} \left\langle \left[3 \left((D'_0(\omega))^2 - 3D''_0(\omega) \right) S'_0(\omega) + \frac{(S'_0(\omega))^3}{4} - 3D'_0(\omega)S''_0(\omega) + S'''_0(\omega) \right] O \right\rangle_{\text{eq}} \\ &+ \mathcal{O}(\varepsilon^4), \end{aligned} \quad (5.20)$$

where we used that for a state observable the nonequilibrium average of the time-reversed observable reduces to an equilibrium average $\langle O\theta \rangle = \langle O(x_t) \rangle_{\text{eq}}$. If we consider a perturbation via a potential force the Hamiltonian is linear in the perturbing field ε , and so is the entropy production S . We can thus neglect higher order derivatives of S and Eq. (5.20) simplifies to

$$\begin{aligned} \langle O(x_t) \rangle - \langle O(x_t) \rangle_{\text{eq}} &= \varepsilon \langle S'_0(\omega) O(x_t) \rangle_{\text{eq}} - \varepsilon^2 \langle D'_0(\omega) S'_0(\omega) O(x_t) \rangle_{\text{eq}} \\ &+ \frac{\varepsilon^3}{6} \left\langle \left[3 \left((D'_0(\omega))^2 - D''_0(\omega) \right) S'_0(\omega) + \frac{(S'_0(\omega))^3}{4} \right] O(x_t) \right\rangle_{\text{eq}} + \mathcal{O}(\varepsilon^4). \end{aligned} \quad (5.21)$$

This is the extension to third-order in the scheme developed in Ref. [119]. Note that to first order in the perturbation we recover the fluctuation-dissipation theorem, a purely entropic contribution. We note that if the frenetic component D is constant, i.e. it remains unchanged under a small perturbation, the third-order response will be nonzero (in contrast to the second-order response [119]). On the other hand, in case of $S'_0 = 0$ the response vanishes up to third order.

5.3 Derivation of nonlinear Langevin equation

The third-order response formula in Eq. (5.21) can be used to derive a nonlinear Langevin equation for the case of a Brownian probe particle suspended in a complex bath. The derivation is feasible because the response behaviour of the bath directly couples to the probe particle and essentially governs its dynamical evolution. In this section, we follow along the lines of Ref. [54] where the authors derived a nonlinear Langevin equation up to second order in probe displacement. We consider a small (colloidal) probe particle with time-dependent spatial position $x_t = (x_t(k), k = 1, 2, 3)$ in contact with the bulk phase of a complex bath. For convenience, we adopt the notation of Ref. [54] and abbreviate the degrees of freedom of the bath at time t as η_t . The level of description of the bath is not necessarily a microscopic one but can already be coarse grained to a mesoscopic scale. A clear separation in length scales between probe particle and bath constituents, however, is generally required so that a continuum description of the bath is applicable. The bath is assumed to be in thermal equilibrium if the probe is at rest. In order to isolate effects due to nonlinear bath dynamics, we neglect the influence of a nonlinear coupling between probe particle and bath on the nonlinear dynamical evolution equation of the probe. We thus assume the interaction potential between bath and probe to be $\partial_{x_k} U(x, \eta_t) = a_k(\eta_t)$, i.e. linear in probe position. The interaction potential U , induced by the probe motion, may be perceived as a time-dependent external potential acting upon the bath. The distortion of the complex bath via the probe motion leads to a back reaction of the bath on the probe particle and causes a friction force in response to its motion. Once again we aim to describe the probe dynamics in an effective manner where just like in the equilibrium case a systematic friction force and a random force/noise term appears. In classical mechanics, the equation of motion of the probe of mass M suspended in the complex bath is given by Newton's equation of motion

$$M\ddot{x}_t = F(x_t, \eta_t) + F_t^{\text{ext}}. \quad (5.22)$$

The interaction force $F(x_t, \eta_t) = -\nabla_x U(x_t, \eta_t)$ is the negative gradient of the interaction potential and F_t^{ext} is an external force which is of no significance for the method of the derivation.

In the following derivation, it is important to distinguish between averages $\langle \cdot \rangle_{x_t}$ and $\langle \cdot \rangle^{\omega^t}$. Both averages are meant with respect to bath variables η_t and are characterized by a dynamical ensemble specified on path space as defined in Eq. (5.13). The former one denotes the average over thermal equilibrium of the bath at fixed probe position x_t . The process that it describes is the one with a constant interaction potential $U(x_t, \eta)$ in time. Note that in a Newtonian liquid this average would suffice to specify any averaged path observable, as in such a fluid the time scales associated with the (slow) probe and the (fast) bath degrees of freedom are well separated. Consequently, even if the probe particle is strongly driven through a Newtonian fluid the bath variables relax so rapidly that on the time scale of the probe the bath always remains in equilibrium. This allows for a Markovian description and

the average $\langle \cdot \rangle_{x_t}$ does not know about previous probe positions (the bath has no memory). Under these circumstances the bath process η_t is reversible with inverse temperature $\beta = (k_B T)^{-1}$. For the probe at rest we may define the equilibrium free energy $\mathcal{F}(x)$. The mean force acting upon the probe in thermal equilibrium can then be expressed by $\langle F(x_t, \eta_t) \rangle_{x_t} = -\nabla_x \mathcal{F}(x_t)$. In a complex bath the situation is fundamentally different: Due to its own intricate microstructure the relaxation time of the bath can be comparable to the one associated with probe motion. This is taken into account in the (nonequilibrium) average $\langle \cdot \rangle^{\omega^t}$ which is over the time-dependent bath (snapshot) configuration of the η_t . In contrast to the equilibrium average it does not only depend on the current position x_t of the probe, but incorporates its whole trajectory $\omega^t = (x_s, s < t)$ under which the bath has evolved. This leads to memory effects in the forces as will be shown below.

We want to derive a nonlinear Langevin equation in the displacement of the probe particle. The perturbation of bath variables η_t induced by the probe motion is assumed to be small which allows to apply the nonlinear response formula in Eq. (5.21). A small displacement means that the position x_s at a time $s < t$ is close to x_t . By introducing the (largest) bath relaxation time τ_{bath} , we demand the work done by the probe on the bath within a single period of relaxation time, $(x_{t-\tau_{\text{bath}}} - x_t) \cdot \nabla_x U(x_t, \eta_t)$, to be small compared to the thermal energy β^{-1} . It is useful to rewrite Newton's equation of motion (5.22) in such a way that the response of the force due to the perturbed bath dynamics appears [54]

$$M\ddot{x}_t - F_t^{\text{ext}} = -\nabla_x \mathcal{F}(x_t) + \left[\langle F(x_t, \eta_t) \rangle^{\omega^t} + \nabla_x \mathcal{F}(x_t) \right] + \xi_t. \quad (5.23)$$

In this equation, we defined the fluctuating part of the force as noise

$$\xi_t \equiv F(x_t, \eta_t) - \langle F(x_t, \eta_t) \rangle^{\omega^t}. \quad (5.24)$$

The perturbation of the bath might again be realized by dragging the particle through the bath at constant velocity v_0 by means of an optical tweezer. We assume that the system is in equilibrium at some time far in the past and we choose the initial probe position to be $x_{s=-\infty} = x_t$.¹ The probe motion acts as a perturbation of the bath via the time-dependent potential

$$\begin{aligned} U(x_s, \eta) &= U(x_t, \eta) - V_s(\eta), \quad s \leq t \\ V_s(\eta) &= (x_s - x_t) \cdot F(x_t, \eta) + \dots \end{aligned} \quad (5.25)$$

The perturbation protocol is contained in $V_s(\eta)$ where the force $F(x_t, \eta)$ between probe and bath couples to the probe displacement. Note that in principle higher order terms in the probe displacement can occur in V_s which are linked to higher derivatives of the interaction force F . Since we assume the potential U to be linear

¹Recall that an initial condition in the infinite past has no physical influence on the particle's evolution at time t . Even though the choice of initial condition might appear peculiar at first glance, it is mathematically useful, e.g., in Eq. (5.27).

in probe position, we can discard these terms and use

$$U(x, \eta) = x \cdot a(\eta), \quad V_s(\eta) = -(x_s - x_t) \cdot a(\eta). \quad (5.26)$$

Starting from basic thermodynamic energy considerations, we can express the entropic part \mathcal{S} in terms of the perturbation potential V_s [29, 54]

$$\begin{aligned} \mathcal{S} &= \beta \left[V_t(\eta_t) - V_{-\infty}(\eta_{-\infty}) - \int_{-\infty}^t ds \frac{\partial V_s}{\partial s}(\eta_s) \right] \\ &= \beta \int_{-\infty}^t ds \dot{x}_s \cdot a(\eta_s) = \beta W. \end{aligned} \quad (5.27)$$

In the last step, we introduced the work done on the bath exerted by the moving probe up to time t

$$W = \int_{-\infty}^t ds \nabla_x U \cdot \dot{x}_s \quad (5.28)$$

We need to compute the response of the force acting upon the tracer particle due to the back reaction of the perturbed bath. In the following, we present the results up to third order in probe displacement. The first and second order have already been computed in Ref. [54]. To first order we find

$$\begin{aligned} \langle F(l)(x_t, \eta_t) \rangle^{\omega^t} - \langle F(l)(x_t, \eta_t) \rangle_{x_t} &= \frac{\partial}{\partial x(l)} \mathcal{F}(x_t) - \langle a_l(\eta_t) \rangle^{\omega^t} \\ &= -\beta \int_0^\infty ds \gamma_s^{lk}(x_t) \dot{x}_{t-s}(k) = \beta \left\langle W; \frac{\partial U(x_t, \eta_t)}{\partial x(l)} \right\rangle^{\omega^t} \end{aligned} \quad (5.29)$$

which is a purely dissipative contribution and may be identified with the linear non-Markovian friction force we already used in the previous chapter. The memory matrix γ_s is linked to the force-force correlations in equilibrium and for the given case of linear coupling reads

$$\gamma_s^{lk}(x_t) = \beta \langle a_l(\eta_0); a_i(\eta_s) \rangle_{x_t}. \quad (5.30)$$

The second-order response involves the time-symmetric part of the action, the so-called dynamical activity, and is found to be

$$\begin{aligned} \frac{\partial}{\partial x(l)} \mathcal{F}(x_t) - \langle a_l(\eta_t) \rangle^{\omega^t} &= \text{Eq. (5.29)} + \\ &- \frac{\beta^2}{2} \int_0^\infty ds \int_0^\infty ds' \dot{x}_{t-s}(j)(x_t(k) - x_{t-s'}(k)) \langle \mathcal{D}_k^{x_t}(\eta_s); a_j(\eta_{s'}); a_l(\eta_{s+s'}) \rangle_{x_t}. \end{aligned} \quad (5.31)$$

Note that this term is no longer purely dissipative but involves the time-symmetric part of the action which depends on kinetic details of the bath (see Ref. [119] for

examples). In the derivation one assumes the following general form of D'_0 [54]

$$D'_0 = \frac{\beta}{2} \int_{-\infty}^t ds (x_s(j) - x_t(j)) \mathcal{D}_j^{x_t}(\eta_s). \quad (5.32)$$

The second-order response requires the computation of a three-point correlation function and introduces a novel time scale associated with the kinematics of the bath. This contribution, however, is only visible if the probe particle samples the nonlinear response of the bath and thus reflects the nonlinear nature of the elastic microstructure of a complex bath. As mentioned before, this term vanishes identically for systems that are isotropic and homogeneous. For these kind of systems the scheme needs to be extended to third order and apart from a purely dissipative contribution also the next higher Taylor coefficient in the expansion of the dynamical activity appears (see Eq. (5.21)). This coefficient takes on the following general form

$$D''_0 = \frac{\beta^2}{4} \int_{-\infty}^t ds \int_{-\infty}^t ds' (x_s(i) - x_t(i))(x_{s'}(j) - x_t(j)) \mathcal{D}_{ij}^{x_t}(\eta_s, \eta_{s'}). \quad (5.33)$$

Note that in contrast to Eq. (5.32) the coefficient is now quadratic in displacement and we introduced the matrix \mathcal{D}_{ij} which in general depends on the snapshot configuration of the baths at two different instances. We then find for the third order the following response relation

$$\begin{aligned} \frac{\partial}{\partial x(l)} \mathcal{F}(x_t) - \langle a_l(\eta_t) \rangle^{\omega_t} &= \text{Eq. (5.29)} + \text{Eq. (5.31)} + \\ &- \frac{\beta^3}{8} \left[\int_0^\infty ds \int_0^\infty ds' \int_0^\infty ds'' \left(\dot{x}_{t-s}(i)(x_t(j) - x_{t-s'}(j))(x_t(k) - x_{t-s''}(k)) \right. \right. \\ &\times \langle (\mathcal{D}_k^{x_t}(\eta_{s+s'}) \mathcal{D}_j^{x_t}(\eta_{s+s''}) - \mathcal{D}_{kj}^{x_t}(\eta_{s+s'}, \eta_{s+s''})) a_i(\eta_{s'+s''}) a_l(\eta_{s+s'+s''}) \rangle_{x_t} \\ &\left. \left. + \frac{1}{3} \dot{x}_{t-s}(i) \dot{x}_{t-s'}(j) \dot{x}_{t-s''}(k) \langle a_k(\eta_{s+s'}) a_j(\eta_{s+s''}) a_i(\eta_{s'+s''}) a_l(\eta_{s+s'+s''}) \rangle_{x_t} \right) \right]. \end{aligned} \quad (5.34)$$

The (multiplicative [38]) noise must be treated in second-order approximation $\xi \rightarrow \xi^{(2)}$ and by virtue of Eq. (5.24) we find

$$\xi_t^{(2)}(k) = \frac{\partial}{\partial x(k)} \mathcal{F}(x_t) + \beta \langle W ; a_k(\eta_t) \rangle_{x_t} - \frac{\beta^2}{2} \langle \tilde{D}'_0 ; W ; a_k(\eta_t) \rangle + F(k)(x_t, \eta_t), \quad (5.35)$$

where $D'_0 = \frac{\beta}{2} \tilde{D}'_0$. The covariance of the noise must be averaged with the second-order perturbation of the equilibrium average $\langle \cdot \rangle_{x_t}$, i.e.

$$\mathcal{P} = e^{-\mathcal{A}} \mathcal{P}_{\text{eq}} = \mathcal{P}_{\text{eq}} \left(1 - (D'_0 - S'_0/2) + \frac{1}{2} ((D'_0 - S'_0/2) - D''_0) \right). \quad (5.36)$$

For the noise correlator we find

$$\begin{aligned}
 \langle \xi_t^{(2)}(k); \xi_s^{(2)}(i) \rangle^{\omega^t} &= \langle a_k(\eta_t); a_i(\eta_s) \rangle_{x_t} - \frac{\beta}{2} \langle (\tilde{D}'_0 - W); a_k(\eta_t); a_i(\eta_s) \rangle_{x_t} \\
 &+ \frac{\beta}{2} [\langle W; a_k(\eta_t) \rangle_{x_t} \langle a_i(\eta_s) \rangle_{x_t} + \langle W; a_i(\eta_s) \rangle_{x_t} \langle a_k(\eta_t) \rangle_{x_t}] \\
 &+ \frac{\beta^2}{8} \langle (-\tilde{D}''_0 + \tilde{D}_0'^2 - 4\tilde{D}'_0 W + 2W^2)(a_k(\eta_t) - \langle a_k(\eta_t) \rangle_{x_t})(a_i(\eta_s) - \langle a_i(\eta_s) \rangle_{x_t}) \rangle_{x_t},
 \end{aligned} \tag{5.37}$$

where we used $D_0'' = \frac{\beta^2}{4} \tilde{D}_0''$. Insertion of the third-order response into Eq. (5.23) yields the following generalized Langevin to third order in in particle velocity

$$\begin{aligned}
 M\ddot{x}_t(i) - F_t^{\text{ext}}(i) &= -\partial_i \mathcal{F}(x_t) - \int_0^\infty ds \gamma_{s,ij}^{(1,S)} \dot{x}_{t-s}(j) \\
 &- \int_0^\infty ds \int_0^\infty ds' \gamma_{s,s';ijk}^{(2,SD)} \dot{x}_{t-s}(j) \dot{x}_{t-s'}(k) \\
 &- \int_0^\infty ds \int_0^\infty ds' \int_0^\infty ds'' \left(\gamma_{s,s',s'';ijkl}^{(3,SD)} + \gamma_{s,s',s'';ijkl}^{(3,S)} \right) \dot{x}_{t-s}(j) \dot{x}_{t-s'}(k) \dot{x}_{t-s''}(l) + \xi_t^{(2)}(l).
 \end{aligned} \tag{5.38}$$

In this equation, we added the superscript $(1, S)$ to the linear memory kernel (already defined in Eq. (5.30) to indicate that it is a purely dissipative contribution. In second order, the contribution is no longer purely dissipative and the dynamical activity of the bath enters the description. The memory kernel $\gamma^{(2,SD)}$ of this order is a tensor of rank three and depends on two independent time variables. It is defined as²

$$\gamma_{s,s';ijk}^{(2,SD)} = -\frac{\beta^2}{2} \int_0^{s'} ds'' \langle a_i(\eta_{s+s''}); a_j(\eta_{s''}); \mathcal{D}_k^{x_t}(\eta_s) \rangle_{x_t}. \tag{5.39}$$

Finally, the third order consists of a purely dissipative contribution and a mixed contribution of D and S . The purely entropic contribution is contained in the rank-four memory tensor $\gamma^{(3,S)}$ (dependent on three time variables) given by

$$\gamma_{s,s',s'';ijkl}^{(3,S)} = \frac{\beta^3}{24} \langle a_i(\eta_{s'+s''}) a_j(\eta_{s+s''}) a_k(\eta_{s+s'}) a_l(\eta_{s+s'+s''}) \rangle_{x_t}. \tag{5.40}$$

The mixed contribution of D and S is written into $\gamma^{(3,SD)}$ which reads

$$\begin{aligned}
 \gamma_{s,s',s'';ijkl}^{(3,SD)} &= \frac{\beta^3}{8} \int_0^{s'} ds_3 \int_0^{s''} ds_4 \\
 &\times \langle a_i(\eta_{s_3+s_4}) (D_j^{x_t}(\eta_{s+s_4}) D_k^{x_t}(\eta_{s+s_3}) - D_{jk}^{x_t}(\eta_{s+s_4}, \eta_{s+s_3})) a_l(\eta_{s+s_3+s_4}) \rangle_{x_t}.
 \end{aligned} \tag{5.41}$$

²Note that we performed a partial integration to recast the displacements $(x_t - x_{t-s})$ in Eq. (5.31) and (5.34) into velocities. The boundary term vanishes as we impose the initial condition $x_{s=-\infty} = x_t$. The lower integration limit in the integrals in Eq. (5.39) and Eq. (5.41) must be real numbers but else can be chosen arbitrarily, which reflects that the indefinite integral in the partial integration is only determined in a unique way up to a constant. We set the lower limits to zero in the two relations.

Note that while this tensor vanishes identically if D remains unchanged under the perturbation, $\gamma^{(3,S)}$ is a purely dissipative contribution. The different contributions in the response of the bath reflect distinct time scales of the system. The dissipative part describes time scale of the energy flux into the bath due to probe motion. On the other hand, the elastic time scale of the bath is probed by nonlinear motion and the kinematic details of the bath enter the evolution equation of the probe.

5.4 Phenomenological equation

In the previous section, we derived an exact nonlinear Langevin equation by exploiting the fact that the distortion via probe motion reacts back on the dynamics of the probe particle. Beyond the linear regime the noise was rendered multiplicative, i.e. it explicitly depended on the probe degrees of freedom [38]. This situation necessitates the specification of the stochastic calculus if the contribution by solvent molecules in the noise correlator is assumed to be delta correlated because the noise strength may change during an infinitesimal jump of the probe particle. Most commonly one uses the Itô or Stratonovich calculus to derive a corresponding Fokker-Planck equation for the probability distribution function by means of the so-called Kramers-Moyal expansion [38, 125]. In Itô's definition the strength of the noise depends only on the initial position of the infinitesimal jump. In the corresponding Fokker-Planck equation no new terms appear which is at the cost of new rules for integration and differentiation specified by the so-called Itô calculus. In the Stratonovich definition the noise strength changes during the jump and a so-called "spurious drift" appears in the Fokker-Planck equation. In this calculus, rules of ordinary calculus do hold. Linear or linearized Langevin equation do not suffer from this issue since the noise is additive, i.e. independent of the probe degrees of freedom [38]. In this limit the two different interpretations are identical.

Motivated by the exact derivation of the nonlinear generalized Langevin equation in Eq. (5.38) to third order in particle velocity³, we may use the general structure of this equation to postulate a phenomenological nonlinear Langevin equation in probe velocity. For simplicity, we restrict again to the one-dimensional case and assume

³Note that in the derivation we assumed a linear coupling between particle and bath. If we relax this condition and allow for nonlinear particle-bath coupling, bath correlations with derivatives of the force appear. The underlying structure of the nonlinear generalized Langevin equation, however, remains the same (see also Ref. [54] for a discussion of the second order).

the bath to be homogeneous⁴

$$\begin{aligned}
 m\ddot{x}(t) = & - \int_{-\infty}^t ds \Gamma^{(1)}(t-s)\dot{x}(s) - \int_{-\infty}^t ds_1 \int_{-\infty}^t ds_2 \Gamma^{(2)}(t-s_1, t-s_2)\dot{x}(s_1)\dot{x}(s_2) \\
 & - \int_{-\infty}^t ds_1 \int_{-\infty}^t ds_2 \int_{-\infty}^t ds_3 \Gamma^{(3)}(t-s_1, t-s_2, t-s_3)\dot{x}(s_1)\dot{x}(s_2)\dot{x}(s_3) \\
 & + F_{\text{ext}}(x, t) + f(t).
 \end{aligned} \tag{5.42}$$

Recall that according to the exact result in the previous section the noise-term is a nonlinear functional of the past trajectory, i.e. $f(t) = \mathcal{F}\{\dot{x}(t')\}_{t' \leq t}$. We can think of the phenomenological equation (5.42) also in terms of a so-called Volterra series [64]. The Volterra series describes a functional expansion of the nonlinear friction force $\mathcal{G}\{\dot{x}(t')\}_{t' \leq t}$ (as well as of the noise) which in general is a functional of the past trajectory. The n -th order memory kernel $\Gamma^{(n)}$ then describes the n -th summand of this series and we truncated it after the third order; the first nonlinear order which contributes to the response in a homogeneous and isotropic system. A time-dependent external force $F_{\text{ext}}(x, t)$ may operate on the probe and we note that the first moment of the noise vanishes⁵, i.e. $\langle f(t) \rangle = 0$.

5.4.1 Particle in equilibrium

We first want to investigate Eq. (5.42) in the equilibrium case of a particle in a harmonic trap. This corresponds to the situation in Chapter 3 and we set the external force to $F_{\text{ext}}(x) = -\kappa x(t)$. Notably, the external potential does not explicitly depend on time in the equilibrium case. The following perturbative analysis of this equation in orders of nonlinear memory kernels $\Gamma^{(2)}$ and $\Gamma^{(3)}$, respectively, is similar to the one presented in Refs. [126–128] for the case of a stochastic nonlinear Helmholtz equation. We want to transform the equation of motion (5.42) into Fourier space. For the n -th summand of the Volterra series we find

$$\begin{aligned}
 & \mathcal{F} \left[\int ds_1 \dots ds_n \Gamma_+^{(n)}(t-s_1, \dots, t-s_n) \dot{x}(s_1) \cdot \dots \cdot \dot{x}(s_n) \right] \\
 & = \frac{1}{(2\pi)^{n-1}} \int d\omega_1 \dots \int d\omega_n \delta(\omega - \omega_\sigma) \Gamma_+^{(n)}(\omega_1, \dots, \omega_n) i\omega_1 x(\omega_1) \cdot \dots \cdot i\omega_n x(\omega_n),
 \end{aligned} \tag{5.43}$$

with Fourier transforms $h(\omega) = \int_{-\infty}^{\infty} dt e^{-i\omega t} h(t)$. Note that we defined $\omega_\sigma = \omega_1 + \dots + \omega_n$ and $\Gamma_+^{(n)}(t) \equiv \Gamma^{(n)}(t)\theta(t)$. The external force is linear in the particle's position

⁴For homogeneous systems, the averages in the definitions of memory kernels in the previous section do not depend on probe position x . Note that we performed variable transformations to write the time differences in into the arguments of the memory kernels in contrast to Eq. (5.38).

⁵This statement holds true for both equilibrium as well as nonequilibrium, as we *define* the noise to be the fluctuating part of the total force, $f(t) \equiv \delta F(t) = F(t) - \langle F(t) \rangle$.

and can be easily transformed into Fourier space via $\mathcal{F}(F_{\text{ext}})(\omega) = -\kappa x(\omega)$. The phenomenological Langevin equation (5.42) thus turns in Fourier space into

$$\chi^{-1}x + \mathcal{M}[xx] + \mathcal{N}[xxx] = f(\omega). \quad (5.44)$$

Here we defined the frequency-dependent function/linear operators

$$\chi^{-1}(\omega) = -m\omega^2 + \kappa + i\omega\Gamma_+^{(1)}(\omega), \quad (5.45)$$

$$\mathcal{M}[xx](\omega) = \frac{1}{2\pi} \int d\omega_1 \int d\omega_2 \delta(\omega - \omega_\sigma) \Gamma_+^{(2)}(\omega_1, \omega_2) i\omega_1 x(\omega_1) i\omega_2 x(\omega_2), \quad (5.46)$$

$$\begin{aligned} \mathcal{N}[xxx](\omega) &= \frac{1}{(2\pi)^2} \int d\omega_1 \int d\omega_2 \int d\omega_3 \\ &\times \delta(\omega - \omega_\sigma) \Gamma_+^{(3)}(\omega_1, \omega_2, \omega_3) i\omega_1 x(\omega_1) i\omega_2 x(\omega_2) i\omega_3 x(\omega_3). \end{aligned} \quad (5.47)$$

We aim to linearize Eq. (5.44) in particle position $x(\omega)$. A suitable constraint that we can impose on the linearized equation is that it must yield the same linear-response function as the nonlinear equation. In order to meet this condition, we compute the linear response of the nonlinear equation in a perturbative manner up to linear order in the nonlinear memory kernels⁶. The system is perturbed by an external (time-dependent) force $F_{\text{pert}}(t)$ which is under our control. In the perturbed system, it is useful to separate x into a mean part⁷ and fluctuations, i.e. $x = \langle x \rangle + \delta x$. We then obtain for the averaged Eq. (5.44)

$$\chi^{-1}\langle x \rangle + \mathcal{M}[\langle x \rangle \langle x \rangle + \langle \delta x \delta x \rangle] + \mathcal{N}[\langle x \rangle \langle x \rangle \langle x \rangle + 3\langle \delta x \delta x \rangle \langle x \rangle + \langle \delta x \delta x \delta x \rangle] = F_{\text{pert}}(\omega). \quad (5.48)$$

Note that we used the symmetry property of the operator \mathcal{N}

$$\mathcal{N}[\langle \delta x \delta x \rangle \langle x \rangle] = \mathcal{N}[\langle x \rangle \langle \delta x \delta x \rangle] = \mathcal{N}[\langle \delta x \langle x \rangle \delta x \rangle] \quad (5.49)$$

which is a consequence of the intrinsic symmetry of the memory kernel. This property is implied by a possible commutation of spatial variables in the definition of Eq. (5.47). Upon rearrangement of the spatial variables and renaming the integration variables, it is obvious that the memory kernel remains the same if one interchanges a pair of frequency indices. Note that in the averaged equation (5.48) the three-point correlator of the fluctuations occur which in general is unknown in case of a non-Gaussian distribution function of the noise. In a perturbative series, however, (where we assume $\Gamma^{(2)}$ and $\Gamma^{(3)}$ to be small perturbations of the linear system) we only keep the leading order of the nonlinear memory kernels and we may replace arguments in \mathcal{M} and \mathcal{N} by the solution of the linear problem, i.e. for the case $\Gamma^{(2)} = \Gamma^{(3)} = 0$. For any linear equation of motion the superposition principle holds and it is safe to assume that noise and fluctuations are Gaussian distributed

⁶From general symmetry considerations it is already clear that $\Gamma^{(2)}$ cannot contribute to the response function in an isotropic and homogeneous system (the friction force must change sign under time reversal). Yet, for the sake of generality we show this below.

⁷We distinguish averages in the perturbed system $\langle \cdot \rangle$ and in equilibrium $\langle \cdot \rangle_{\text{eq}}$.

random variables⁸. By virtue of Wick's theorem [38], the odd moments of random variables vanish, i.e. in particular $\langle \delta x \delta x \delta x \rangle = 0$. The equation of motion in Fourier space simplifies to

$$\chi^{-1} \langle x \rangle + \mathcal{M}[\langle x \rangle \langle x \rangle + \langle \delta x \delta x \rangle] + \mathcal{N}[\langle x \rangle \langle x \rangle \langle x \rangle + 3 \langle \delta x \delta x \rangle \langle x \rangle] = F_{\text{pert}}(\omega). \quad (5.50)$$

We assume that the perturbation has been switched on at some time far in the past and the system is in the stationary state. Under such conditions the correlation functions in time-domain are functions of time differences and in Fourier space we can apply the Wiener-Khintchine theorem [38]

$$\langle \delta x(\omega) \delta x(\omega') \rangle = 2\pi \delta(\omega + \omega') \langle |\delta x(\omega)|^2 \rangle. \quad (5.51)$$

The spectral density is the Fourier transform of the correlation function for stationary processes, i.e. $\langle |\delta x(\omega)|^2 \rangle = \int_{-\infty}^{\infty} d\omega' e^{-i\omega t} \langle x(t)x(0) \rangle$. We can then rewrite the term $\mathcal{M}[\langle \delta x \delta x \rangle]$ as

$$\mathcal{M}[\langle \delta x \delta x \rangle] = \delta(\omega) \int d\omega_1 \Gamma_+^{(2)}(\omega_1, -\omega_1) \omega_1^2 \langle |\delta x(\omega_1)|^2 \rangle = 0. \quad (5.52)$$

Note that this term vanishes identically for any frequency⁹. We thus find the final form of the averaged Langevin equation in leading order in $\Gamma^{(2)}$ and $\Gamma^{(3)}$

$$(\chi^{-1} + 3\mathcal{N}[\langle \delta x \delta x \rangle]) \langle x \rangle + \mathcal{M}[\langle x \rangle \langle x \rangle] + \mathcal{N}[\langle x \rangle \langle x \rangle \langle x \rangle] = F_{\text{pert}}(\omega), \quad (5.53)$$

where we used the notation $\mathcal{N}[\langle \delta x \delta x \rangle] \langle x \rangle \equiv \mathcal{N}[\langle \delta x \delta x \rangle \langle x \rangle]$. This notation is motivated by the fact that

$$\mathcal{N}[\langle \delta x \delta x \rangle] = \frac{i\omega}{2\pi} \int d\omega_1 \Gamma_+^{(3)}(\omega_1, -\omega_1, \omega) \omega_1^2 \langle |\delta x(\omega_1)|^2 \rangle \quad (5.54)$$

does no longer involve an operation over ω_3 , i.e. $\mathcal{N}[\langle \delta x \delta x \rangle \langle x \rangle]$ reduces to a multiplication of the operator in Eq. (5.54) with the third argument. Recall that in the operators \mathcal{M} and \mathcal{N} the fluctuations and average of the linear problem appear, i.e.

$$\langle x \rangle = (-m\omega^2 + \kappa + i\omega\Gamma_+^{(1)})^{-1} F_{\text{pert}}, \quad (5.55)$$

$$\delta x = (-m\omega^2 + \kappa + i\omega\Gamma_+^{(1)})^{-1} f. \quad (5.56)$$

⁸Recall that a quadratic microscopic Hamiltonian leads to linear equations of motion and the noise is a Gaussian random variable [12, 75]. In Fokker-Planck dynamics, a linear drift vector and constant diffusion tensor leads to Gaussian distributions for the stationary as well as for the instationary solutions [38].

⁹At finite frequency ω the delta function immediately renders the term zero. At zero frequency the relation is, however, more subtle. We can still rule out a contribution on physical grounds by arguing that the contribution at $\omega = 0$ corresponds to the quasi-static case where the particle's velocity obeys the Maxwell-Boltzmann distribution. Since the Maxwell-Boltzmann distribution does not know about the shape of the particle, and the quadratic-order term in velocity does not contribute to the response in case of an isotropic particle in a homogeneous system, we can set this term to zero even at $\omega = 0$ (it is then rather a property of $\Gamma^{(2)}$ and the integral must vanish).

The χ as defined in Eq. (5.45) is identified as the response function of the linear problem. Note that the linear-response function is connected to the spatial equilibrium fluctuations via the fluctuation-dissipation theorem [8]

$$\langle \delta x(\omega) \delta x^*(\omega') \rangle_{\text{eq}} = -\frac{4\pi}{\omega\beta} \delta(\omega - \omega') \text{Im}[\chi]. \quad (5.57)$$

With this relation and Eq. (5.56) we find the usual connection between the force-force correlator and the friction memory kernel of a linear generalized Langevin equation

$$\begin{aligned} \langle f(\omega) f^*(\omega') \rangle_{\text{eq}} &= \langle [\chi^{-1} \delta x](\omega) [\chi^{-1} \delta x]^*(\omega') \rangle_{\text{eq}} \\ &= \chi^{-1} \langle \delta x(\omega) \delta x^*(\omega') \rangle_{\text{eq}} (\chi^{-1})^* \\ &= \frac{4\pi}{\beta\omega} \delta(\omega - \omega') \text{Im}[\chi^{-1}] \\ &= 4\pi\beta^{-1} \delta(\omega - \omega') \text{Re}[\Gamma_+^{(1)}]. \end{aligned} \quad (5.58)$$

Application of the Wiener-Khintchine theorem thus yields

$$\beta \langle |f(\omega)|^2 \rangle = 2 \text{Re}[\Gamma_+^{(1)}]. \quad (5.59)$$

How does the presence of nonlinear terms in the equation of motion (5.42) change the linear response of the system? In order to answer this question we need to compute the functional derivative of Eq. (5.53). We obtain¹⁰

$$\begin{aligned} \tilde{\chi} &\equiv \left. \frac{\delta \langle x \rangle}{\delta F_{\text{pert}}} \right|_{F_{\text{pert}} \rightarrow 0} = (-m\omega^2 + \kappa + i\omega\Gamma_+^{(1)} + 3\mathcal{N}[\langle \delta x \delta x \rangle_{\text{eq}}])^{-1} \\ &= \chi - 3\chi \mathcal{N}[\langle \delta x \delta x \rangle_{\text{eq}}] \chi. \end{aligned} \quad (5.60)$$

The linear response function of the nonlinear system is renormalized by the presence of the nonlinear friction force in the Langevin equation. The equilibrium noise is easily extracted by setting $\langle x \rangle_{\text{eq}} = 0$ in Eq. (5.44),

$$f(\omega) = \chi^{-1} \delta x + \mathcal{M}[\delta x \delta x] + \mathcal{N}[\delta x \delta x \delta x]. \quad (5.61)$$

The first moment of the equilibrium noise vanishes by definition and we can compute the equilibrium noise correlator as

$$\begin{aligned} \langle f(\omega) f^*(\omega') \rangle_{\text{eq}} &= \chi^{-1}(\omega) \langle \delta x(\omega) \delta x^*(\omega') \rangle_{\text{eq}} (\chi(\omega')^{-1})^* \\ &\quad + \chi(\omega)^{-1} \langle \delta x(\omega) \mathcal{N}[\delta x \delta x \delta x]^*(\omega') \rangle_{\text{eq}} + \langle \mathcal{N}[\delta x \delta x \delta x](\omega) \delta x^*(\omega') \rangle_{\text{eq}} (\chi^{-1}(\omega'))^*, \end{aligned} \quad (5.62)$$

where we used again that the linear fluctuations are Gaussian distributed random variables. In the four-point correlation functions that appear we can use the symmetry property of the \mathcal{N} -operator and rewrite the equilibrium noise correlator in a

¹⁰Note that the equilibrium correlator $\langle \delta x \delta x \rangle_{\text{eq}}$ now appears in the argument of \mathcal{N} since we compute the linear-response function and need to expand the probability distribution of the correlation function to zeroth order in F_{pert} (as $\langle x \rangle$ is of linear order in F_{pert} according to Eq. (5.55)).

symmetric form

$$\langle f(\omega)f(\omega') \rangle_{\text{eq}} = (\chi^{-1} + 3\mathcal{N}[\langle \delta x \delta x \rangle_{\text{eq}}])_{\omega} \langle \delta x(\omega) \delta x^*(\omega') \rangle_{\text{eq}} ((\chi^{-1})^* + 3\mathcal{N}[\langle \delta x \delta x \rangle_{\text{eq}}]^*)_{\omega'} \quad (5.63)$$

By virtue of the fluctuation dissipation theorem in Eq. (5.57), where we now use the renormalized response function $\tilde{\chi}$, we find

$$\langle f(\omega)f(\omega')^* \rangle_{\text{eq}} = \frac{4}{\beta\omega} \delta(\omega - \omega') \text{Im}[\tilde{\chi}^{-1}]. \quad (5.64)$$

The spectral density of the equilibrium noise thus reads

$$\beta \langle |f(\omega)|^2 \rangle_{\text{eq}} = 2 \text{Re} \left[\Gamma_+^{(1)}(\omega) + \frac{3\omega}{2\pi} \int d\omega_1 \Gamma_+^{(3)}(\omega_1, -\omega_1, \omega) \omega_1^2 \langle |\delta x(\omega_1)|^2 \rangle_{\text{eq}} \right] \quad (5.65)$$

and we can read off the renormalized memory kernel of the linearized equation of motion

$$\tilde{\Gamma}_+^{(1)}(\omega) = \Gamma_+^{(1)}(\omega) + \frac{3\omega}{2\pi} \int d\omega_1 \Gamma_+^{(3)}(\omega_1, -\omega_1, \omega) \omega_1^2 \langle |\delta x(\omega_1)|^2 \rangle_{\text{eq}}. \quad (5.66)$$

The linearized equation of motion in Fourier space is thus given in terms of the renormalized noise correlator (Eq. (5.65)) and memory kernel (Eq. (5.66))

$$-m\omega^2 x(\omega) = -i\omega \tilde{\Gamma}_+^{(1)} - \kappa x(\omega) + f(\omega). \quad (5.67)$$

Interestingly, the spectral density of the particle's position appears in the renormalized quantities. Since Eq. (5.66) holds up to linear order in $\Gamma^{(2)}$ and $\Gamma^{(3)}$ the spectral density must be computed with respect to the linear problem. By means of Eq. (5.56) we easily find

$$\langle |\delta x(\omega)|^2 \rangle = \frac{2k_B T \text{Re}[\Gamma_+^{(1)}(\omega)]}{\left| -m\omega^2 + i\omega \Gamma_+^{(1)}(\omega) + \kappa \right|^2}. \quad (5.68)$$

Equivalent to what we found from a microscopic starting point in Sec. 3.1, the friction memory kernel of the linearized equation of motion couples to the trap stiffness κ of the external potential. Note that possible choices of $\Gamma_+^{(3)}$ are restricted by its connection to the spectral density of the equilibrium noise in Eq. (5.65). As a function of two independent arguments, $\Gamma_+^{(3)}$ is antisymmetric in the argument ω but symmetric in ω_1 .

5.4.2 Particle in a nonequilibrium steady state

The linearization in the previous section is only strictly true in equilibrium as we made use of the fluctuation-dissipation theorem in Eq. (5.57). In a nonequilibrium situation there is no known universal analogue to this fundamental theorem of sta-

tistical physics despite certain generalizations in particular cases [29–33]. We now want to investigate the case where the colloidal particle is driven at a constant velocity through the complex bath. In the experimental system of a wormlike micellar bath the driving of the colloid is realized by setting the optical tweezer into motion. The relative motion between tracer particle and bath can in principle be achieved by two equivalent routes: i) the position of the laser spot which gives rise to the optical trapping potential is moved at constant velocity, ii) the trap is hold in place and we move the bath at constant relative velocity against the probe. In classical physics the two scenarios are identical because of the invariance of Newton’s equation of motion under the Galilean transformation that connects the two inertial frame of references (the laboratory frame and the comoving frame of the probe).

As a starting point we use again the phenomenological nonlinear Langevin equation (5.42). In the described nonequilibrium situation, the external force is an explicit function of time and reads $F_{\text{ext}} = -\kappa(x - v_0t)$, where v_0 is the dragging velocity of the harmonic potential. The nonlinearity of the friction force and noise makes the transformation to the comoving frame and the linearization nontrivial. We want to consider the system under stationary conditions, i.e. the motion of the trap started at some time far in the past. In the steady state the bath exerts a mean friction force on the probe particle which on average is balanced by the mean optical force. The force balance under stationary conditions gives us information on the mean position of the particle in the laboratory frame, i.e.

$$|\langle F_\gamma \rangle| = |\langle F_\kappa \rangle| \quad \Rightarrow \quad \langle x \rangle - v_0t = \langle \xi \rangle = \frac{\langle F_\gamma \rangle}{\kappa} = \text{const.} \quad (5.69)$$

Here we introduced the variable $\xi = x - v_0t$ which measures the particle position in the coming frame with respect to the origin of the moving trap. The mean value $\langle \xi \rangle$ thus gives the mean displacement of the particle in this reference frame due to the mean friction force $\langle F_\gamma \rangle$. It is convenient to introduce another coordinate system that describes the fluctuations around the mean position $\langle \xi \rangle$ of the particle. The transformation into this comoving frame that follows the *zero-force point* is given by

$$\delta x = \xi - \langle \xi \rangle = x - v_0t - \langle \xi \rangle = x - \langle x \rangle. \quad (5.70)$$

In order to rewrite the equation of motion with respect to this coordinate system, we need to correctly transform the velocity and the inertial term. By using the fact that the stationary probability distribution is time-independent, we find

$$\delta \dot{x} = \dot{\xi} = \dot{x} - \langle \dot{x} \rangle = \dot{x} - v_0, \quad \delta \ddot{x} = \ddot{x} - \langle \ddot{x} \rangle. \quad (5.71)$$

Since in the nonequilibrium steady state the particle moves on average at the same velocity as the trap, we used $\langle \dot{x} \rangle = v_0$. The transformation rules in Eqs. (5.70) and (5.71) together with the condition of force balance (5.69) in the stationary state allows us to rewrite Eq. (5.42) as

$$m\delta \ddot{x}(t) = F_\gamma(t) - \langle F_\gamma \rangle - \kappa\delta x(t) + f(t). \quad (5.72)$$

This is the equation of motion in the comoving frame where the particle fluctuates around the coordinate origin¹¹. Note that the fluctuating part of the friction force F_γ (i.e. the velocity-dependent part in Eq. (5.42)) appears in this reference frame. We may compute the fluctuating force up to third order in velocity and find¹²

$$\begin{aligned} F_\gamma - \langle F_\gamma \rangle &= - \int ds \tilde{\Gamma}_+^{(1)}(t-s) \dot{x}(s) \\ &- \int ds_1 ds_2 \tilde{\Gamma}_+^{(2)}(t-s_1, t-s_2) (\dot{x}(s_1) \dot{x}(s_2) - \langle \dot{x}(s_1) \dot{x}(s_2) \rangle) \\ &- \int ds_1 ds_2 ds_3 \tilde{\Gamma}_+^{(3)}(t-s_1, t-s_2, -t-s_3) (\dot{x}(s_1) \dot{x}(s_2) \dot{x}(s_3) - \langle \dot{x}(s_1) \dot{x}(s_2) \dot{x}(s_3) \rangle). \end{aligned} \quad (5.73)$$

The transformation into the comoving frame yields a renormalization of memory kernels $\tilde{\Gamma}^{(1)}$ and $\tilde{\Gamma}^{(2)}$. They become functions of dragging velocity v_0 and read

$$\tilde{\Gamma}^{(1)}(t) = \Gamma^{(1)}(t) + 2v_0 \Gamma^{(2)}(t, 0) + 3v_0^2 \Gamma^{(3)}(t, 0, 0), \quad (5.74)$$

$$\tilde{\Gamma}^{(2)}(t_1, t_2) = \Gamma^{(2)}(t_1, t_2) + 3v_0 \Gamma^{(3)}(t_1, t_2, 0). \quad (5.75)$$

Note that in this representation the argument zero in the bare memory kernels (the one without the tilde) involves an integration over time (i.e. these arguments have been Laplace transformed and are evaluated at $s = 0$). Recall that the equation of motion (5.72) is from the perspective/frame of the probe particle being at rest on average. Consequently, the relative motion of the bath is reflected in a velocity-dependent friction kernel (and noise as we will see below). This is another kind of renormalization in comparison to the one we found for the equilibrium case in the previous section. There the renormalization of memory kernel and noise was of thermal nature (cf. Eqs. (5.66) and (5.68)) obtained by a perturbative treatment of the nonlinearity.

A similar analysis is feasible in the nonequilibrium steady state. Transformation of the equation of motion (5.72) into Fourier space yields

$$\chi^{-1} x + \mathcal{M}[xx - \langle xx \rangle] + \mathcal{N}[xxx - \langle xxx \rangle] = f(\omega) + F_{\text{pert}}(\omega). \quad (5.76)$$

Here we included again a time-dependent external perturbation force F_{pert} that is under our control. Furthermore, we defined the frequency-dependent function/linear operators

$$\chi^{-1}(\omega) = -m\omega^2 + \kappa + i\omega \tilde{\Gamma}^{(1)}(\omega) \quad (5.77)$$

$$\mathcal{M}[xx](\omega) = \frac{1}{2\pi} \int d\omega_1 \int d\omega_2 \delta(\omega - \omega_\sigma) \tilde{\Gamma}^{(2)}(\omega_1, \omega_2) i\omega_1 x(\omega_1) i\omega_2 x(\omega_2), \quad (5.78)$$

¹¹The vanishing mean particle position, i.e. $\langle \delta x \rangle = 0$, can be easily seen from Eq. (5.72) by taking the average $\langle \cdot \rangle$ with respect to the stationary distribution function.

¹²Note that we drop the extra δ from $\delta \dot{x}$ from now on to save space.

$$\begin{aligned} \mathcal{N}[xxx](\omega) &= \frac{1}{(2\pi)^2} \int d\omega_1 \int d\omega_2 \int d\omega_3 \\ &\times \delta(\omega - \omega_\sigma) \Gamma^{(3)}(\omega_1, \omega_2, \omega_3) i\omega_1 x(\omega_1) i\omega_2 x(\omega_2) i\omega_3 x(\omega_3). \end{aligned} \quad (5.79)$$

In contrast to the equilibrium case, we use the rescaled memory kernels $\tilde{\Gamma}^{(1)}$ and $\tilde{\Gamma}^{(2)}$ in these definitions. In order to find the linearized equation of motion, we now need to compute the linear-response function around the nonequilibrium steady state. For that purpose we introduce the average with respect to the perturbed distribution $\langle \cdot \rangle_p$. Application of this average with respect to Eq. (5.76) yields

$$\chi^{-1} \langle x \rangle_p + \mathcal{M}[\langle xx \rangle_p - \langle xx \rangle] + \mathcal{N}[\langle xxx \rangle_p - \langle xxx \rangle] = F_{\text{pert}}(\omega). \quad (5.80)$$

Due to the external perturbation the particle's mean position in the moving trap changes and we can write

$$x = \langle x \rangle_p + \delta x. \quad (5.81)$$

The equation of motion can then be rewritten according to

$$\begin{aligned} \chi^{-1} \langle x \rangle_p + \mathcal{M}[\langle \delta x \delta x \rangle_p - \langle \delta x \delta x \rangle - 2\langle \delta x \rangle \langle x \rangle_p] \\ + \mathcal{N}[3(\langle \delta x \delta x \rangle_p - \langle \delta x \delta x \rangle) \langle x \rangle_p + \langle \delta x \delta x \delta x \rangle_p - \langle \delta x \delta x \delta x \rangle - 3\langle \delta x \rangle \langle x \rangle_p \langle x \rangle_p] = F_{\text{pert}}(\omega). \end{aligned} \quad (5.82)$$

Again we may assume that the perturbation was switched on at some time far in the past, so that correlators in the operator \mathcal{M} drop out¹³. Furthermore, we aim at the perturbative equation to linear order in the nonlinear memory kernels. Consequently, the averaging of arguments within the arguments of \mathcal{M} and \mathcal{N} can be assumed Gaussian. Moreover, with $\langle \delta x \rangle = \langle x \rangle - \langle x \rangle_p$ we find

$$\begin{aligned} F_{\text{pert}}(\omega) &= \chi^{-1} \langle x \rangle_p + \mathcal{M}[-2(\langle x \rangle - \langle x \rangle_p) \langle x \rangle_p] \\ &+ \mathcal{N}[3(\langle \delta x \delta x \rangle_p - \langle \delta x \delta x \rangle) \langle x \rangle_p - 3(\langle x \rangle - \langle x \rangle_p) \langle \delta x \delta x \rangle - 3(\langle x \rangle - \langle x \rangle_p) \langle x \rangle_p \langle x \rangle_p]. \end{aligned} \quad (5.83)$$

The linear response function around the nonequilibrium steady state thus reads

$$\begin{aligned} \tilde{\chi} &\equiv \left. \frac{\delta \langle x \rangle_p}{\delta F_{\text{pert}}} \right|_{F_{\text{pert}} \rightarrow 0} = \left(-m\omega^2 + \kappa + i\omega \tilde{\Gamma}^{(1)}(\omega) + 3\mathcal{N}[\langle \delta x \delta x \rangle] \right)^{-1} \\ &= \chi - 3\chi \mathcal{N}[\langle \delta x \delta x \rangle] \chi. \end{aligned} \quad (5.84)$$

Although the appearance of the result is identical to the case of equilibrium in Eq. (5.60), we note that in χ (the response function of the linear problem) now the renormalized memory kernel $\tilde{\Gamma}^{(1)}(t)$ occurs given in Eq. (5.74) (note the v_0 -dependence). Another striking difference to the linear-response function around the equilibrium state is the correlator $\langle \delta x \delta x \rangle$ which must be evaluated in Eq. (5.84)

¹³The same line of argumentation as in the equilibrium case holds for nonzero frequencies. At zero frequency these terms must vanish as well which is a consequence of the isotropy of the system (a property of $\tilde{\Gamma}^{(2)}$).

with respect to the stationary distribution function instead of the equilibrium distribution. Note that from the linear-response relation (5.84) we can read off the renormalized memory kernel that appears in the linearized equation of motion in the comoving frame. In contrast to the equilibrium case, it is obtained in a two step renormalization (transformation into the comoving frame and subsequent linearization in the nonlinear memory kernel) and takes on the form

$$\bar{\Gamma}_+^{(v_0)}(\omega) = \tilde{\Gamma}_+^{(1)}(\omega) + \frac{3}{2\pi} \int d\omega_1 \Gamma_+^{(3)}(\omega_1, -\omega_1, \omega) \omega_1^2 \langle |\delta x(\omega_1)|^2 \rangle. \quad (5.85)$$

Unlike the equilibrium case, the linear memory kernel $\tilde{\Gamma}_+^{(1)}(\omega)$ is already renormalized via Eq. (5.74) and depends on velocity v_0 of the trap. The expansion of the noise correlator under stationary conditions to first order in the nonlinear memory kernels follows the same computational steps as in Sec. 5.4.1. We only provide the final result which for the spectral density of the noise reads

$$\langle |f(\omega)|^2 \rangle = (\chi^{-1} + 3\mathcal{N}[\langle \delta x \delta x \rangle])_\omega \langle |\delta x(\omega)|^2 \rangle ((\chi^{-1})^* + 3\mathcal{N}[\langle \delta x \delta x \rangle]^*)_\omega \quad (5.86)$$

We emphasize that the noise is now also a function of dragging velocity v_0 of the trap via the renormalized memory kernel in Eq. (5.74). In contrast to the equilibrium case, we cannot invoke the fluctuation-dissipation theorem¹⁴ anymore to link this correlator to the memory kernel. Note that in this case relation Eq. (5.86) is an implicit equation of the noise correlator (recall that the position spectral density of the linear generalized Langevin equation is proportional to the noise spectral density). In principle, such an equation could be solve in an iterative fashion. The linearized equation of motion in the comoving frame is then given in terms of the renormalized memory kernel (Eq. (5.85)) and noise correlator (Eq. (5.86)) written in time domain as

$$m\ddot{x}(t) = - \int_{-\infty}^t \bar{\Gamma}^{(v_0)}(t-s) \dot{x}(s) - \kappa x(t) + f^{(v_0)}(t). \quad (5.87)$$

Summarizing the results of the previous two sections about the phenomenological nonlinear Langevin equation (5.42), we found that a perturbative analysis in equilibrium leads to a thermal renormalization of the type of which we already worked out from a microscopic starting point in Chapter 3. In particular, we observed a dependence on the trap stiffness κ in the renormalized friction memory kernel (see Eq. (5.66) and Eq. (5.68)) if the particle is confined by a harmonic trap. As stated before such a dependence in a linearized equation appears to be quite general irrespective of the actual type of the external potential. In nonequilibrium the situation is more complex because of the nontrivial transformation into the comoving frame. While this transformation itself leads to a renormalization, the subsequent thermal renormalization is then additive. The study of the phenomenological nonlinear Langevin equation and its dependencies in the linearized version will prove useful in the following section where we resort to this model a model equation of the form of Eq. (5.87)

¹⁴Despite a universal nonequilibrium analogue to this fundamental theorem of statistical physics has not been found yet, certain generalizations do exist in particular cases [29–33].

to describe nonequilibrium phenomena of a colloidal particle in a wormlike micellar system.

6 Oscillating modes of overdamped driven colloids

In this chapter, we revisit the experimental system of a colloidal particle in a wormlike micellar solution already investigated in Chapter 3. Here we investigate the case of nonequilibrium steady state dynamics and resort to the performed analysis of nonlinear generalized Langevin equations in the previous chapter. In particular, we study the case where the confining harmonic trap is dragged at constant velocity v_0 through the complex micellar bath. In the experimental system of a wormlike micellar bath the driving of the colloid is realized by setting the optical tweezer into motion. The relative motion between tracer particle and bath can in principle be achieved by two equivalent routes: i) the position of the laser spot, which gives rise to the optical trapping potential, is moved at constant velocity, ii) the trap is hold in place and we move the bath at constant relative velocity against the probe. These two scenarios are identical in classical physics because of the invariance of Newton's equation of motion under the Galilean transformation that connects the two inertial frame of references (the laboratory frame and the comoving frame of the probe). The study of fluctuations in the comoving frame of the experimental system will reveal a new harmonic oscillator state with non-trivial fluctuations, which in overdamped dynamics are strictly ruled out in equilibrium. The experimental observations are conveniently described via a linear generalized Langevin equation of the form we derived in the previous chapter. The results presented in this chapter are based to a large extent on the findings published in Ref. [4]¹.

6.1 State of the art

Driven colloidal particles suspended in purely viscous (Newtonian) solvents have provided valuable insight in understanding nonequilibrium processes. Due to the clear separation of time scales between the degrees of freedom of the tracer particle and the bath degrees of freedom they can be described by Markovian Langevin equations. In the Markovian limit any time scale associated with probe motion (the

¹J. Berner, B. Müller, J. R. Gomez-Solano, M. Krüger, and C. Bechinger. Oscillating modes of driven colloids in overdamped systems. *Nat. Commun.*, 9(1):999, 2018. This article is licensed under a Creative Commons Attribution 4.0 International License (see <http://creativecommons.org/licenses/by/4.0/>). Any reprint and/or adaptation of figures taken from this reference will be indicated in the corresponding figure caption in this chapter.

Brownian diffusion time and the time scale of driving) is well separated from the relaxation time scale of the solvent. Consequently, the velocity distribution of the bath molecules is unaffected by the driving of the particle. For that reason the bath acts as a genuine equilibrium thermostat irrespective of how fast the particle is dragged through the fluid. The ratio of the solvent relaxation time τ_S and Brownian diffusion time τ_B defined as the parameter M in Eq. (2.4) is thus supposed to be small in the given limit. Consequently, the memory kernel is presumed to be delta correlated and in particular *independent* of velocity, i.e.

$$\Gamma^{(v_0)}(t) \stackrel{M \ll 1}{\equiv} 2\gamma\delta(t). \quad (6.1)$$

The noise is typically assumed to be Gaussian white and, by virtue of the fluctuation-dissipation theorem, independent of the driving velocity as well. Indeed, many experiments have confirmed that the Markovian assumption remains valid even in the case of strong external driving forces (Ref. [39] provides an excellent overview over this topic). On the theoretical side, the time scale separation and the postulation of a weak coupling of colloidal particles to the thermal bath opens up a consistent description in terms of stochastic thermodynamics [32, 39, 47]. In the Markovian limit, the equation of motion in the comoving frame can be given by the linear Langevin equation

$$m\ddot{x}(t) = -\gamma\dot{x}(t) - \kappa x(t) + f(t). \quad (6.2)$$

Notably, this equation of motion only depends on the probe position at time t and does not take into account the probe's history. While this equation is expected to hold for purely viscous solvents, i.e. Newtonian fluids, experimental measurements in viscoelastic fluids like semi-dilute polymer solutions [129], micellar systems [53], or dense colloidal suspensions [111] demonstrate that the theoretical description must be necessarily a non-Markovian equation of motion, e.g., of the form Eq. (5.87).

Viscoelastic fluids exhibit a large structural relaxation time τ_S and the argument of a separation of time scales between particle and bath degrees of freedom is no longer applicable. As a consequence, when the particle is driven through such a fluid, the bath can no longer be regarded to remain in equilibrium. Instead the particle dynamics will be strongly affected by the deformation of the complex microstructure of the bath. Experimental studies reported the occurrence of unsteady particle motion [130, 131], and in general showed a strong deviation from the behaviour in simple Newtonian liquids [50, 52, 53, 111–113, 118, 129, 132, 133]. Note that these findings are typically caused by nonlinear rheological properties of viscoelastic fluids (e.g. the decay of viscosity commonly known as shear thinning with increasing driving velocities), which can be observed in both micro- and macrorheological experiments [18, 50, 52, 134].

6.2 The regime of measurement

In contrast to previous studies, the experiments presented in this chapter are performed in the regime of low driving velocities. A suitable dimensionless parameter to distinguish the different regimes is given in terms of the Weissenberg number Wi introduced in Eq. (2.3). It describes the ratio of the (structural) relaxation time of the solvent and the time scale of driving. Here, we consider the regime of small Weissenberg numbers, i.e. $Wi < 1$. Another distinct feature of the experimental system in comparison to previous studies is the separation of length scales between probe particle and bath. Since the radius of the probe particle is much larger than the effective dimension of the bath particles there is no dependence on the size ratio and we are in the asymptotic limit. Furthermore, we restrict ourselves to the case of steady-state dynamics. In the steady state we can define a (micro-)viscosity by means of the force balance between frictional force and optical restoring force

$$\eta \equiv \frac{\kappa |\langle \xi \rangle|}{6\pi v_0 R}. \quad (6.3)$$

The viscosity η is plotted in Fig. 6.1 as a function of velocity/Weissenberg number for the wormlike micellar system. From the analysis in equilibrium and literature [60, 61, 67, 114] we know that the so-called flow curve depends on the confinement potential, i.e. in case of a harmonic potential the friction force acting upon the particle depends on the stiffness κ . In order to make the following analysis of the micellar system comparable for different Weissenberg numbers the experimental trap stiffness is fixed at $\kappa = 2.81 \mu\text{N}/\text{m}$. There is another subtlety we want to comment on in the flow curve in Fig. 6.1: While the values of viscosity for finite velocities were evaluated via the relation (6.3), the relation is of no use for the experimental system in the static limit $v_0 = 0$. The reason for it is that for very small velocities $v_0 \rightarrow 0$ the displacement $\langle \xi \rangle$ from the center of the trap decreases as well. Indeed, in the linear response regime it must scale linearly in velocity so that the viscosity becomes independent of v_0 . Experimentally these very small displacements are difficult to resolve because of the limited spatial resolution. From linear response theory we obtained in Eq. (4.11) that the friction coefficient in the limit $v_0 \rightarrow 0$ is simply given by the $s = 0$ value of the Laplace transform of the friction memory kernel Γ . Extrapolation of the numerical black curves in Fig. (3.12), that fitted the experimental equilibrium data very well, yields the static values of viscosity in Fig. 6.1 for the three different trap stiffnesses investigated in Sec. 3.3. For $\kappa = 2.81 \mu\text{N}/\text{m}$ this value is surprisingly more than twice as large as the measured value for the smallest driving velocity at $Wi = 0.04$. The static value describes the linear response regime of the system and we expect a strong decrease in viscosity between $Wi = 0 \dots 0.04$ for this trap stiffness. The resolution of this regime is currently under experimental investigation and cannot yet be provided here. More importantly, we observe that the viscosity appears to be independent of velocity not only in the linear-response regime of the system but also in the regime $Wi = 0.04 \dots 0.34$ (cf. the blue curve in Fig. 6.1). For even larger driving velocities than the ones illustrated in Fig. 6.1 we expect the viscosity to fall of even further to finally reach the limiting plateau of the pure

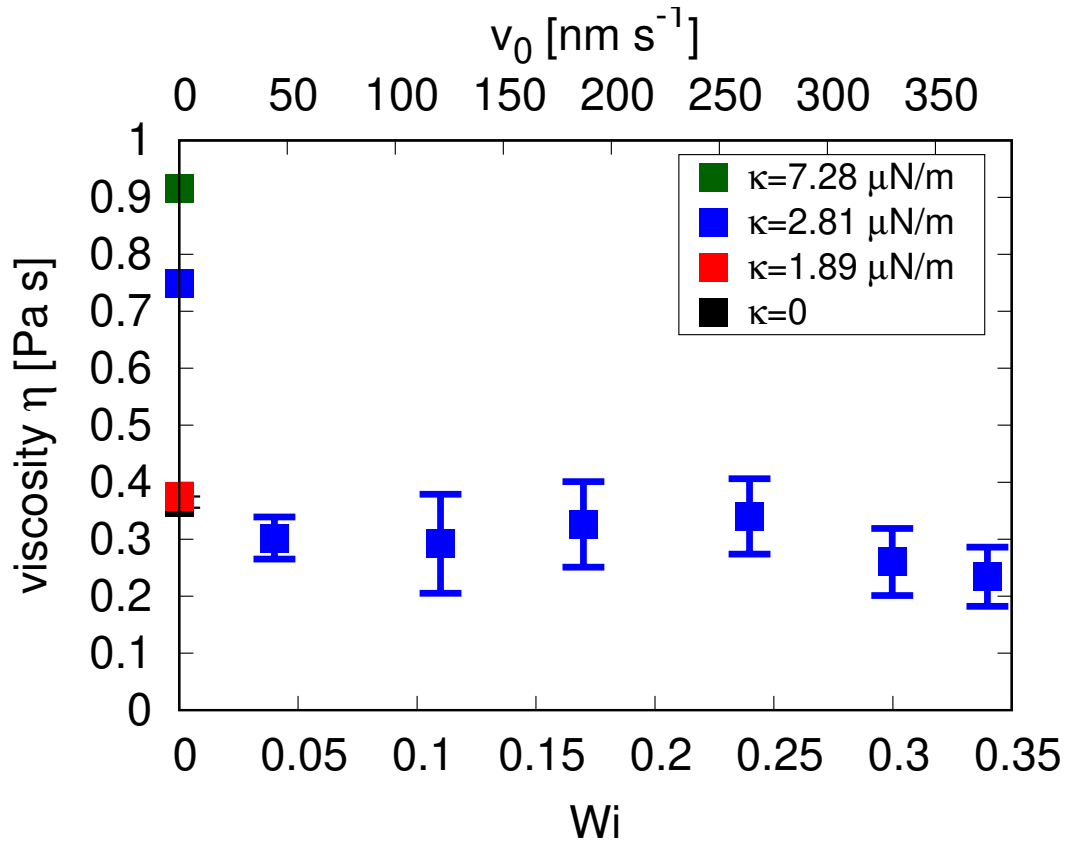


Figure 6.1: Viscosity η obtained from the force balance of friction force and optical force in Eq. (6.3) as a function of trap velocity v_0 and corresponding Weissenberg number. The values at $Wi = 0$ for finite trap stiffness κ are obtained from the linear-response relation in Eq. (4.11). The static value in the absence of the trap is obtained from the mean-squared displacement of a free diffusion measurement. Provision and use of experimental data granted by Johannes Berner (Bechinger group, University of Konstanz). Adapted and reprinted from Ref. [4].

solvent viscosity (i.e. excluding the contribution of the micellar particles). We thus anticipate the full experimental flow curve to exhibit (at least) three plateaus: the linear-response regime, an intermediate transient plateau for finite driving velocities, and the final plateau of the solvent viscosity. Here we investigate the intermediate transient plateau which shows a new harmonic oscillator state with non-trivial fluctuations. This oscillator state is strictly ruled out in equilibrium systems for the case of highly overdamped motion as will be proven below.

6.3 Experimental observations

The experimental system studied in this section is identical to the one for the equilibrium case (for details see Sec. 3.3). We emphasize again that the measurements are conducted under highly overdamped conditions with Reynolds numbers of the

order of 10^{-9} , so that inertial effects in the fluids are negligibly small. Figure 6.2 compares the particle motion in equilibrium ($Wi = 0$) and for nonequilibrium conditions ($Wi = 0.34$). Recall that fluctuations of the particle in nonequilibrium are recorded in the comoving frame around the particle's mean position quantified by $x(t) = \xi(t) - \langle \xi(t) \rangle$. As observed earlier the particle behaves as an almost ideal random walker in equilibrium (see the upper panel in Fig. 6.2 and the distribution function follows the Boltzmann distribution in that case (see Fig. 3.3). In contrast, the nonequilibrium trajectory shown in the lower panel of Fig. 6.2 looks different on both the qualitative and quantitative level. We observe strong differences in the fluctuations around the mean particle position. In the driven state the fluctuations appear to be more involved showing and the trajectories show an almost oscillatory-like motion (if we would smoothen out the trajectory). On the other hand, the particle reaches values of displacements that are highly unlikely in its equilibrium counterpart. This fact is also reflected in the probability distribution of particle positions that exhibits considerable deviations from the corresponding equilibrium distribution as illustrated in Fig. 6.3. The unexpected behaviour in the regime of finite but very small Wi is also corroborated by the corresponding mean-squared displacements (MSDs), $\langle (x(t) - x(0))^2 \rangle$, which are shown in Fig. 6.4 for six different Wi . In equilibrium, the MSD grows monotonically and reaches, in the limit of large times t , a plateau value of $2k_B T / \kappa$ (indicated by the horizontal black dashed line) in accordance with the equipartition theorem. In contrast, the MSD curves at finite driving velocities of the trap show a distinct behaviour reaching a maximum value that considerably exceeds the equilibrium long-time value. This is clear indication that the particle can explore a larger configurational space in a moving trap compared to a static trap. Another striking feature of the nonequilibrium MSD curves is the apparent nonmonotonicity of the curves at larger times. Note that this behaviour of MSD curves is strictly ruled out in equilibrium as we will show below.

The oscillatory-like behaviour of trajectories can be made even more evident by considering the average particle position $\langle x(t) \rangle_{x_0}$ over time if the particle has been released from a certain initial position x_0 . The so-called mean conditional displacements (MCDs) can be defined in terms of the conditional probability $P(x, t | x_0, 0)$ as

$$\langle x(t) \rangle_{x_0} \equiv \int dx P(x, t | x_0, 0) x. \quad (6.4)$$

$P(x, t | x_0, 0)$ is the probability to find the particle at position x at time t , provided that it was at x_0 at time $t = 0$. The previous formal definition applies to the continuous case. In the case of discrete experimental data we may use instead the following weighted sum

$$\langle x(t_n) \rangle_{x_0} = \frac{1}{n(x_0)} \sum_i n(x_i, x_0, t_n) x_i. \quad (6.5)$$

In the discrete case we replaced the conditional probability with the corresponding statistical frequencies $n(x_i, x_0, t_n)$, i.e. the number of (random) occurrences x_i at time

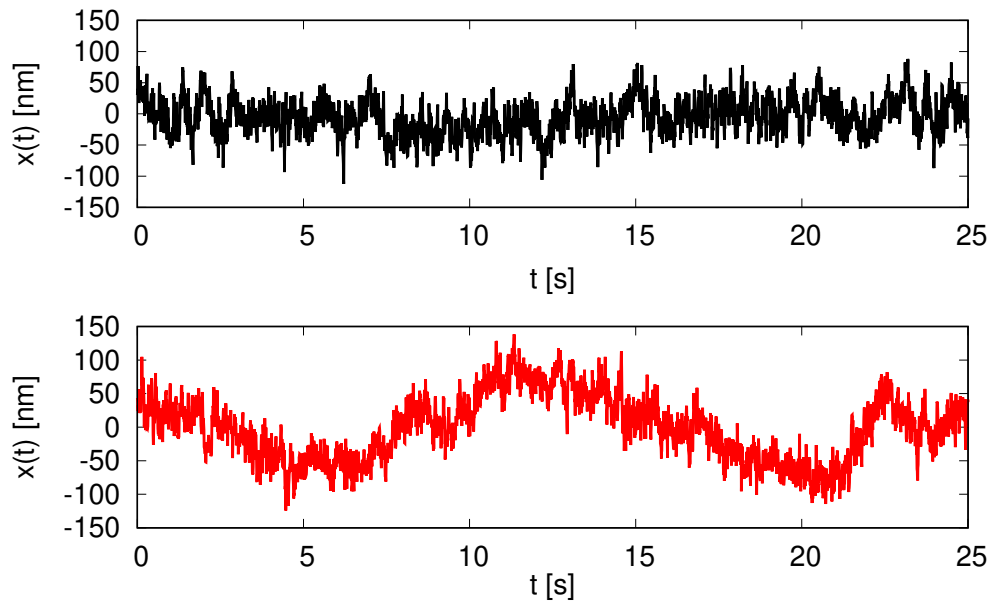


Figure 6.2: Experimental trajectories of a harmonically confined particle for $Wi = 0$ and for finite Wi . The latter is measured in the comoving frame under stationary conditions. In contrast to Newtonian fluids, we observe strong differences in the fluctuations of the two states. Provision and use of experimental data granted by Johannes Berner (Bechinger group, University of Konstanz). Adapted and reprinted from Ref. [4].

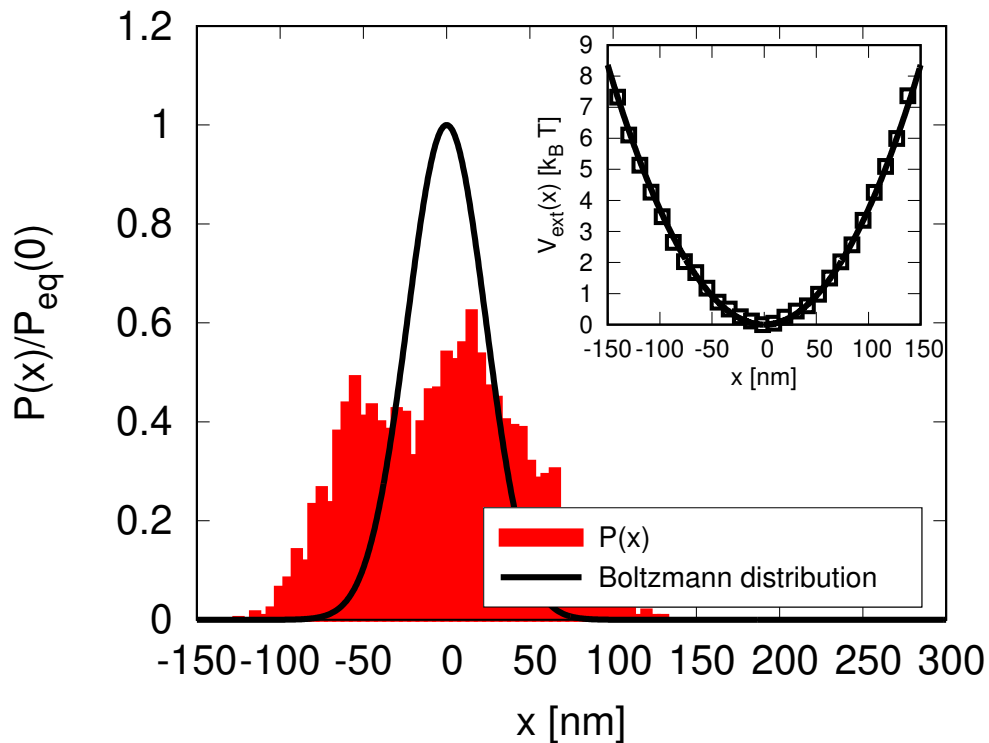


Figure 6.3: Probability distribution $P(x)$ of particle positions in the comoving frame in a wormlike micellar bath out of thermal equilibrium. For comparison we included the Boltzmann distribution of the corresponding equilibrium measurement from which we can extract the trap stiffness κ by using a parabolic fit (solid line) of the measured trap potential (symbols). Adapted and reprinted from Ref. [4].

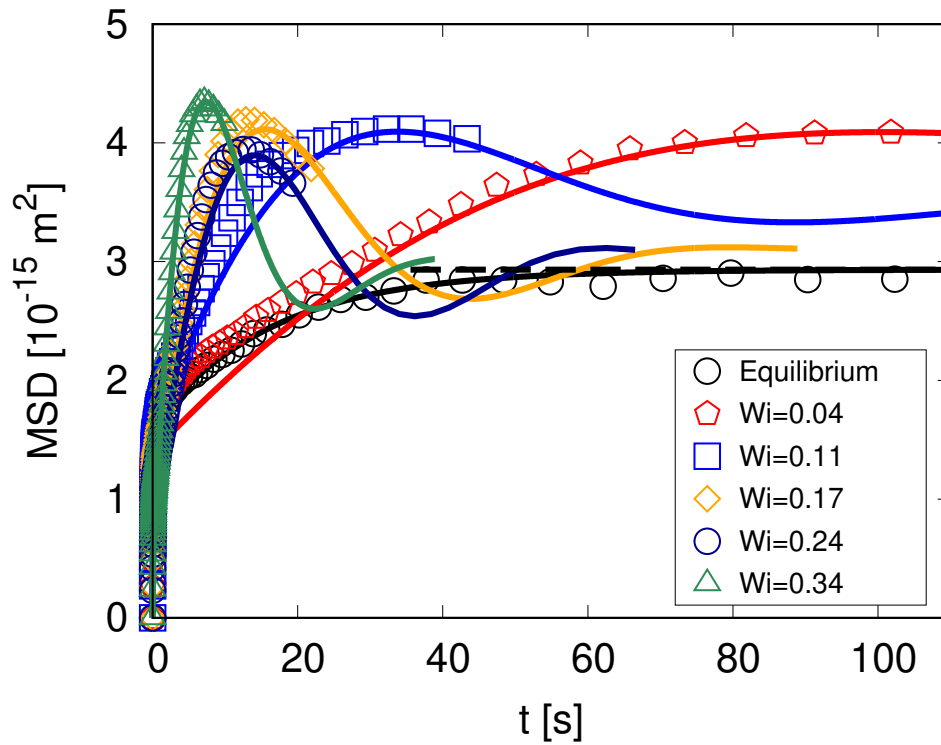


Figure 6.4: Experimental mean-squared displacements in equilibrium and nonequilibrium. In equilibrium the MSD is monotonic and saturates to $2k_B T/\kappa$ (horizontal dashed black line) according to the equipartition theorem. In contrast, in the case of finite driving the MSDs grow much quicker and higher and appear to become nonmonotonic for large times. Provision and use of experimental raw data granted by Johannes Berner (Bechinger group, University of Konstanz). Adapted and reprinted from Ref. [4].

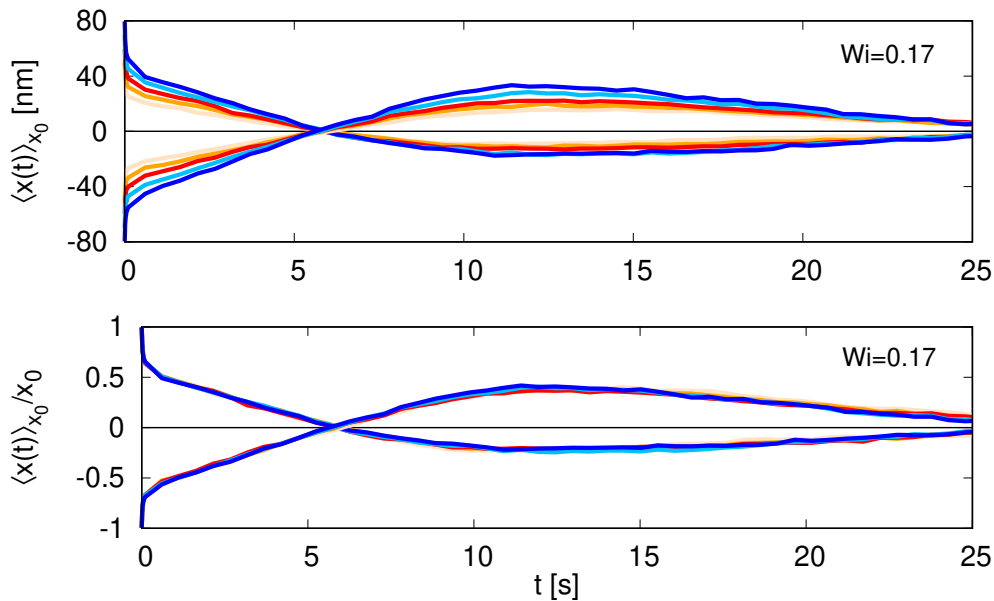


Figure 6.5: Upper panel: The experimental MCDs are computed for various intervals $\Delta x_0 = 10$ nm of initial conditions x_0 . Lower panel: After normalisation on x_0 the curves collapse to a single line. Reprinted from Ref. [4].

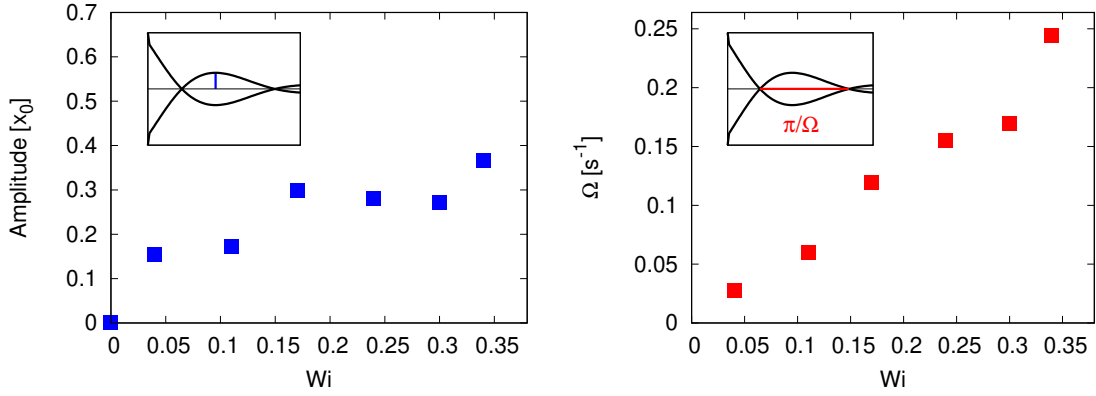


Figure 6.6: Oscillation amplitude and frequency of the MCD curves (shown in Fig. 6.7) over Weissenberg number. The insets illustrate how these quantities are derived from experimental data. Both curves decrease with decreasing Weissenberg number, i.e. towards equilibrium. The decreasing frequency implies that the relaxation of the particle’s position is particularly slow at small Wi . We estimated the frequency from the first half cycle of oscillations due to the limited length of experimental trajectories. Reprinted from Ref. [4].

step t_n if the initial position x_0 was fixed at $t_0 = 0$. It is normalized by $n(x_0)$, which gives the number of (random) occurrences of equal initial displacements $x(t_n) = x_0$ in a given experimental trajectory. Notably, the sum in Eq. (6.5) runs over all possible outcomes x_i of the experiment. For decent statistics it is convenient to collect the occurrences of initial points in intervals of $\Delta x_0 = 10 \mu\text{m}$ and average over them. Furthermore, we note that when computing the MCD curves one should leave out the values around zero that are within the experimental uncertainty of spatial resolution.

The experimental MCD curves are computed from (long) trajectories for different intervals Δx_0 of starting points. Note that the length of experimental trajectories is limited not only by the length of the sample cell used in the experiment but also by the arrangement of mirrors used to deflect the laser spot. The distance that can be covered by the particle in the bulk medium is roughly $20 \mu\text{m}$. This restricts the numerical analysis of observables to a certain point in time which decreases with increasing Weissenberg number. It is important to emphasize that the MCD curves scale linearly in the initial condition x_0 . This observation is verified in Fig. 6.5 where we assembled the curves in intervals of $\Delta x_0 = 10 \mu\text{m}$ at $Wi = 0.17$. After normalisation on the respective initial condition x_0 the curves collapse almost perfectly to a single line (cf. lower panel in Fig. 6.5). Note that the linearity of MCDs in initial condition x_0 is also found for the other Weissenberg numbers as considered in this chapter. The property is significant as it motivates the usage of a linear equation in x of the form of Eq. (5.87). Moreover, it allows us to average over the normalised curves with positive and negative initial condition x_0 to improve overall statistics.

This procedure is performed for six different Weissenberg numbers and we illustrate the results in Fig. 6.7. The first panel, $Wi = 0$, shows the equilibrium behaviour

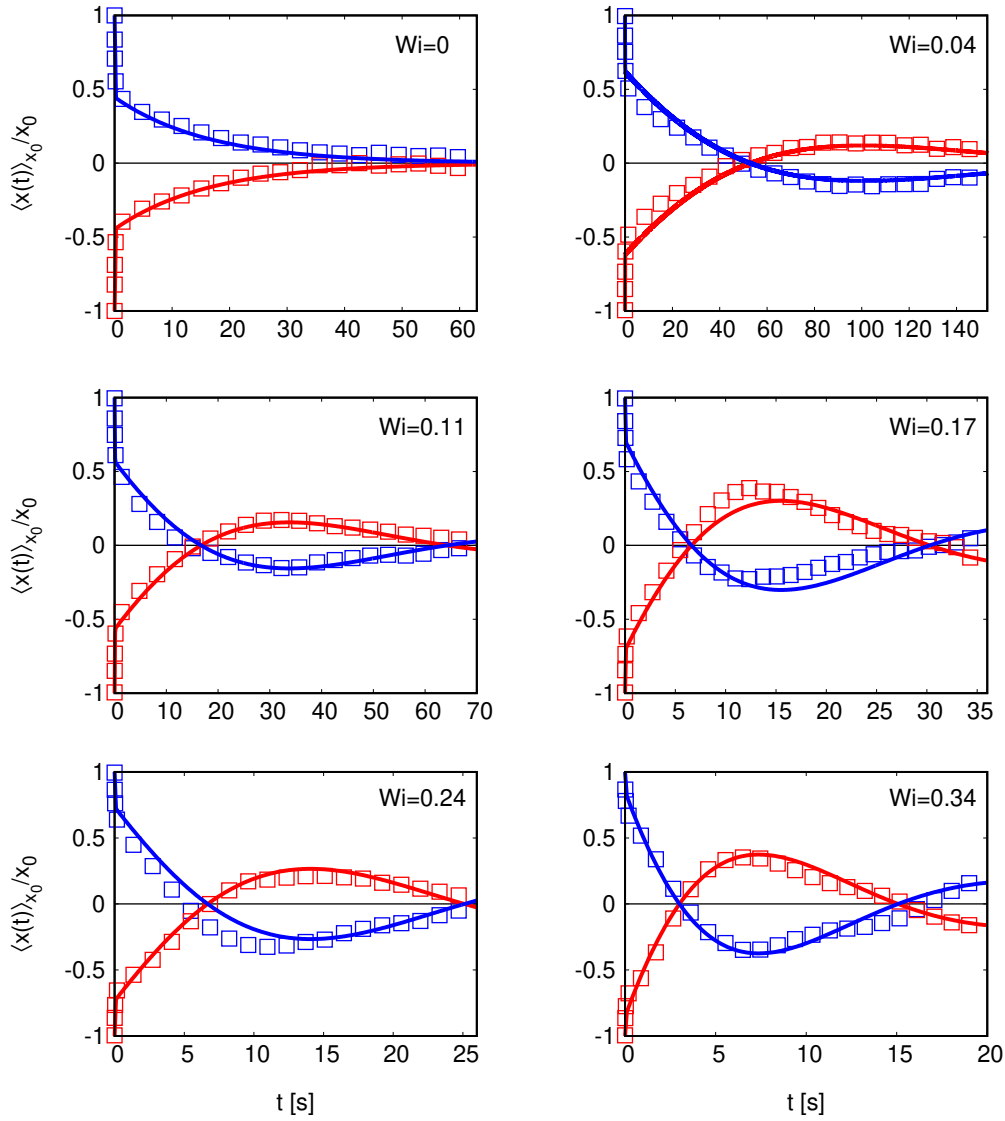


Figure 6.7: Mean-conditional curves in equilibrium and at finite driving of the trap. In equilibrium, the MCD relaxes exponentially, as expected for any complex fluid under overdamped conditions. For finite driving, MCDs show pronounced oscillatory behaviour, which, especially for small Wi , drastically increases the system's correlation time (e.g., more than 150 s for $Wi = 0.04$). Provision and use of experimental data granted by Johannes Berner (Bechinger group, University of Konstanz). Adapted and reprinted from Ref. [4].

of the particle in a static trap. As expected for a highly overdamped system the MCD decays monotonically, exhibiting a rapid initial decay and a subsequent slower exponential-like decay. This kind of two-step behaviour is intuitively clear: When being released from its initial condition x_0 , the particle initially feels only the low friction force induced by the solvent molecules but a strong restoring force due to the optical trap. On a larger time scale, the particle is affected by the viscoelasticity of the medium and the interaction with micellar particles increases the friction force. Combined with the confined motion in the trap the particle position relaxes monotonically to zero on a time scale roughly given by the ratio of the particle's friction and the trap stiffness κ . In equilibrium, this behaviour is expected as the Smoluchowski operator, including interactions between the colloidal probe and the surrounding micellar particles, has real negative eigenvalues. The MCD curve is thus a sum of positive exponentially decaying functions as we will prove below. For finite driving velocities, the MCD curves in Fig. 6.7 are qualitatively different. They do not decay monotonically, but show oscillations whose amplitudes increase with Weissenberg number. Most interestingly, the oscillation period appears to be extremely large for small driving velocities (about 100s for $Wi = 0.04$, the slowest drive accessible in the experiments). In the regime of small driving velocities the particle position relaxes much slower than in equilibrium. It is noteworthy to point out that even in nonequilibrium the MCDs are symmetric and there is no difference whether the particle is released from a positive or negative value of x_0 . In Figure 6.6, we show the dependence of amplitude and frequency of oscillations over Weissenberg numbers. Both quantities exhibit a gradual decrease as equilibrium ($Wi = 0$) is approached.

6.4 Negative memory modes

How can we understand the origin of particle oscillations in an overdamped system? In order to answer this question, we recall that on the Brownian diffusion time scale, the particle's motion is a balance of a frictional force, an optical force, and a stochastic 'noise'. For a viscoelastic bath, the frictional force at time t is in general a nonlinear functional $\mathcal{G}\{\dot{x}(t') + v_0\}_{t' \leq t}$ of the past trajectory, and so is the noise. In the previous section, we observed that the experimental MCD curves scale linearly in initial position x_0 . This supports the idea of a linear equation of motion and we may use the phenomenological Langevin equation derived in Eq. (5.87). In the overdamped limit we may drop the inertial term and obtain the first-order differential equation

$$\int_{-\infty}^t ds \Gamma^{(v_0)}(t-s) \dot{x}(s) = -\kappa x(t) + f^{(v_0)}(t). \quad (6.6)$$

The phenomenological equation used here is in contrast to other approaches which can be deployed to describe nonlinear stochastic systems [54, 100, 135–137]. Formally, the velocity-dependent memory kernel $\Gamma^{(v_0)}$ is the functional derivative of the

Wi	κ	γ_∞	γ_0	τ	γ_1	τ_1	γ_2	τ_2
0	2.8	0.18	20.6	9.1	–	–	–	–
0.04	2.3	0.19	6.8	25.0	-1135.1	27.0	–	–
0.11	2.3	0.19	5.3	28.0	-204.5	17.8	109.3	10.0
0.17	2.6	0.18	6.5	28.0	-67.3	15.0	17.3	2.0
0.24	2.7	0.21	7.1	14.8	-126.4	11.0	23.0	2.1
0.34	2.7	0.18	6.0	16.0	-84.1	12.0	6.4	0.4

Table 6.1: Values of parameters as used in Fig. 6.4 and Fig. 6.7, respectively. The trap stiffness κ is given in units of $\mu\text{N/m}$, friction coefficients γ are given in units of $\mu\text{Ns/m}$, and memory relaxation times τ in s.

average of \mathcal{G} around the nonequilibrium steady state,

$$\Gamma^{(v_0)}(t-s) = \left. \frac{\delta \langle \mathcal{G} \{ \dot{x} + t \} (t) \rangle}{\delta \dot{x}(s)} \right|_{\dot{x}=0}. \quad (6.7)$$

A similar formal definition is applicable to the noise $f^{(v_0)}$, which is then independent of \dot{x} and $\langle f^{(v_0)}(t) \rangle = 0$. In Chapter 5, we approximated \mathcal{G} by a series expansion in orders of velocities $\dot{x}(t) + v_0$ (see Sec. 5.3 and the initial equation (5.42) of the phenomenological abstraction). The nonlinearity of \mathcal{G} makes the transformation into the comoving frame as well as the linearization nontrivial. As a consequence, the memory kernel of the linearized equation in the comoving frame is a function of the dragging velocity². In this linearized phenomenological model, we can compute the MCD curves directly from Eq. (6.6),

$$\langle \hat{x} \rangle_{x_0}(s) = \frac{x_0 \hat{\Gamma}^{(v_0)}(s)}{s \hat{\Gamma}^{(v_0)}(s) + \kappa}, \quad (6.8)$$

with Laplace transforms $\hat{h}(s) = \int_0^\infty dt e^{-st} h(t)$. It is noteworthy that velocities average to zero for $t < 0$, e.g. by preparing the system at $t = 0$ in position x_0 in the nonequilibrium steady state. Equation (6.8) uniquely relates the MCD curve to the nonequilibrium memory kernel $\Gamma^{(v)}$, i.e. knowledge of one of the quantities implies knowledge of the other. On the other hand, this relation is independent of noise $f^{(v)}$. An accurate description of the experimental MCD curves is thus reduced to finding a suitable model of the nonequilibrium memory kernel $\Gamma^{(v)}$. In fact, solving Eq. (6.8) for $\Gamma^{(v)}$ and a numerical Laplace transformation of the experimental MCD curve reveals that the experimental memory kernel in nonequilibrium is no longer positive for all times t as opposed to the equilibrium case.

In equilibrium, well-established models for the memory kernel $\Gamma^{(0)}$ have been developed by Maxwell [138] and Jeffreys [51, 139], which consider a memory time τ ,

²In a sense, this is the natural nonequilibrium extension to the statement that the memory kernel depends on trap stiffness κ in the static case.

$$\Gamma^{(0)}(t) = 2\gamma_\infty\delta(t) + \frac{\gamma_0 - \gamma_\infty}{\tau}e^{-\frac{t}{\tau}}. \quad (6.9)$$

Here, γ_∞ and γ_0 are friction coefficients at infinite and zero frequencies, respectively. In this effective model one assumes a separation of time scales between interactions of the probe particle with solvent molecules and with other Brownian particles. While the former interactions form the Markovian part of the memory kernel and have only an impact on the tracer particle at time t , the latter interactions are non-Markovian and their history, characterized by the relaxation time τ , influences the future dynamical evolution of the probe. Note that the time integral over the memory kernel equals γ_0 which can be referred to as the zero-shear friction coefficient. The friction coefficients and relaxation time of this model can now be adjusted in such manner to obtain best agreement with the experimental data. The best fit result is shown in Fig. 6.7 in the form of solid lines. As expected, after a rapid initial decay the MCD decays monotonically to zero in accordance with the experimental curve. Note that the parameters are provided in Table 6.1. The friction coefficient $\gamma_0 = 20.6 \mu\text{Ns/m}$ can be recast in the corresponding zero-shear viscosity via $\eta = \frac{\gamma_0}{6\pi R} = 0.8 \text{ Pa s}$ which is in good agreement with the value we found in Fig. 6.1 from the numerical extrapolation of curves in Fig. 3.12. The relaxation time $\tau = 9.1 \text{ s}$ is of the order of seconds as expected for the micellar system.

The nonequilibrium MCD curves, however, cannot be grasped within the model of Eq. (6.9). Such a model always leads to monotonically decaying MCD curves in agreement with equilibrium statistical mechanics. In overdamped dynamics, the Smoluchowski equation describes the time evolution of the probability function $P(\mathbf{X}, t)$ of a interacting constituents in a system. We have already become familiar with this important equation in Sec. 3.2.3 and here we want to exploit some general properties of the Smoluchowski operator to prove the absence of oscillations in the equilibrium MCDs. Recall that the adjoint of the Smoluchowski operator is Hermitian with respect to the weighted inner product (weighted with the equilibrium probability distribution P_{eq}) [18]

$$\langle g^* \Omega^\dagger h \rangle_{\text{eq}} = \langle h \Omega^\dagger g^* \rangle_{\text{eq}} = - \left\langle \sum_{ij} \frac{\partial g^*}{\partial \mathbf{r}_i} \cdot \mathbf{D}_{ij} \cdot \frac{\partial h}{\partial \mathbf{r}_j} \right\rangle_{\text{eq}}. \quad (6.10)$$

The eigenvalues of Ω^\dagger are thus real and the set of eigenfunctions $\Omega^\dagger \phi_n = \lambda_n \phi_n$ for a orthogonal basis, i.e. for normalised functions fulfill $\langle \phi_n^* \phi_m \rangle_{\text{eq}} = \delta_{nm}$. By definition the microscopic diffusion matrices \mathbf{D}_{ij} are positive semi-definite [38], and consequently we find Ω^\dagger to be negative semi-definite

$$\langle g^* \Omega^\dagger g \rangle_{\text{eq}} \leq 0 \quad (6.11)$$

i.e. $\lambda_n \leq 0$ for any n . All modes are strictly overdamped, and we can express any equilibrium correlation function $\langle g(t)g(0) \rangle_{\text{eq}}$ as a sum of positive exponentially

decaying functions

$$\langle g(t)g(0) \rangle_{\text{eq}} = \langle g^* e^{\Omega t} g \rangle_{\text{eq}} = \sum_n |c_n|^2 e^{\lambda_n t} \quad (6.12)$$

where we expanded the arbitrary phase space observable $g = \sum_n c_n \phi_n$ in the eigenbasis of the Smoluchowski operator. In Laplace space it is easy to see that

$$\frac{\langle \hat{x}(s)x_0 \rangle_{\text{eq}}}{\langle x^2 \rangle_{\text{eq}}} = \frac{\langle \hat{x} \rangle_{x_0}(s)}{x_0}. \quad (6.13)$$

In time domain this relation translates into (we may use $\langle x^2 \rangle_{\text{eq}} = (\beta\kappa)^{-1}$ with $\beta = (k_B T)^{-1}$ the inverse temperature)

$$\frac{\langle x(t) \rangle_{x_0}^{\text{eq}}}{x_0} = \beta\kappa \langle x(t)x(0) \rangle_{\text{eq}}. \quad (6.14)$$

Consequently, the equilibrium MCDs are strictly monotonic and show no oscillatory behaviour in a complex suspension. A similar argumentation can be used to prove that the equilibrium memory kernel is a positive function for all times t under overdamped conditions. We recall that the fluctuation-dissipation theorem relates the linear response function of a system to a small external perturbation to its thermal equilibrium fluctuations. For the trapped Brownian particle we have

$$\Gamma^{(0)}(|t|) = \langle f(t)f(0) \rangle_{\text{eq}}. \quad (6.15)$$

By virtue of the same arguments as before, $\Gamma^{(0)}$ is positive for all times t .

The correct description of the nonequilibrium MCD curves requires the memory kernel to be negative in a certain regime of time. Aiming at a simple model, we amend Eq. (6.9) by another generic exponential term to account for finite driving,

$$\Gamma^{(v_0)} = 2\gamma_\infty \delta(t) + \frac{\gamma_0 - \gamma_\infty - \gamma_1}{\tau} e^{-\frac{t}{\tau}} + \frac{\gamma_1}{\tau_1} e^{-\frac{t}{\tau_1}}. \quad (6.16)$$

Notably, the parameters of this kernel are now itself a function of dragging velocity v_0 or Weissenberg number, respectively. Note we use $\tau_1 > \tau$ throughout the following analysis³. Most importantly, the new coefficient γ_1 is negative, so that $\Gamma^{(v)}(t)$ is negative for long times in contrast to the equilibrium kernel. The concept of negative memory has been used in other fields of rheology as well, e.g. in the description of so-called stress overshoots. These overshoots can occur when macroscopic shear is applied abruptly to a system and the resulting stress encounters a maximum as a function of time before the yield stress is finally overcome [134, 140–143]. The phenomenon can be linked to the concept of negative memory as was demonstrated in Refs. [134, 143] starting from a microscopic starting point.

³This condition ensures that the non-Markovian contribution of the memory kernel is positive at $t = 0$ provided that $\gamma_0 > \gamma_\infty$.

Similar to the equilibrium case we can vary the parameters of the model in Eq. (6.16) to find best agreement with the experimental curves. In the regime of small driving velocities we assume the connection between the memory kernel and the viscosity measured in the flow curve to be approximately true⁴, i.e.

$$\gamma_0 = \int_0^\infty dt \Gamma^{(v)}(t) \approx 6\pi\eta R. \quad (6.17)$$

This reduces the parameter space to the variation of four parameters. We also note that for larger driving, above $Wi = 0.11$, we used one additional exponential term in contrast to Eq. (6.9) to obtain quantitative agreement with the experimental curve. The results with the extension of Jeffreys model are shown in Fig. 6.7. The theoretical curves now show the oscillatory behaviour which was observed in the experimental MCDs and almost perfectly agree with their experimental counterparts. Notably, the final relaxation in the theoretical MCD curves can be much larger than the individual relaxation times given in Table 6.1. In contrast to the negative memory modes found in the above mentioned studies of macroscopic shear, we study the interplay of frictional forces with optical restoring forces. Oscillations as observed in the nonequilibrium MCDs are typically features of inertia, as second-differential equations (Newton's equation of motion) easily allow for sinusoidal solutions. The notion of inertia allows a reconsideration of the overdamped generalized Langevin equation (6.6). Indeed, we can mathematically recast the first-order overdamped equation of motion into a second-order differential equation by partial integration. We find

$$\int_{-\infty}^t ds \mathcal{M}^{(v_0)}(t-s)\ddot{x}(s) = -\gamma_0\dot{x}(t) - \kappa x(t) + f^{(v_0)}(t). \quad (6.18)$$

In this equation, the friction coefficient γ_0 at zero frequency appears, and we identify $\mathcal{M}^{(v_0)}(t-s) \equiv -\int_{-\infty}^s dh \Gamma^{(v_0)}(t-h)$ with the memory kernel of inertia. Noteworthy, the memory of the system is now related to inertial effects while the friction coefficient is time-independent and reduces to the zero frequency contribution of the memory kernel. The effective mass of the system may now be interpreted as the zero-frequency contribution of $\tilde{\mathcal{M}}^{(v_0)}(\omega)$ and by mimicking Newton's equation of motion we define

$$m \equiv \int_0^\infty dt \mathcal{M}^{(v_0)}(t) = -(\gamma_0 - \gamma_\infty - \gamma_1)\tau - \gamma_1\tau_1. \quad (6.19)$$

In equilibrium, the memory kernel $\Gamma^{(0)}$ in Eq. (6.16) is necessarily a sum of positive exponentially decaying functions and consequently m strictly takes a negative value. In nonequilibrium, however, the *defined* mass m is positive if the amplitude γ_1 is negative and $\tau_1 > \tau$. For instance, we find a mass of $m = 2.1$ g for the parameters

⁴Strictly speaking, this relation is only true in the linear-response regime and beyond it no analytical connection between the memory kernel $\Gamma^{(v)}$ and the (microrheological) viscosity can be established. In the variation of parameters, we allowed γ_0 to vary within the range of errorbars of Fig. 6.1 which seems to be a reasonable approximation of the uncertainty of this parameter beyond the actual linear-response regime.

used for $Wi = 0.04$ in Table 6.1. This corresponds to an effective mass 10^{10} times the actual (physical) mass of the particle. Due to the negative memory, the particle thus behaves like a massive particle with inertia even in the overdamped limit.

With the given model of memory friction in Eq. (6.16) at hand, we observe that Eq. (6.6) shows two distinct types of solutions of the MCD curves. Depending on the exact parameter values, there are either purely exponential solutions, $\sim e^{-|\nu|t}$ or damped oscillating modes, $\sim e^{-(|\nu|+i|\Omega|)t}$, characterized by a frequency Ω . In particular, oscillatory solutions only occur in a finite range of κ (with all other parameters fixed). Beyond this narrow range of κ the MCD curves exhibit a purely exponential decay. The necessity of resonant conditions provides a possible explanation why such oscillations have not been observed in previous experiments in a viscoelastic colloidal suspension [111]. Indeed, a variation of κ in the experiment at finite Wi indicates that there is a resonant value of trap stiffness. In Fig. 6.7, we show the experimental MCD curves at $Wi = 0.24$ for three different values of κ . Obviously, the trap stiffness used in the creation of Fig. 6.7 shows a particularly large oscillation amplitude, while larger and smaller stiffnesses show less pronounced oscillatory behaviour. A critical value of trap stiffness can be analytically determined to

$$\kappa_c = \frac{\gamma_0 - 2\gamma_1}{\tau_1 - \tau} \pm \frac{2\sqrt{\gamma_1(\gamma_1 - \gamma_0)}}{\tau_1 - \tau}. \quad (6.20)$$

Here, we used the memory kernel in Eq. (6.16) and neglected the contribution of the solvent ($\gamma_\infty = 0$). The analytical form in Eq. (6.20) shows a critical point at $|\gamma_1| = 0$, from which κ_c grows as a square root in $|\gamma_1|$. The upper limit corresponds to the physical situation where the particle moves at constant velocity (constant strain rate conditions). Oscillatory behaviour in the MCDs is not possible because the optical restoring force is so strong that the particle cannot overshoot its mean position. On the other hand, if the trap is too soft the particle dynamics becomes diffusive and due to the very weak restoring force the particle slowly relaxes to its mean position in the MCD. In both cases, oscillating modes are thus excluded. While the principal behaviour of the MCD curves upon varying trap stiffness is captured by Eq. (6.20), its predictive power in terms of a dynamical phase diagram [4] is limited. The reason for it is that in a complex bath memory kernel is a function of κ itself (recall the results from Sec. 3.2.3). In this way, Eq. (6.20) must be regarded as an implicit function of κ . Due to the lack of knowledge of the exact κ -dependence of the memory kernel, we do not provide a phase diagram here.

By virtue of the overdamped generalized Langevin equation (6.6), we can also compute the mean-squared displacement. It can be computed as the inverse Fourier transform of the spectral density

$$\langle (x(t) - x(0))^2 \rangle = \frac{1}{\pi} \int_{-\infty}^{\infty} d\omega (1 - e^{i\omega t}) \frac{\langle |\tilde{f}^{(v_0)}(\omega)|^2 \rangle}{|\omega \tilde{\Gamma}^{(v_0)}(\omega) - i\kappa|^2}, \quad (6.21)$$

with Fourier transforms $\tilde{h}(\omega) = \int_{-\infty}^{\infty} dt e^{-i\omega t} h(t)$. The MSD involves the noise correlator in contrast to the noise-free MCD curves in Eq. (6.8). In equilibrium, the sec-

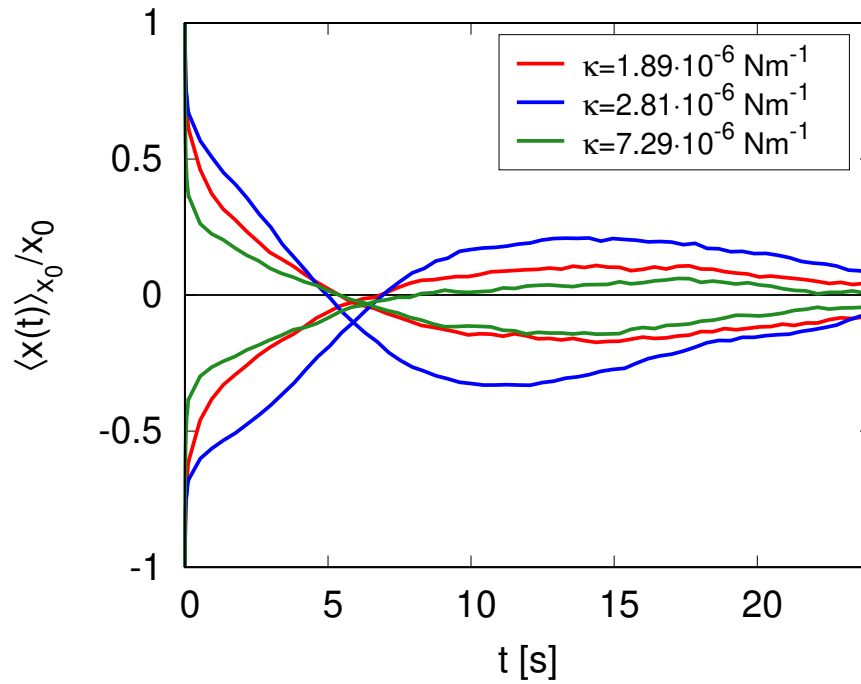


Figure 6.8: Variation of trap stiffness in the experimental mean-conditional displacement. The curves are plotted at the same Weissenberg number $Wi = 0.24$. The blue curve corresponds to the value of κ used in the creation of Fig. 6.7 and seems to show a resonant-like behaviour. Provision and use of experimental data granted by Johannes Berner (Bechinger group, University of Konstanz). Reprinted from Ref. [4].

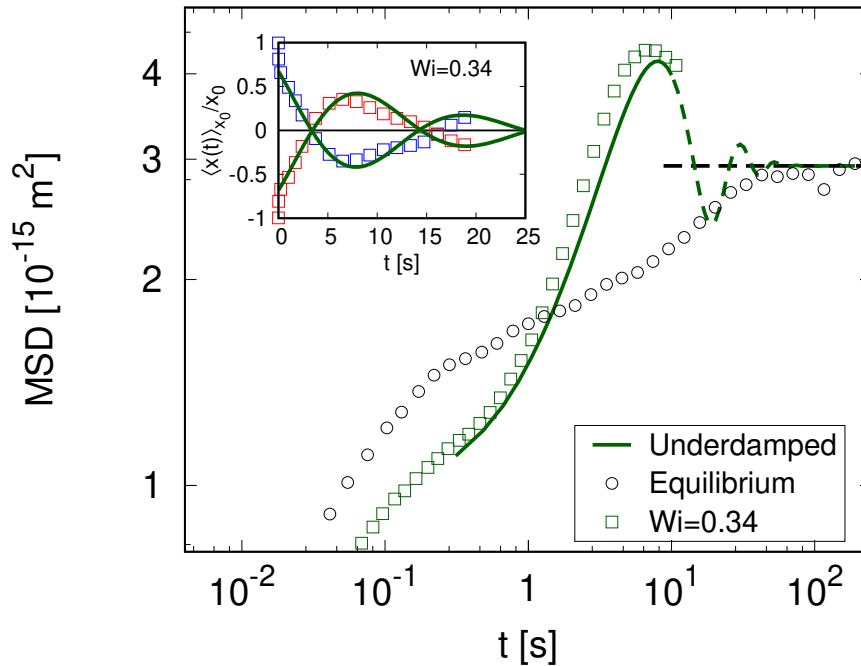


Figure 6.9: Solution of a (stochastic) underdamped harmonic oscillator of a massive particle for $Wi = 0.34$. The main graph shows the MSD (compare Fig. 6.4 and note the log scale), whereas the inset shows the corresponding MCD (compare Fig. 6.7 for the same Wi). Reprinted from Ref. [4].

ond moment of the noise is linked to the friction memory kernel via the fluctuation-dissipation theorem (see Eq. (3.25)). In nonequilibrium this relation no longer holds in general. For small driving velocities, however, it seems to be a good approximation as is shown in Fig. 6.4 by the solid lines where we used the same parameters as in the creation of the MCD curves and obtain remarkable agreement with the experiment⁵.

Note that the onset of oscillations in the nonequilibrium steady state was also observed in a semi-dilute polymer solution [4]. The observation of oscillations in two independent systems suggests the effect to be generic for viscoelastic solvents with large structural relaxation times.

We close this section by reproducing the experimental results at $Wi = 0.34$ with a model system of a (stochastic) underdamped harmonic oscillator. This picks up on the idea that the overdamped equation of motion (6.6) with negative memory modes corresponds to an underdamped equation of motion (recall Eq. (6.18)) with (positive) particle mass m . One can test this analogy quantitatively by using an underdamped oscillator in an equilibrium bath. The underdamped equation of motion in the Markovian limit is given by

$$m\ddot{x}(t) + \gamma\dot{x}(t) = -\kappa x(t) + f(t). \quad (6.22)$$

The noise term is assumed white Gaussian, i.e. its statistical properties are fully specified by its first two moments, $\langle f(t) \rangle_{\text{eq}} = 0$ and $\langle f(t)f(t') \rangle_{\text{eq}} = 2\gamma k_B T \delta(t - t')$. As shown in Fig. 6.9, the results of this simple model are in excellent agreement with the experimental MSD and MCD curve, respectively. The parameters used for the solid lines in this figure are $\kappa = 2.8 \mu\text{Nm}^{-1}$, $m = 32 \text{ mg}$, and $\gamma = 5 \mu\text{Nsm}^{-1}$. Note that the value of the friction coefficient γ is of the order of the nonequilibrium zero-frequency coefficient γ_0 in Table 6.1. Since the short-time behaviour is fundamentally different in this model, we shifted the theoretical curves by an offset time $t_0 = 3.0 \text{ s}$ into negative t -direction to map this behaviour accordingly. Strong effects of inertia allow the particle to temporarily explore a larger part of phase space and we see the typically overshoot behaviour in the MSD in the main graph of Fig. 6.9. For very large times, the MSD of the massive particle converges to its equilibrium value $2k_B T/\kappa$. The behaviour of the complex nonequilibrium system is thus well described by a single parameter, the effective mass. The notion of effective mass has proven useful before, e.g., in the description of conduction electrons [144].

⁵We allowed a slight variation of κ which can be attributed to the enhanced nonequilibrium fluctuations and/or a small anharmonicity of the potential shown in Fig. 6.3

γ	γ_{b_1}	γ_{b_2}	$V_{0,1}$	$V_{0,2}$	$d_{0,1}$	$d_{0,2}$
0.25	1	10	4	8	4	50

Table 6.2: Values of parameters as used in Fig. 6.11 and Fig. 6.12, respectively. The potential barriers $V_{0,i}$ are given in units of $k_B T$, and the interaction length scales $d_{0,i}$ in units of $\sqrt{\frac{k_B T}{\kappa}}$.

6.5 Stochastic Prandtl-Tomlinson model in nonequilibrium

The stochastic PT model provided an accurate description of the measured experimental observables as outlined in Sec. 3.5. Here, we want to revisit the model and study its properties in the nonequilibrium steady state where the harmonic confinement potential of the probe particle is dragged at constant velocity v_0 . Again, by using the force balance between the optical restoring force and the friction force, we can define

$$\gamma(v_0) = \lim_{t \rightarrow \infty} \frac{|\langle F \rangle(t)|}{v_0} = \frac{\kappa |\langle x \rangle(t) - v_0 t|}{v_0}. \quad (6.23)$$

We expect $\gamma(v_0)$ to be a function of velocity as we now consider the full response force beyond the linear-response regime. In the linear-response regime, $v_0 \rightarrow 0$, the curves must converge to the $s = 0$ value of the corresponding Laplace-transformed memory kernel, i.e. $\lim_{v_0 \rightarrow 0} \gamma(v_0) = \hat{\Gamma}(s = 0)$ (cf. Eq. (4.11)). Indeed, this behaviour is observed in Fig. 6.10 where we simulate the flow curve for values of κ spanning five orders of magnitude. Note that the values of $\hat{\Gamma}(s = 0)$ obtained from Fig. 3.9 are included as horizontal solid lines in the figure. Overall, the κ -dependence in absolute numbers seems to be largest in the linear-response regime. For dragging velocities beyond this regime, the effective friction experienced by the particle decreases over velocity for any value of κ . The reason for it is that the impact of the coupled bath particle becomes less significant if the tracer particle is strongly driven. Note that in this case the time scale of driving $\tau_D \sim v_0^{-1}$ and the Brownian diffusion time τ_B of the bath particle are well separated. Ultimately, in the limit of very large velocities, $\tau_D \ll \tau_B$, the curves collapse to a single line and reduce to the bare friction coefficient of the probe particle, i.e. $\lim_{v_0 \rightarrow \infty} \gamma(v_0) = \gamma$. In this regime, the bath particle is at rest as seen from the perspective of the tracer particle. Notably, there is a point of intersection between the curves roughly at $v_0 \approx 2$. This behaviour of the flow curve is in contrast to the strict monotonicity of $\lim_{v_0 \rightarrow 0} \gamma(v_0)$ upon varying κ which we illustrated in Fig. 4.2. In the nonlinear-response regime, there is the case that the particle feels less friction in a stiffer trap than in a weaker one.

In the discussion of the experimental flow curve (see Fig. 6.1), we suspected the regime of measurement to be a transient regime, where the viscosity is approximately constant over velocity just as one would expect from the actual linear-response

regime. Such a flow curve behaviour can be mimicked by the stochastic PT model if one couples another bath particle to the confined tracer particle. The second bath particle must exhibit a distinct length scale of interaction with the tracer particle as compared to the scale of the first bath particle. The principal appearance of the flow curve in such a three-particle model is shown in Fig. 6.11 (note the logscale) for a set of model parameters given in Table 6.2. After a strong initial decay beyond the linear-response regime, the flow curve exhibits a transient regime where the particle's friction remains virtually unchanged (see inset). For even larger trap velocities v_0 , the friction coefficient decays further to finally reach the bare friction coefficient (set to $\gamma = 0.25$). While these results are still preliminary, and the experimental system is currently under investigation to resolve the flow curve for even smaller driving velocities, the stochastic PT model with many particles might be a good candidate to qualitatively and quantitatively describe the expected behaviour.

Not surprisingly, the stochastic PT model also exhibits oscillatory behaviour in the MCD curves when the harmonic trap is dragged at finite velocity v_0 . Here, we use again a three particle model with distinct interaction length scales. The MCD curves in Fig. 6.12 are computed from simulated trajectories. The use of two bath particles is convenient to separate the time scale of the equilibrium exponential decay from the time scales of oscillations. On a qualitative level, the stochastic PT model shows the same behaviour as the experimental system in Fig. 6.7. In equilibrium, the particle position relaxes to zero in a monotonic way. It cannot escape the potential well of the interaction potentials which is set to be much higher than the thermal energy $k_B T$ of the particle (see Table 6.2). In nonequilibrium, the particle is actively dragged through the sinusoidal interaction potential which is reflected by the onset of oscillations in the nonequilibrium MCD curves. Note that the plots for the many particle PT model are yet preliminary and allow only for a qualitative comparison with the experimental results. We leave the discussion on a quantitative level for future work. Nevertheless, it appears as if the stochastic PT model could be used to also describe the nonequilibrium properties of the experiment in a convenient fashion.

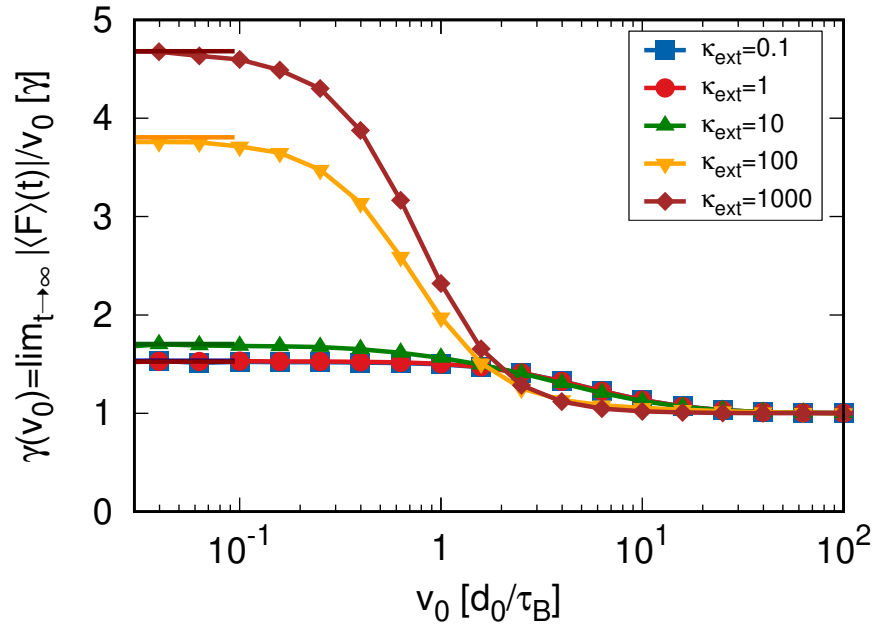


Figure 6.10: Flow curve $\gamma(v_0)$ of the stochastic PT model in units of the probe's bare friction coefficient γ upon varying trap stiffness κ . The parameters are given in the units discussed in Sec. 3.4.4. In the limit of small driving velocities v_0 , the curves asymptotically approach their corresponding linear-response values (cf. Fig. 3.9). For large driving velocities, $v_0 \gg 1$, the curves collapse to a single line and reduce to the bare friction coefficient γ .

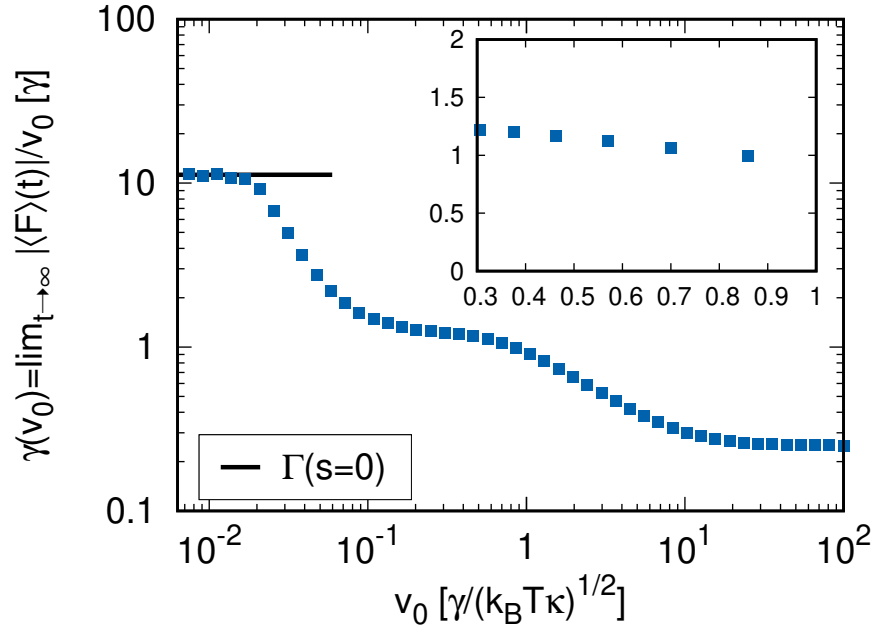


Figure 6.11: Flow curve $\gamma(v_0)$ of the stochastic PT model with two coupled bath particles whose interaction length scales are well separated (note the logscale). The inset shows the magnification of the transient regime where the friction changes only weakly.

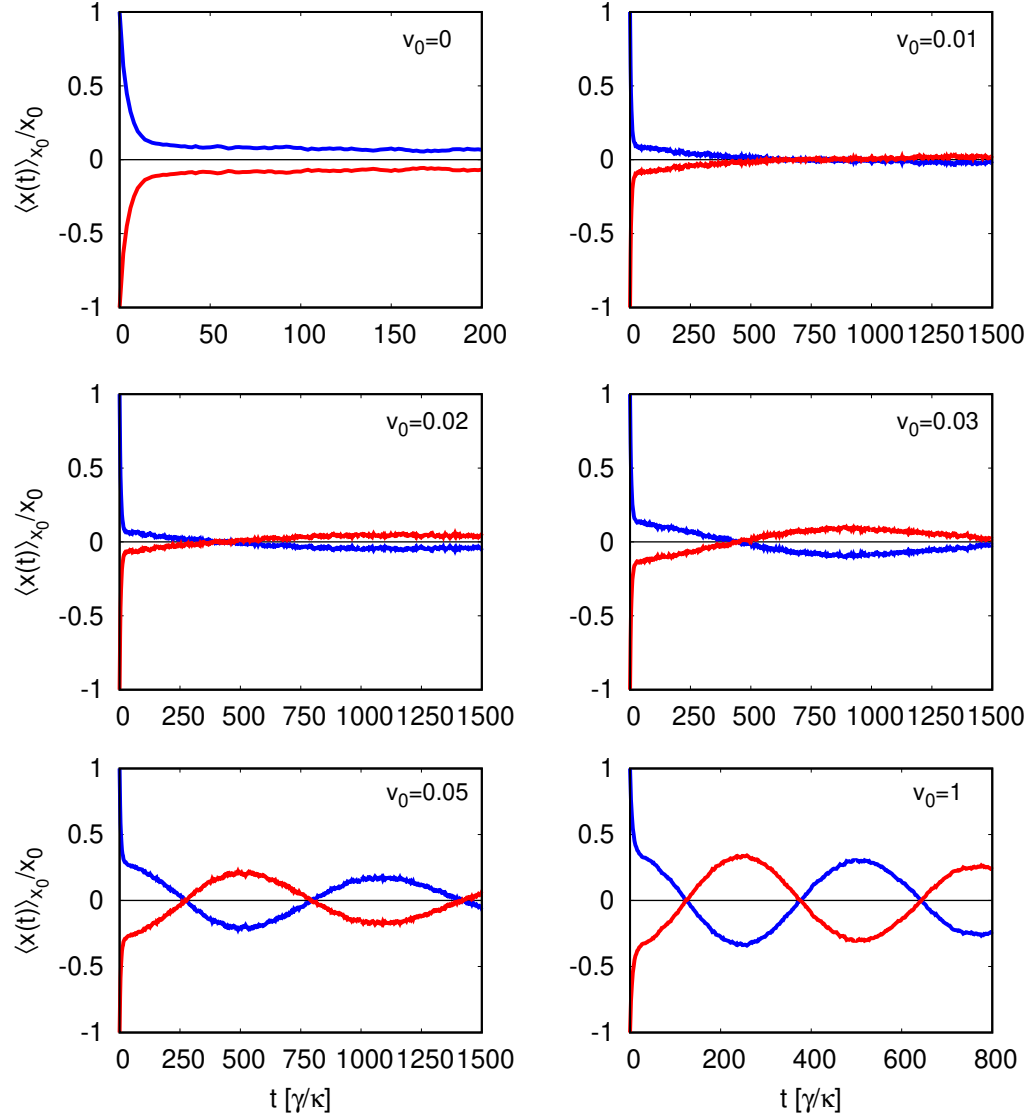


Figure 6.12: Mean-conditional curves in the stochastic PT model in equilibrium and at finite driving of the trap. The harmonically confined tracer particle is coupled to two bath particles with distinct length scale of interaction. In equilibrium, the tracer's position relaxes exponentially. For finite driving, we observe the onset of oscillations as the particle is dragged through the sinusoidal interaction potential.

Summary and outlook

In this thesis, we studied the behaviour of Brownian particles suspended in complex baths. The complexity of the bath was introduced by considering fluids that go beyond a purely viscous impact on the Brownian particle as is commonly assumed for the case of Newtonian solvents. Experimentally such baths are realized by viscoelastic fluids that exhibit a complex microstructure of their own. The elastic properties of these material result in large structural relaxation times that can become comparable to the time scale associated with colloidal probe motion on the mesoscopic scale.

Even in equilibrium the theoretical description of the probe particle's evolution equation must therefore be modified and memory effects need to be taken into account. In equilibrium, well-known projection operator techniques allow to integrate out the bath degrees of freedom. As a consequence, the effective evolution equation of the probe degrees of freedom turn non-Markovian, i.e. dependent on all previous states of the particle. A small time expansion of the friction memory kernel of this generalized Langevin equation revealed that the underlying nonlinear interactions of an equilibrium system are reflected in the linear coefficients of the effective evolution equation. We attributed the intriguing interdependences, such as the dependence of the memory kernel on the external trap stiffness κ , the particle's mass m , or, in the overdamped case, on its bare diffusivity, to a so-called fluctuation renormalization. An investigation of the findings in the experimental system of a harmonically confined colloidal particle suspended in a wormlike micellar bath confirmed the theoretically predicted dependence on the external trap stiffness. We developed a simple model system of two nonlinearly coupled Brownian particles to mimic the interaction between the colloidal particle and the bath. A stochastic Prandtl-Tomlinson model accurately described the experimental results on a quantitative level with insightful model parameters.

We then established a connection of these results to microrheological quantities, such as the friction coefficient or the mobility of a particle. The dependence on the external trap stiffness translated to these physically measurable quantities. This observation as well as the investigation of the limiting cases of a very stiff external confinement potential confirmed the results of previous related work by other authors. In microrheology, the modes of constant velocity and constant force are distinct due to the different origin of fluctuations in a mesoscopic system.

The application of a recently presented novel approach of nonlinear response the-

ory based on path integral techniques allowed us to derive a nonlinear generalized Langevin equation up to third order in probe displacement. While this equation turned out to be exact up to the given order, we used it to abstract a phenomenological equation based on the underlying structure of the equation. A subsequent linearization of the equation in both equilibrium and under nonequilibrium steady state conditions revealed a renormalization of the memory kernel. In equilibrium, the renormalization is of thermal nature and just like for the microscopic starting point we find a dependence on the properties of the external potential. In nonequilibrium, the situation is more complex and already the transformation into the comoving frame is nontrivial. Besides the thermal renormalization of the memory kernel, we found that it also becomes a function of the dragging velocity of the trap in the comoving frame (and so does the noise).

The linearized generalized Langevin equation provided a suitable description of the phenomenon of oscillating modes observed in the experimental system when the trap is dragged at constant velocity through the micellar bath. Indeed, such underdamped modes can be ruled out in an equilibrium overdamped system. In the nonequilibrium case, they render the memory kernel partially negative (over time), so that the overdamped equation of motion suddenly shows the property of an underdamped harmonic oscillator with an effective mass. We closed by revisiting the stochastic Prandtl-Tomlinson model under nonequilibrium steady state conditions. The obtained flow curve and mean-conditional displacement curves appeared to be qualitatively similar to the experimental ones. By extending this simple model system in different ways (e.g. additional particles, a change of the interaction potential between different particles), we believe that the stochastic Prandtl-Tomlinson model might be a suitable candidate to describe the phenomena of complex particle-bath systems both in equilibrium and nonequilibrium. While the resolution of the experimental flow curve over a larger range of velocities is currently under investigation, a modulation of trap stiffness might be useful to create stochastic resonances for the oscillating modes found in the nonequilibrium steady state. We leave the study of these effects to future work.

Zusammenfassung

In der vorliegenden Arbeit wird das Verhalten von Brownschen Teilchen in komplexen Flüssigkeiten untersucht. Die Komplexität der Flüssigkeit ist gegeben durch eine zugrundeliegende nicht-triviale Mikrostruktur der Lösung. Diese erlaubt bei der Bewegung eines Kolloids in der Flüssigkeit nicht nur die Dissipation von Energie, sondern besitzt auch eine elastische Komponente, in der Energie gespeichert werden kann. In diesem Sinne unterscheiden sich komplexe Flüssigkeiten fundamental von einfachen, sogenannten Newtonschen Flüssigkeiten, die keinerlei elastische Komponente aufweisen und deren Relaxationszeiten daher als verschwindend gering angenommen werden können im Vergleich zu den Zeitskalen der Kolloidbewegung. In experimentellen Systemen werden komplexe Flüssigkeiten durch den Einsatz sogenannter viskoelastischer Flüssigkeiten umgesetzt. Viskoelastische Eigenschaften spielen eine wichtige Rolle in der Natur sowie in industriellen Anwendungen und finden sich in diversen physikalischen Systemen (z.B. in biologischen Flüssigkeiten, semi-diluten Polymerlösungen, Mizellensystemen, oder in dichten kolloidalen Suspensionen) wieder. Die elastische Komponente dieser Flüssigkeiten führt zu großen strukturellen Relaxationszeiten der Freiheitsgrade des Bades, die oftmals in der Größenordnung von Sekunden liegen und daher auf einfache Art und Weise in Experimenten beobachtet werden können. Wird das viskoelastische Bad zum Beispiel durch die Bewegung des Kolloids gestört, so bewirkt die elastische Komponente des Bades eine Rückkopplung auf das Teilchen, die sich in der zukünftigen Bewegung des Teilchens widerspiegelt. Die effektiven Gleichungen, mit denen die Bewegung von Teilchen in Flüssigkeiten typischerweise beschrieben werden, müssen aus diesem Grund verändert werden. Diese Gleichungen müssen nunmehr das Erinnerungsvermögen („Gedächtnis“) des Systems sowie kinematische Details des Bades beinhalten.

Bereits in der Gleichgewichtsbeschreibung der Kolloidbewegung macht sich der Unterschied zu einer Newtonschen Flüssigkeit bemerkbar. Ausgehend von mikroskopischen Bewegungsgleichungen, die alle Freiheitsgrade des Systems explizit berücksichtigen, kann mit bekannten Projektionsoperatorentechniken eine effektive verallgemeinerte, nicht-Markovsche Langevin Gleichung hergeleitet werden. Diese untersuchen wir für den Fall eines harmonisch gefangenen Kolloids. Dabei entwickeln wir die Kernelfunktion der Reibungskraft für kleine Zeiten. Wir finden heraus, dass diese Funktion im Falle einer nichtlinearen Teilchen-Bad Kopplung erstaunliche Abhängigkeiten aufweist. So kann die Reibungskraft beispielsweise von der externen Fallenstärke abhängen, von der Masse des Teilchens, oder im überdämpften Fall von dem Reibungskoeffizient des Kolloids. Dieses Ergebnis widerspricht der intuitiven Annahme, dass die Reibungskraft nur Eigenschaften des Bades beinhalten sollte.

Die gefundenen Abhängigkeiten der Kernelfunktion werden im Falle der Fallenstärke durch die experimentellen Ergebnisse in einer wurmartigen Mizellenlösung bestätigt. Um die experimentellen Ergebnisse quantitativ zu beschreiben, entwickeln wir ein einfaches Modell zweier nichtlinearer gekoppelter Brownscher Teilchen. Während sich das eine Teilchen in einer harmonischen Falle befindet, stellt das andere Teilchen das komplexe Bad dar, das an das Teilchen gekoppelt ist. Durch die Variation des Interaktionspotentials dieser beiden Teilchen finden wir im Falle eines stochastischen Prandtl-Tomlinson Modells eine geeignete Beschreibung, um die experimentellen Messergebnisse zu reproduzieren. Die verwendeten Modellparameter liefern wichtige Einsichten über die Längen- und Zeitskalen des experimentellen Systems.

Im nächsten Schritt verknüpfen wir die gewonnenen Erkenntnisse mit aus der Mikrorheologie bekannten Messgrößen. Auch in mikrorheologischen Größen taucht die Abhängigkeit von der externen Fallenstärke auf, eine Tatsache, die bereits in früheren Studien beobachtet wurde. Anhand der abgeleiteten Gleichungen diskutieren wir den Fall einer besonders steifen Falle und einer besonders schwachen Falle im Rahmen der linearen Antworttheorie. Es zeigt sich, dass in der mikrorheologischen Beschreibung die beiden Modi, konstante Geschwindigkeit und konstante Kraft, grundlegend verschieden sind. Diese Beobachtung ist darauf zurückzuführen, dass sich die Fluktuationen des Systems in den beiden Modi unterschiedlich verhalten.

Auf dem Weg zu einer Beschreibung im Nichtgleichgewicht leiten wir eine exakte nichtlineare Langevin Gleichung her, die bis zur dritten Ordnung in der Teilchengeschwindigkeit gültig ist. In der Herleitung der Gleichung verwenden wir einen neuartigen Ansatz der nichtlinearen Antworttheorie, der auf Pfadintegralen basiert. Die Struktur der exakten Gleichung erlaubt uns eine phänomenologische Modellgleichung abzuleiten. Die phänomenologische Gleichung wird anschließend sowohl im Gleichgewicht als auch unter stationären Nichtgleichgewichtsbedingungen linearisiert. Im Zuge der Linearisierung wird die Kernelfunktion der Reibungskraft renormalisiert. Während wir im Gleichgewicht eine Renormalisierung thermischer Natur finden, wie wir sie bereits im Falle der mikroskopischen Herleitung beobachtet hatten, ist die Situation im stationären Nichtgleichgewicht komplexer. Hier sorgt bereits die Transformation in das mitbewegte Bezugssystem für eine Renormalisierung der linearen Kernelfunktion. Wir finden heraus, dass diese Funktion (ebenso wie das Rauschen) abhängig ist von der Geschwindigkeit der Falle, mit der das Teilchen durch das Bad gezogen wird.

Die linearisierte Gleichung im mitbewegten Bezugssystem der Falle liefert eine geeignete Beschreibung der oszillierenden Moden, die im experimentellen Mizellensystem im stationären Nichtgleichgewichtszustand beobachtet werden. Diese oszillierenden Moden sind für ein überdämpftes Gleichgewichtssystem strikt ausgeschlossen. Die oszillierenden Moden im Nichtgleichgewicht sorgen dafür, dass die Kernelfunktion in der effektiven Langevin Beschreibung für bestimmte Zeiten negativ wird. Es kann gezeigt werden, dass die eigentlich überdämpfte Bewegungsgleichung in diesem Fall einer unterdämpften Gleichung mit einer positiven effektiven Masse entspricht. Abschließend greifen wir erneut das stochastische Prandtl-Tomlinson Modell auf

und untersuchen seine Eigenschaften im Nichtgleichgewichtsfall. Insbesondere simulieren wir den geschwindigkeitsabhängigen Reibungskoeffizienten und die mittlere Teilchenposition bei gegebener Anfangsbedingung. Diese Kurven zeigen qualitative Übereinstimmung mit den experimentellen Resultaten. Wir glauben daher, dass das stochastische Prandtl-Tomlinson Modell unter der Einbeziehung möglicher Modifikationen (z.B. zusätzliche Teilchen, Änderung der Interaktionspotenziale zwischen den Teilchen) geeignet ist, die Phänomene komplexer Kolloid-Bad System im Gleichgewicht und Nichtgleichgewicht in geeigneter Weise zu beschreiben.

A Nonlinear external potential in overdamped dynamics

In this appendix, we want to derive the correction term in the memory kernel due to the presence of an anharmonic external potential for the case of overdamped dynamics. Notably, the projection operator technique presented in Sec. 3.1 is not restricted to Hamilton dynamics and the Liouville equation, but applicable to any linear operator equation of the form

$$\frac{\partial}{\partial t}A(t) = \mathcal{T}A(t). \quad (1.1)$$

In order to derive an evolution equation for the one dimensional correlator $C_{xx}(t)$ in overdamped dynamics we naturally choose $\mathcal{T} = \Omega^\dagger$ and $A = x$. We obtain the first-order differential equation

$$\frac{\partial}{\partial t}C_{xx}(t) = i\Omega C_{xx}(t) + \int_0^t dt' M(t-t')C_{xx}(t'). \quad (1.2)$$

In the following, we consider a single particle in an anharmonic external field, i.e. the Hermitian adjoint of the Smoluchowski operator reads

$$\Omega^\dagger = D(\partial_x^2 + \beta F_{\text{ext}}\partial_x) \quad (1.3)$$

with diffusion coefficient $D = \frac{k_B T}{\gamma}$ and $F_{\text{ext}} = -ax - bx^3$. The frequency matrix $i\Omega$ is computed as

$$i\Omega = \frac{\langle x\Omega^\dagger x \rangle_{\text{eq}}}{\langle x^2 \rangle_{\text{eq}}} = -\frac{\kappa}{\gamma}, \quad (1.4)$$

where we defined the effective spring constant $\kappa = \frac{k_B T}{\langle x^2 \rangle_{\text{eq}}}$. By rewriting Eq. (1.2), we obtain

$$\gamma \frac{\partial}{\partial t}C_{xx}(t) = -\kappa C_{xx}(t) + \int_0^t dt' \Gamma(t-t')C_{xx}(t'). \quad (1.5)$$

For the computation of the memory kernel we require projected dynamics. With the projector $P(\cdot) = \frac{\langle x \cdot \rangle}{\langle x^2 \rangle}x$ and $P + Q = 1$ we have

$$\Gamma(t) = \gamma M(t) = \gamma \frac{\langle x\Omega^\dagger Q e^{Q\Omega^\dagger t} Q\Omega^\dagger x \rangle}{\langle x^2 \rangle}. \quad (1.6)$$

It is useful to separate the perturbative part of the evolution operator Ω^\dagger from the linear part Ω_0^\dagger

$$\Omega^\dagger = \Omega_0^\dagger - D\beta b x^3 \partial_x, \quad (1.7)$$

where we defined $\Omega_0^\dagger = D(\partial_x^2 - \beta a x \partial_x)$. The linear contribution does not contribute to the memory kernel since

$$Q\Omega_0^\dagger x = 0 \quad (1.8)$$

and we conclude that the leading-order term is at least of $\mathcal{O}(b^2)$. On the other hand, we have

$$Q(\Omega^\dagger - \Omega_0^\dagger)x = \gamma^{-1}b \left(\frac{\langle x^4 \rangle}{\langle x^2 \rangle} x - x^3 \right) \equiv \mathcal{F}. \quad (1.9)$$

The defined function \mathcal{F} is an eigenfunction of the operator $Q\Omega_0^\dagger$ obeying

$$Q\Omega_0^\dagger \mathcal{F} = -3D\beta a \mathcal{F}. \quad (1.10)$$

The eigenvalue equation proves useful in the application of exponential operator in Eq. (1.6). In leading order in b we find

$$\Gamma(t) = \gamma \frac{\langle \mathcal{F} e^{Q\Omega_0^\dagger t} \mathcal{F} \rangle}{\langle x^2 \rangle} + \mathcal{O}(b^3) = 6\gamma^{-1} \left(\frac{k_B T}{a} \right)^2 b^2 e^{-3\frac{t}{\gamma a}} + \mathcal{O}(b^3). \quad (1.11)$$

The time-integrated memory kernel in the Markov limit yields

$$\hat{\Gamma}(0) = \int_0^\infty dt \Gamma(t) = 2 \left(\frac{k_B T}{a} \right)^2 \frac{b^2}{a}. \quad (1.12)$$

Even though the correction term looks very similar to the one in Eq. (4.44), they are not identical due to their different origin in their corresponding equations of motion/dynamics.

B Entropic and frenetic part – An example

In this appendix, we exemplarily derive the entropic and frenetic part, S and D , respectively, for the case of overdamped diffusion by application of simple path integral techniques [119, 145]. The overdamped equation of motion in the Itô calculus is defined by

$$\dot{x}_s = \chi(x_s)f(x_s) + \nabla\mathcal{D}(x_s) + \sqrt{2\mathcal{D}(x_s)}\xi_s. \quad (2.1)$$

The mobility $\chi = \beta\mathcal{D}(x)$ is proportional to the diffusion matrix \mathcal{D} and fulfills the Stokes-Einstein-Sutherland relation. The probe particle is in contact with a heat bath specified by inverse temperature β . The system of equations is Markovian and the noise is assumed to be Gaussian white, i.e.

$$\langle \xi_s^i \rangle = 0, \quad \langle \xi_s^i \xi_{s'}^j \rangle = \delta_{ij} \delta(s - s'). \quad (2.2)$$

In equilibrium, the force f acting upon the particle is conservative and is characterized by a potential $U(x)$. The system is perturbed by a small external potential at time $t = 0$,

$$f(x_t) = -\nabla U \xrightarrow{\text{perturb}} f(x_t) = -\nabla(U - \varepsilon V), \quad t > 0 \quad (2.3)$$

We assume that the diffusion matrix \mathcal{D} is not influenced by this external perturbation. In path integral formalism infinitely many paths exist (in contrast to classical mechanics where the physical path is characterized by the extremal action) which are taken into account with different weights. In Sec. 5.2, the perturbed dynamical ensemble was described via an action $\mathcal{A}_\varepsilon(\omega)$ which can be written in terms of a time-symmetric part $D = D\theta$ and a time-antisymmetric part $S = -S\theta$ upon time reversal defined on paths $\omega = (x_s, 0 \leq s \leq t)$ via $(\theta\omega)_s = \pi x_{t-s}$. The two parts can then be expressed in terms of the action \mathcal{A}_ε

$$D(\omega) = \frac{1}{2} (\mathcal{A}_\varepsilon(\omega) + \mathcal{A}_\varepsilon(\theta\omega)), \quad (2.4)$$

$$S(\omega) = \mathcal{A}_\varepsilon(\theta\omega) - \mathcal{A}_\varepsilon(\omega). \quad (2.5)$$

In the Martin-Siggia-Rose formalism, and for a Markovian process with Gaussian

white noise, this action may be identified as [146]

$$\mathcal{A}_\varepsilon = \frac{1}{2} \int_0^t ds (\xi_s^2 - \lim_{\varepsilon \rightarrow 0} \xi_s^2) = D - \frac{S}{2}. \quad (2.6)$$

Note that we subtracted the perturbation-independent term $\lim_{\varepsilon \rightarrow 0} \xi_s^2$. In the last step, we separated the action into D and S , respectively. From the equation of motion (2.1) we may compute

$$\begin{aligned} \xi_j^2 = \frac{1}{2} & \left(\mathcal{D}_{im}^{-1} \dot{x}_i \dot{x}_m + 2\beta \dot{x}_i \partial_i U - \mathcal{D}_{im}^{-1} (\dot{x}_i \partial_l \mathcal{D}_{ml} + \dot{x}_m \partial_k \mathcal{D}_{ik}) \right. \\ & \left. \beta^2 \mathcal{D}_{kl} \partial_l U \partial_k U - 2\beta \partial_l \mathcal{D}_{kl} \partial_k U + \mathcal{D}_{im}^{-1} \partial_k \mathcal{D}_{ik} \partial_l \mathcal{D}_{ml} \right. \\ & \left. \varepsilon \left[-2\beta \partial_k V (\dot{x}_k + \beta \mathcal{D}_{kl} \partial_l U - \partial_l \mathcal{D}_{kl}) \right] + \varepsilon^2 \beta^2 \partial_k V \mathcal{D}_{kl} \partial_l V \right). \end{aligned} \quad (2.7)$$

Note that we used Einstein's summation convention, i.e. sums are indicated by indices that appear twice in products. Applied to a specific trajectory $\omega(x, \dot{x}, s)$ with $0 < s < t$ the time reversal operator θ implies

$$\theta \omega(x, \dot{x}, s) = \omega(x, -\dot{x}, t - s). \quad (2.8)$$

By taking into account that velocities change sign under time reversal, and using the conversion between Itô and Stratonovich integrals [125], we find [119, 145]

$$D'_0 = \frac{\beta}{2} \int_0^t ds [-\chi_{ij} \partial_j U \partial_i V + \partial_i \mathcal{D}_{ij} \partial_j V] = \frac{\beta}{2} \int_0^t ds \Omega^\dagger V(x_s), \quad (2.9)$$

$$D''_0 = \int_0^t ds \frac{\beta^2}{2} \mathcal{D}_{ij} \partial_i V \partial_j V, \quad (2.10)$$

where we expanded $D = \varepsilon D'_0 + \frac{\varepsilon^2}{2} D''_0$ in orders of perturbation. Note that the Taylor coefficient D'_0 can be rewritten in terms of the Hermitian conjugate of the equilibrium Smoluchowski operator

$$\Omega^\dagger = (\nabla - \beta \nabla U) \cdot \mathcal{D}(x_s) \cdot \nabla. \quad (2.11)$$

On the other hand, for the entropic part $S = \varepsilon S'_0$ we find [119, 145]

$$S'_0 = \beta [V(x_t) - V(x_0)]. \quad (2.12)$$

As expected for a potential perturbation there is no higher-order term than the linear one in the expansion of the time-antisymmetric part of the action.

Bibliography

- [1] B. Müller and M. Krüger. Anisotropic particles near surfaces: Propulsion force and friction. *Phys. Rev. A*, 93:032511, 2016.
- [2] B. Müller, R. Incardone, M. Antezza, T. Emig, and M. Krüger. Many-body heat radiation and heat transfer in the presence of a nonabsorbing background medium. *Phys. Rev. B*, 95:085413, 2017.
- [3] K. Asheichyk, B. Müller, and M. Krüger. Heat radiation and transfer for point particles in arbitrary geometries. *Phys. Rev. B*, 96:155402, 2017.
- [4] J. Berner, B. Müller, J. R. Gomez-Solano, M. Krüger, and C. Bechinger. Oscillating modes of driven colloids in overdamped systems. *Nat. Commun.*, 9(1):999, 2018.
- [5] B. Müller, J. Berner, C. Bechinger, and M. Krüger. Properties of a nonlinear bath: Experiments, theory, and a stochastic Prandtl-Tomlinson model. *arXiv:1909.12812*, 2019.
- [6] E. Nelson. *Quantum fluctuations*. Princeton University Press, 1985.
- [7] H. L. Pécseli. *Fluctuations in physical systems*. Cambridge University Press, 2000.
- [8] F. Schwabl and W. D. Brewer. *Statistical Mechanics*. Advanced Texts in Physics. Springer Berlin Heidelberg, 2006.
- [9] D. Dalvit, P. Milonni, D. Roberts, and F. Da Rosa. *Casimir physics*, volume 834. Springer, 2011.
- [10] R. Klages, W. Just, and C. Jarzynski. *Nonequilibrium statistical physics of small systems*. Wiley Online Library, 2013.
- [11] J.-P. Hansen and I. R. McDonald. *Theory of simple liquids: with applications to soft matter*. Academic Press, 2013.
- [12] R. Zwanzig. *Nonequilibrium statistical mechanics*. Oxford University Press, 2001.

- [13] D. B. Newell and E. Tiesinga. The international system of units (SI). Technical report, 2019.
- [14] P. Gaspard. *Chaos, scattering and statistical mechanics*, volume 9. Cambridge University Press, 2005.
- [15] P. W. Milonni. *The quantum vacuum: an introduction to quantum electrodynamics*. Academic Press, 2013.
- [16] W. Heisenberg. Über den anschaulichen Inhalt der quantentheoretischen Kinematik und Mechanik. In *Original Scientific Papers Wissenschaftliche Originalarbeiten*, pages 478–504. Springer, 1985.
- [17] H. B. G. Casimir. On the attraction between two perfectly conducting plates. In *Proc. Kon. Ned. Akad. Wet.*, volume 51, page 793, 1948.
- [18] J. K. G. Dhont. *An introduction to dynamics of colloids*, volume 2. Elsevier, 1996.
- [19] R. Brown. A brief account of microscopical observations made in the months of june, july and august 1827, on the particles contained in the pollen of plants; and on the general existence of active molecules in organic and inorganic bodies. *Philos. Mag.*, 4(21):161–173, 1828.
- [20] A. Einstein. Über die von der molekularkinetischen Theorie der Wärme geforderte Bewegung von in ruhenden Flüssigkeiten suspendierten Teilchen. *Ann. Phys.*, 322(8):549–560, 1905.
- [21] W. Sutherland. A dynamical theory of diffusion for non-electrolytes and the molecular mass of albumin. *Philos. Mag.*, 9(54):781–785, 1905.
- [22] M. von Smoluchowski. Zur kinetischen Theorie der Brownschen Molekularbewegung und der Suspensionen. *Ann. Phys.*, 326(14):756–780, 1906.
- [23] H. B. Callen and T. A. Welton. Irreversibility and generalized noise. *Phys. Rev.*, 83(1):34, 1951.
- [24] R. Kubo. Statistical-mechanical theory of irreversible processes. i. general theory and simple applications to magnetic and conduction problems. *J. Phys. Soc. Jpn.*, 12(6):570–586, 1957.
- [25] R. Kubo. The fluctuation-dissipation theorem. *Rep. Prog. Phys.*, 29(1):255, 1966.
- [26] P. Langevin. Sur la théorie du mouvement brownien. *Compt. Rendus*, 146:530–533, 1908.

-
- [27] J. Perrin and J. Donau. Die Brown'sche Bewegung und die wahre Existenz der Moleküle. *Kolloidchemische Beihefte*, 1(6-7):221–300, 1910.
- [28] G. S. Agarwal. Fluctuation-dissipation theorems for systems in non-thermal equilibrium and applications. *Z. Phys.*, 252(1):25–38, 1972.
- [29] M. Baiesi, C. Maes, and B. Wynants. Fluctuations and response of nonequilibrium states. *Phys. Rev. Lett.*, 103(1):010602, 2009.
- [30] J. R. Gomez-Solano, A. Petrosyan, S. Ciliberto, and C. Maes. Fluctuations and response in a non-equilibrium micron-sized system. *J. Stat. Mech.: Theory Exp.*, 2011(01):P01008, 2011.
- [31] J. Prost, J.-F. Joanny, and J. M. R. Parrondo. Generalized fluctuation-dissipation theorem for steady-state systems. *Phys. Rev. Lett.*, 103(9):090601, 2009.
- [32] U. Seifert and T. Speck. Fluctuation-dissipation theorem in nonequilibrium steady states. *EPL*, 89(1):10007, 2010.
- [33] E. Lippiello, M. Baiesi, and A. Sarracino. Nonequilibrium fluctuation-dissipation theorem and heat production. *Phys. Rev. Lett.*, 112(14):140602, 2014.
- [34] N. P. Cheremisinoff. *Encyclopedia of Fluid Mechanics: Polymer Flow Engineering*, volume 9. Gulf Publishing Company, 1990.
- [35] S. Toyabe, H.-R. Jiang, T. Nakamura, Y. Murayama, and M. Sano. Experimental test of a new equality: Measuring heat dissipation in an optically driven colloidal system. *Phys. Rev. E*, 75(1):011122, 2007.
- [36] V. Blickle, T. Speck, C. Lutz, U. Seifert, and C. Bechinger. Einstein relation generalized to nonequilibrium. *Phys. Rev. Lett.*, 98(21):210601, 2007.
- [37] J. R. Gomez-Solano, A. Petrosyan, S. Ciliberto, R. Chetrite, and K. Gawędzki. Experimental verification of a modified fluctuation-dissipation relation for a micron-sized particle in a nonequilibrium steady state. *Phys. Rev. Lett.*, 103(4):040601, 2009.
- [38] H. Risken. *Fokker-planck equation*. Springer, 1996.
- [39] S. Ciliberto. Experiments in stochastic thermodynamics: Short history and perspectives. *Phys. Rev. X*, 7(2):021051, 2017.
- [40] K. Sekimoto. Langevin equation and thermodynamics. *Prog. Theor. Exp. Phys.*, 130:17–27, 1998.

- [41] G. Gallavotti and E. G. D. Cohen. Dynamical ensembles in nonequilibrium statistical mechanics. *Phys. Rev. Lett.*, 74(14):2694, 1995.
- [42] C. Jarzynski. Nonequilibrium equality for free energy differences. *Phys. Rev. Lett.*, 78(14):2690, 1997.
- [43] G. E. Crooks. Entropy production fluctuation theorem and the nonequilibrium work relation for free energy differences. *Phys. Rev. E*, 60(3):2721, 1999.
- [44] T. Hatano and S. Sasa. Steady-state thermodynamics of Langevin systems. *Phys. Rev. Lett.*, 86(16):3463, 2001.
- [45] U. Seifert. Entropy production along a stochastic trajectory and an integral fluctuation theorem. *Phys. Rev. Lett.*, 95(4):040602, 2005.
- [46] G. Verley, R. Chetrite, and D. Lacoste. Inequalities generalizing the second law of thermodynamics for transitions between nonstationary states. *Phys. Rev. Lett.*, 108(12):120601, 2012.
- [47] U. Seifert. Stochastic thermodynamics, fluctuation theorems and molecular machines. *Rep. Prog. Phys.*, 75(12):126001, 2012.
- [48] T. G. Mason and D. A. Weitz. Optical measurements of frequency-dependent linear viscoelastic moduli of complex fluids. *Phys. Rev. Lett.*, 74(7):1250, 1995.
- [49] J. Yang. Viscoelastic wormlike micelles and their applications. *Curr. Opin. Colloid Interface Sci.*, 7(5-6):276–281, 2002.
- [50] I. Gazuz, A. M. Puertas, T. Voigtmann, and M. Fuchs. Active and nonlinear microrheology in dense colloidal suspensions. *Phys. Rev. Lett.*, 102(24):248302, 2009.
- [51] Y. L. Raikher, V. V. Rusakov, and R. Perzynski. Brownian motion in a viscoelastic medium modelled by a Jeffreys fluid. *Soft Matter*, 9(45):10857–10865, 2013.
- [52] J. R. Gomez-Solano and C. Bechinger. Probing linear and nonlinear microrheology of viscoelastic fluids. *EPL*, 108(5):54008, 2014.
- [53] J. R. Gomez-Solano and C. Bechinger. Transient dynamics of a colloidal particle driven through a viscoelastic fluid. *New J. Phys.*, 17(10):103032, 2015.
- [54] M. Krüger and C. Maes. The modified Langevin description for probes in a nonlinear medium. *J. Phys. Condens. Matter*, 29(6), 2016.

-
- [55] J.-F. Berret. Local viscoelasticity of living cells measured by rotational magnetic spectroscopy. *Nat. Commun.*, 7:10134, 2016.
- [56] J. R. Gomez-Solano, A. Blokhuis, and C. Bechinger. Dynamics of self-propelled janus particles in viscoelastic fluids. *Phys. Rev. Lett.*, 116(13):138301, 2016.
- [57] C. Lozano, J. R. Gomez-Solano, and C. Bechinger. Run-and-tumble-like motion of active colloids in viscoelastic media. *New J. Phys.*, 20(1):015008, 2018.
- [58] M. Gruber. *Theory of microrheology in complex fluids*. PhD thesis, Universität Konstanz, Konstanz, 2019.
- [59] R. G. Larson. *The structure and rheology of complex fluids*, volume 150. Oxford university press New York, 1999.
- [60] T. M. Squires and J. F. Brady. A simple paradigm for active and nonlinear microrheology. *Phys. Fluids*, 17(7):073101, 2005.
- [61] R. R. Brau, J. M. Ferrer, H. Lee, C. E. Castro, B. K. Tam, P. B. Tarsa, P. Matsudaira, M. C. Boyce, R. D. Kamm, and M. J. Lang. Passive and active microrheology with optical tweezers. *J. Opt.*, 9(8):S103, 2007.
- [62] L. G. Wilson and W. C. K. Poon. Small-world rheology: an introduction to probe-based active microrheology. *Phys. Chem. Chem. Phys.*, 13(22):10617–10630, 2011.
- [63] A. Freed. *Soft solids*. Springer, 2016.
- [64] R. E. Langer et al. Vito volterra, theory of functionals and of integral and integro-differential equations. *Bull. Am. Math. Soc.*, 38(9, Part 1):623–623, 1932.
- [65] C. T. Culbertson, S. C. Jacobson, and J. M. Ramsey. Diffusion coefficient measurements in microfluidic devices. *Talanta*, 56(2):365–373, 2002.
- [66] C. B. Müller, A. Loman, V. Pacheco, F. Koberling, D. Willbold, W. Richtering, and J. Enderlein. Precise measurement of diffusion by multi-color dual-focus fluorescence correlation spectroscopy. *EPL*, 83(4):46001, 2008.
- [67] A. Yao, M. Tassieri, M. Padgett, and J. Cooper. Microrheology with optical tweezers. *Lab Chip*, 9(17):2568–2575, 2009.
- [68] P. H. Jones, O. M. Maragò, and G. Volpe. *Optical tweezers: Principles and applications*. Cambridge University Press, 2015.

- [69] N. Phan-Thien and N. Mai-Duy. *Understanding viscoelasticity: an introduction to rheology*. Springer, 2017.
- [70] R. J. Poole. The Deborah and Weissenberg numbers. *British Soc. Rheol. Rheol. Bull*, 53:32–39, 2012.
- [71] R. Zwanzig. Memory effects in irreversible thermodynamics. *Phys. Rev.*, 124:983–992, Nov 1961.
- [72] H. Mori. Transport, collective motion, and brownian motion. *Prog. Theor. Phys.*, 33(3):423–455, 1965.
- [73] H. Goldstein, C. Poole, and J. Safko. *Classical mechanics*, 2002.
- [74] J. D. Jackson. *Classical electrodynamics*, 1999.
- [75] A. O. Caldeira and A. J. Leggett. Influence of dissipation on quantum tunneling in macroscopic systems. *Phys. Rev. Lett.*, 46(4):211, 1981.
- [76] J. O. Daldrop, B. G. Kowalik, and R. R. Netz. External potential modifies friction of molecular solutes in water. *Phys. Rev. X*, 7:041065, Dec 2017.
- [77] K. Sture, J. Nordholm, and R. Zwanzig. Strategies for fluctuation renormalization in nonlinear transport theory. *J. Stat. Phys.*, 11(2):143–158, Aug 1974.
- [78] H. Fujisaka. Fluctuation Renormalization in Nonlinear Dynamics. *Prog. Theor. Exp. Phys.*, 55(2):430–437, 02 1976.
- [79] L. J. Magid, Z. Han, Z. Li, and P. D. Butler. Tuning the contour lengths and persistence lengths of cationic micelles: the role of electrostatics and specific ion binding. *J. Phys. Chem. B*, 104(29):6717–6727, 2000.
- [80] L. M. Walker. Rheology and structure of worm-like micelles. *Curr. Opin. Colloid Interface Sci.*, 6(5-6):451–456, 2001.
- [81] M. E. Cates and S. M. Fielding. Rheology of giant micelles. *Adv. Phys*, 55(7-8):799–879, 2006.
- [82] C. A. Dreiss. Wormlike micelles: where do we stand? recent developments, linear rheology and scattering techniques. *Soft Matter*, 3(8):956–970, 2007.
- [83] M. Akram, S. Yousuf, T. Sarwar, et al. Micellization and interfacial behavior of 16-e2-16 in presence of inorganic and organic salt counterions. *Colloids Surf.*, 441:281–290, 2014.
- [84] M. Buchanan, M. Atakhorrani, J. F. Palierne, F. C. MacKintosh, and C. F.

- Schmidt. High-frequency microrheology of wormlike micelles. *Phys. Rev. E*, 72:011504, Jul 2005.
- [85] J. C. Crocker and D. G. Grier. Methods of digital video microscopy for colloidal studies. *J. Colloid Interface Sci.*, 179(1):298–310, 1996.
- [86] J. C. Lindon, G. E. Tranter, and D. Koppelaar. *Encyclopedia of spectroscopy and spectrometry*. Academic Press, 2016.
- [87] W. Van Meegen, T. C. Mortensen, S. R. Williams, and J. Müller. Measurement of the self-intermediate scattering function of suspensions of hard spherical particles near the glass transition. *Phys. Rev. E*, 58(5):6073, 1998.
- [88] P. S. Burada, P. Hänggi, F. Marchesoni, G. Schmid, and P. Talkner. Diffusion in confined geometries. *ChemPhysChem*, 10(1):45–54, 2009.
- [89] D. Ernst and J. Köhler. Measuring a diffusion coefficient by single-particle tracking: statistical analysis of experimental mean squared displacement curves. *Phys. Chem. Chem. Phys.*, 15(3):845–849, 2013.
- [90] A. Dechant. Estimating the free-space diffusion coefficient of trapped particles. *EPL*, 125(2):20010, 2019.
- [91] D. Frenkel and B. Smit. *Understanding molecular simulation: from algorithms to applications*, volume 1. Elsevier, 2001.
- [92] M. P. Allen and D. J. Tildesley. *Computer simulation of liquids*. Oxford university press, 2017.
- [93] D. L. Ermak. A computer simulation of charged particles in solution. i. technique and equilibrium properties. *J. Chem. Phys.*, 62(10):4189–4196, 1975.
- [94] D. L. Ermak and J. A. McCammon. Brownian dynamics with hydrodynamic interactions. *J. Chem. Phys.*, 69(4):1352–1360, 1978.
- [95] S. H. Northrup, S. A. Allison, and J. A. McCammon. Brownian dynamics simulation of diffusion-influenced bimolecular reactions. *J. Chem. Phys.*, 80(4):1517–1524, 1984.
- [96] P. Bhattacharya, S. K. Saha, A. Yadav, P. E. Phelan, and R. S. Prasher. Brownian dynamics simulation to determine the effective thermal conductivity of nanofluids. *J. Appl. Phys.*, 95(11):6492–6494, 2004.
- [97] R. Erban. From molecular dynamics to brownian dynamics. *Proc. Royal Soc. A*, 470(2167):20140036, 2014.

- [98] P. S. Doyle and P. T. Underhill. Brownian dynamics simulations of polymers and soft matter. In *Handbook of materials modeling*, pages 2619–2630. Springer, 2005.
- [99] K. Debrabant. Runge-Kutta methods for third order weak approximation of sdes with multidimensional additive noise. *BIT Numer. Math.*, 50(3):541–558, 2010.
- [100] R. Zwanzig. Nonlinear generalized Langevin equations. *J. Stat. Phys.*, 9(3):215–220, 1973.
- [101] R. N. Bracewell and R. N. Bracewell. *The Fourier transform and its applications*, volume 31999. McGraw-Hill New York, 1986.
- [102] J. Goldstone. Field theories with superconductor solutions. *Il Nuovo Cimento (1955-1965)*, 19(1):154–164, 1961.
- [103] J. Kappler, V. B. Hinrichsen, and R. R. Netz. Non-markovian barrier crossing with two-time-scale memory is dominated by the faster memory component. *Eur. Phys. J. E*, 42(9):119, 2019.
- [104] L. Prandtl. Ein Gedankenmodell zur kinetischen Theorie der festen Körper. *J. Appl. Math. Mech.*, 8(2):85–106, 1928.
- [105] V. L. Popov and J. A. T. Gray. Prandtl-Tomlinson model: History and applications in friction, plasticity, and nanotechnologies. *J. Appl. Math. Mech.*, 92(9):683–708, 2012.
- [106] E. Gnecco, R. Bennewitz, T. Gyalog, C. Loppacher, M. Bammerlin, E. Meyer, and H.-J. Güntherodt. Velocity dependence of atomic friction. *Phys. Rev. Lett.*, 84(6):1172, 2000.
- [107] L. Jansen, H. Hölscher, H. Fuchs, and A. Schirmeisen. Temperature dependence of atomic-scale stick-slip friction. *Phys. Rev. Lett.*, 104(25):256101, 2010.
- [108] M. H. Müser. Velocity dependence of kinetic friction in the Prandtl-Tomlinson model. *Phys. Rev. B*, 84(12):125419, 2011.
- [109] P. Cicuta and A. M. Donald. Microrheology: a review of the method and applications. *Soft Matter*, 3(12):1449–1455, 2007.
- [110] T. M. Squires and T. G. Mason. Fluid mechanics of microrheology. *Annu. Rev. Fluid Mech.*, 42, 2010.
- [111] L. G. Wilson, A. W. Harrison, W. C. K. Poon, and A. M. Puertas. Microrheology and the fluctuation theorem in dense colloids. *EPL*, 93(5):58007, 2011.

-
- [112] C. J. Harrer, D. Winter, J. Horbach, M. Fuchs, and T. Voigtmann. Force-induced diffusion in microrheology. *J. Phys. Condens. Matter*, 24(46):464105, 2012.
- [113] A. M. Puertas and T. Voigtmann. Microrheology of colloidal systems. *J. Phys. Condens. Matter*, 26(24):243101, 2014.
- [114] A. I. Bishop, T. A. Nieminen, N. R. Heckenberg, and H. Rubinsztein-Dunlop. Optical microrheology using rotating laser-trapped particles. *Phys. Rev. Lett.*, 92(19):198104, 2004.
- [115] M. D. Graham. *Microhydrodynamics, Brownian motion, and complex fluids*, volume 58. Cambridge University Press, 2018.
- [116] F. Penna, J. Dzubiella, and P. Tarazona. Dynamic density functional study of a driven colloidal particle in polymer solutions. *Phys. Rev. E*, 68(6):061407, 2003.
- [117] M. Rauscher, A. Domínguez, M. Krüger, and F. Penna. A dynamic density functional theory for particles in a flowing solvent. *J. Chem. Phys.*, 127(24):244906, 2007.
- [118] O. Bénichou, A. Bodrova, D. Chakraborty, P. Illien, A. Law, C. Mejía-Monasterio, G. Oshanin, and R. Voituriez. Geometry-induced superdiffusion in driven crowded systems. *Phys. Rev. Lett.*, 111(26):260601, 2013.
- [119] U. Basu, M. Krüger, A. Lazarescu, and C. Maes. Frenetic aspects of second order response. *Phys. Chem. Chem. Phys.*, 17(9):6653–6666, 2015.
- [120] D. J. Evans and G. Morriss. *Statistical mechanics of nonequilibrium liquids*. Cambridge University Press, 2008.
- [121] C. P. Enz. *A course on Many-body theory Applied to Solid-state Physics*, volume 11. World Scientific Publishing Company, 1992.
- [122] C. Maes and K. Netočný. Time-reversal and entropy. *J. Stat. Phys.*, 110(1-2):269–310, 2003.
- [123] C. Maes and M. H. van Wieren. Time-symmetric fluctuations in nonequilibrium systems. *Phys. Rev. Lett.*, 96(24):240601, 2006.
- [124] G. E. Crooks. Nonequilibrium measurements of free energy differences for microscopically reversible markovian systems. *J. Stat. Phys.*, 90(5-6):1481–1487, 1998.
- [125] C. W. Gardiner et al. *Handbook of stochastic methods*, volume 3.

- [126] H. Soo and M. Krüger. Fluctuational electrodynamics for nonlinear media. *EPL*, 115(4):41002, 2016.
- [127] H. Soo and M. Krüger. Fluctuational electrodynamics for nonlinear materials in and out of thermal equilibrium. *Phys. Rev. B*, 97(4), 2018.
- [128] H. Soo. *Fluctuational electrodynamics for nonlinear materials in and out of equilibrium*. PhD thesis, Universität Göttingen, Göttingen, 2019.
- [129] C. Gutsche, F. Kremer, M. Krüger, M. Rauscher, R. Weeber, and J. Harting. Colloids dragged through a polymer solution: Experiment, theory, and simulation. *J. Chem. Phys.*, 129(8):084902, 2008.
- [130] A. Jayaraman and A. Belmonte. Oscillations of a solid sphere falling through a wormlike micellar fluid. *Physical Review E*, 67(6):065301, 2003.
- [131] N. Z. Handzy and A. Belmonte. Oscillatory rise of bubbles in wormlike micellar fluids with different microstructures. *Phys. Rev. Lett.*, 92(12):124501, 2004.
- [132] S. Leitmann and T. Franosch. Nonlinear response in the driven lattice lorentz gas. *Phys. Rev. Lett.*, 111(19):190603, 2013.
- [133] D. Winter, J. Horbach, P. Virnau, and K. Binder. Active nonlinear microrheology in a glass-forming Yukawa fluid. *Phys. Rev. Lett.*, 108(2):028303, 2012.
- [134] M. Fuchs and M. E. Cates. Schematic models for dynamic yielding of sheared colloidal glasses. *Faraday Discuss.*, 123:267–286, 2003.
- [135] Y. L. Klimontovich. Nonlinear brownian motion. *Phys.-Uspekhi*, 37(8):737, 1994.
- [136] W. Ebeling. Nonlinear brownian motion–mean square displacement. *Condensed Matter Physics*, 2004.
- [137] V. Lisý, J. Tóthová, and L. Glod. Diffusion in a medium with nonlinear friction. *Int. J. Thermophys.*, 35(11):2001–2010, 2014.
- [138] J. C. Maxwell. Iv. on the dynamical theory of gases. *Philos. Trans. Royal Soc.*, (157):49–88, 1867.
- [139] H. Jeffreys. A modification of Lomnitz’s law of creep in rocks. *Geophys. J. Int.*, 1(1):92–95, 1958.
- [140] P. Sollich. Rheological constitutive equation for a model of soft glassy materials. *Phys. Rev. E*, 58(1):738, 1998.

- [141] S. M. Fielding, P. Sollich, and M. E. Cates. Aging and rheology in soft materials. *J. Rheol.*, 44(2):323–369, 2000.
- [142] M. L. Falk and J. S. Langer. Deformation and failure of amorphous, solidlike materials. *Annu. Rev. Condens. Matter Phys.*, 2(1):353–373, 2011.
- [143] C. P. Amann, M. Siebenbürger, M. Krüger, F. Weysser, M. Ballauff, and M. Fuchs. Overshoots in stress-strain curves: Colloid experiments and schematic mode coupling theory. *J. Rheol.*, 57(1):149–175, 2013.
- [144] P. Phillips. *Advanced solid state physics*. Cambridge University Press, 2012.
- [145] B. Wynants. *Structures of Nonequilibrium Fluctuations*. PhD thesis, Queen Mary, University of London, 2010.
- [146] A. Altland and B. D. Simons. *Condensed matter field theory*. Cambridge university press, 2010.

Acknowledgments

The journey of this thesis started almost three years ago and many people contributed to the successful outcome in various ways. First and foremost, I would like to thank Prof. Matthias Krüger who gave me the opportunity to work in his group on this exciting project about Brownian motion under his supervision. During our uncountable hours of discussion, I enormously profited by his expertise in the field and helpful instructions. After working in his group for so many years now, he has had a tremendous positive impact on my development of becoming a young scientist and guided me the way through the academic jungle. I will certainly miss the regular discourse with him on the scientific level but also on topics beyond. Even though some behaviour of data is more linear than other (or “definitely not linear”), our discussions have been fruitful and resulted in the many papers we published together over the years.

I am grateful to Prof. Marcus Müller, the second examiner of the thesis, and Dr. Claus Heussinger for joining my thesis committee and for giving me the possibility to present my work. I would also like to thank the further members of the examination board, Prof. Reiner Kree, Prof. Tim Salditt, Prof. Peter Sollich, and Prof. Annette Zippelius for taking over responsibility as examiners in the oral examination of this thesis.

I highly appreciate the extensive collaboration with the group of Clemens Bechinger. The precise measurements of Johannes Berner and provision of data increased the value of this thesis in a considerable way and without it the thesis would not be complete. Things became a little bit more complicated when both of our groups left the Swabian capital (at least in terms of personal meetings). However, apart from this, our joint cooperation was anything but repulsive. Our many Skype meetings with Clemens Bechinger, Johannes Berner, and Juan Ruben Gomez-Solano kept the project going and were helpful to discuss new ideas and results of both theory and experiment. Our collaboration is proof to me that theory and experiment should always work hand in hand to get the best out of the “two worlds”.

I acknowledge discussions with Mike Reppert in the early stages of this work which helped me to set off and have a good access to the topic.

I also want to thank my former and current fellow group members, Heino Soo, Christian Rohwer, Kiryl Asheichyk, Miru Lee, Rohit Jain, Fenna Müller, and Tristan Holsten for interesting discussion, activities outside the office, and a pleasant time in the group.

I appreciate the support of my family and friends who kept me grounded and visited me during my time in Göttingen. In the words of William Shakespeare, “What’s past is prologue”, and I hope the future looks bright to everyone.

Curriculum vitae

Personal information

Name	Boris Müller
Date of birth	February 14, 1992
Place of birth	Waiblingen, Germany

Education

Oct 2011 – Sep 2014	Bachelor of Science in Physics University of Stuttgart, Germany Bachelor thesis: “Electromagnetic self-propulsion for small objects in the near-field”
---------------------	--

Oct 2014 – Oct 2016	Master of Science in Physics University of Stuttgart, Germany Master thesis: “Electromagnetic radiation in complex environments: Many body systems and background medium
---------------------	--

Nov 2016 – Jan 2018	Doctoral studies University of Stuttgart, Germany
---------------------	--

Feb 2018 – Dec 2019	Doctoral studies (cont.) University of Göttingen, Germany
---------------------	--

Conferences

Apr 2016	WE-Heraeus-Seminar on Heat Transfer and Heat Conduction on the Nanoscale, Bad Honnef, Germany Poster: “Many body heat radiation”
----------	---

Jul 2017	10th Liquid Matter Conference, Ljubljana, Slovenia Poster: “Oscillations in non-equilibrium Brownian motion”
----------	---

May 2018 WE-Heraeus-Seminar on Fluctuation-Induced Phenomena in Complex Systems, Bad Honnef, Germany
Talk & Poster: “Oscillating Modes of Driven Colloids in Overdamped Systems”

Publications

Mar 2016 B. Müller and M. Krüger. Anisotropic particles near surfaces: Propulsion force and friction. *Phys. Rev. A*, 93:032511

Feb 2017 B. Müller, R. Incardone, M. Antezza, T. Emig, and M. Krüger. Many-body heat radiation and heat transfer in the presence of a nonabsorbing background medium. *Phys. Rev. B*, 95:085413

Oct 2017 K. Asheichyk, B. Müller, and M. Krüger. Heat radiation and transfer for point particles in arbitrary geometries. *Phys. Rev. B*, 96:155402

Feb 2018 J. Berner, B. Müller, J. R. Gomez-Solano, M. Krüger, and C. Bechinger. Oscillating modes of driven colloids in overdamped systems. *Nat. Commun.*, 9(1):999

Sep 2019 B. Müller, J. Berner, C. Bechinger, and M. Krüger. Properties of a nonlinear bath: Experiments, theory, and a stochastic Prandtl-Tomlinson model. *arXiv:1909.12812*